KfK 5106
Mai 1994

Chemical Interactions between as-received and pre-oxidized Zircaloy-4 and Stainless Steel at High Temperatures

P. Hofmann, M. Markiewicz
Institut für Materialforschung
Projekt Nukleare Sicherheitsforschung

Kernforschungszentrum Karlsruhe

Kernforschungszentrum Karlsruhe
Institut für Materialforschung
Projekt Nukleare Sicherheitsforschung

KfK 5106

Chemical interactions between as-received and pre-oxidized Zircaloy-4 and stainless steel at high temperatures

P. Hofmann, M. Markiewicz*

*Comisión Nacional de Energia Atómica
Av. del Libertador 8250, 1429 Buenos Aires
Argentina

Kernforschungszentrum Karlsruhe GmbH, Karlsruhe

Als Manuskript gedruckt

Kernforschungszentrum Karlsruhe GmbH
Postfach 3640, 76021 Karlsruhe

ISSN 0303-4003

Abstract

The chemical reaction behavior between Zircaloy-4 and 1.4919 (AISI 316) stainless steel, which are used in absorber assemblies of Pressurized Water Reactors (PWR) and Boiling Water Reactors (BWR), has been studied in the temperature range 1000 - 1400°C. Zircaloy was used in the as-received, pre-oxidized and oxygen-containing condition. The maximum temperature was limited by the fast and complete liquefaction of the reaction couple as a result of eutectic chemical interactions. Liquefaction of the components occurs below their melting point.
The effect of oxygen dissolved in Zircaloy plays an important role in the interaction; oxide layers on the Zircaloy surface delay the chemical interactions with stainless steel but cannot prevent them. Oxygen dissolved in Zircaloy reduces the reaction rates and shift the liquefaction temperature to slightly higher levels. The interaction experiments at the examined temperatures with or without pre-oxidized Zircaloy can be described by parabolic rate laws. The Arrhenius equations for the various conditions of interactions are given.

Chemische Wechselwirkungen von Zircaloy-4 im Anlieferungs- und voroxidierten Zustand mit rostfreiem Stahl bei hohen Temperaturen

Zusammenfassung

Es wurden die chemischen Wechselwirkungen zwischen Zircaloy-4 und dem austenitischen Stahl 1.4919 im Temperaturbereich 1000 - 1400°C untersucht. Der Stahl ist Bestandteil der Absorberelemente in Druck- und Siedewasserreaktoren. Das Zircaloy kam im Anlieferungszustand und im voroxidierten Zustand zum Einsatz. Die maximalen Reaktionstemperaturen waren auf 1400°C begrenzt, da es bei höheren Temperaturen zur Verflüssigung der Materialproben infolge chemischer Wechselwirkungen kam.

Oxidschichten auf dem Zircaloy oder gelöster Sauerstoff im Zircaloy verzögern die chemischen Wechselwirkungen, können diese aber nicht verhindern. Die Verflüssigung wird nur zu etwas höheren Temperaturen verschoben. Die verschiedenen chemischen Wechselwirkungen können durch parabolische Zeitgesetze beschrieben werden; die Arrheniusgleichungen werden angegeben.

Contents

1. Introduction

In a severe reactor accident a number of chemical interactions between the various core components of an LWR take place at high temperatures because they are not in thermodynamic equilibrium with each other. Of special interest are the interactions between Zircaloy-4 and stainless steel in absorber assemblies of Pressurized Water Reactors (PWR) and Boiling Water Reactors (BWR).

The absorber assembly of a PWR consists of (Ag, In, Cd) absorber material with stainless steel cladding (AISI 316). The absorber rod is inserted into a Zircaloy-4 guide tube (Figure 1). At high temperatures the absorber rod will deform or balloon and locally contact the Zircaloy guide tube. As a result of chemical interactions, the stainless steel cladding of the absorber rod will fail. The released molten (Ag, In, Cd) absorber alloy will then attack the Zircaloy of the guide tube and fuel rods and dissolve (liquefy) it much below its melting point [1].

The absorber rods in Boiling Water Reactors (BWR) consist of boron carbide (B_4C) pellets or B_4C powder in thin walled stainless steel tubes. The absorber rods are contained in a four-bladed stainless steel assembly. Four fuel rod bundles, each surrounded by a Zircaloy flow channel box arranged around the cross-shaped control element (Figure 1). The boron carbide/stainless steel system is not stable thermodynamically, i.e. chemical interactions have to be expected to take place. Under normal reactor operation conditions the limited chemical interactions between B_4C and stainless steel can be tolerated. But the question is how the absorber rods behave chemically at temperatures beyond 1000°C which have to be assumed to prevail in severe reactor accidents. First scoping tests with small LWR fuel rod bundles containing B_4C absorber rods showed strong chemical interactions at temperatures above 1250°C which resulted in fast liquefaction and subsequent relocation of the absorber rod material[2]. The liquid B_4C/stainless steel reaction products then interact with the Zircaloy flow channel box and the adjacent UO_2/Zircaloy fuel rods(Figure 1). For this reason, it has also been of interest to study the chemical interactions between B_4C and Zircaloy; the results are described in [3].

The objective of this paper is to describe quantitatively the chemical interactions between Zircaloy and stainless steel up to complete liquefaction of the reaction specimens: of particular interest is the knowledge of the reaction kinetics and the determination of the critical temperature at which liquid phases form. As a result of the oxidation of the Zircaloy of the fuel rod cladding and flow channel boxes by the H_2O coolant under conditions of normal reactor operation, the influence

of thin ZrO_2 layers on the Zircaloy/stainless steel interactions has been studied in addition. The oxide layers can prevent or delay the chemical interactions. At high temperature thin ZrO_2 layers will disappear if no steam is available and will form oxygen-stabilized α-Zr(O). It was therefore also important to study the reaction behavior between oxygen-containing (dissolved) Zircaloy and stainless steel.

The following reaction couples have been studied at temperatures ≥ 1000°C:

- stainless steel / as-received Zircaloy;
- stainless steel / pre-oxidized Zircaloy with ZrO_2 layers of 10, 20 and 50 µm; and
- stainless steel / oxygen-containing Zircaloy (about 3.5 wt % oxygen)

The maximum temperature at which experiments could be made was limited by complete liquefaction of the specimens already during heatup. The results of these separate-effects tests are important to understand and describe analytically the complex material behavior in integral experiments like the CORA fuel rod bundle meltdown experiments [4].

2. Experimental procedure

The isothermal annealing experiments were performed with Zircaloy-4 (Zry) capsules into which short cylindrical rods of 1.4919 (AISI 316) stainless steel (ss) were pressed and closed gas-tight by a conical Zry plug. Figure 2 shows the components of a compatibility specimen before being loaded.

The annealing experiments were perfomed in a tube furnace under flowing argon. The specimens were heated up to about 900 °C and then placed into the pre-heated furnace which had the desired annealing temperature. The annealing time started when the temperature of the specimen was 20 K below the annealing temperature. The specimens were cooled down outside the furnace at room temperature. The temperatures investigated ranged from 1000 to 1400°C and the maximum annealing time was 900 minutes.

After annealing, the specimens were mechanically cut and then metallographically prepared for examinations of the reaction zones with an optical microscope. A few specimens were etched to recognize better the various phases. The reaction zone thicknesses were measured at four different locations

of the interface. The kinetics data were evaluated on the basis of the maximum thickness of the reaction zones. In addition, some Scanning Electron Microscopy (SEM)/Energy Dispersive X-Ray (EDX) or SEM/Wave Length Dispersive X-ray (WDX) and Auger Electron Spectroscopy (AES) examinations were performed to obtain information on the chemical compositions of the reaction products and diffusion zones.

To pre-oxidize the Zircaloy specimens, the crucibles were exposed to a steam atmosphere in an apparatus made of stainless steel which was connected to a steam generator. The apparatus was introduced into a furnace maintained at the desired temperature. Figure 3 is a schematic of the system used. The temperature and the time selected for the oxidation were taken from a study carried out by R. Pawel et. al [5] in which the following equation is given for the oxide layer growth:

$$\delta^2/2\,(cm^2/s) = 0.01126\exp(-35890/RT)\,, \quad R = 1.987\ \text{cal/mol·K} \tag{1}$$

The temperatures used to obtain an oxide layer of 10, 20 and 50 µm were 870, 900 and 980°C, respectively. The metallographic examinations showed ZrO_2 layer thicknesses between 9 - 12, 19 - 22 and 49 - 53 µm. To study the effect of the oxygen on the interaction between α-Zr(O) and stainless steel, it was necessary, to introduce first oxygen into the Zircaloy and then to homogenize the specimens to obtain a homogeneous distribution of oxygen. The oxygen concentration in the Zircaloy was around 3 weight percent; which had been determined by weight measurements. The oxidation was carried out in a steam atmosphere.

The combinations of temperature and time needed for the oxidation were taken from the study carried out by Ballinger [6] who gives the following equation for the total oxygen absorbed:

$$w\,(mg/cm^2) = 195.3\sqrt{t\,(s)}\exp(-33370/RT) \tag{2}$$

The weight gains in our specimens are in agreement with this equation, the average of 21 crucibles was 3.17 weight percent. After oxidation, the crucibles were annealed for 22 hours at 1200°C in a dynamic vacuum of 9 x 10^{-6} mbar to homogenize the oxygen distribution. The average weight gain after this treatment was about 0.28 weight percent. According to the DISOL code [7] the oxygen concentration difference between the centre of the crucible wall and the outside or inside surface of the wall should be lower than 0.025 mg/mm^3 after 20 hours. To avoid damage to the thin oxide layer on the inner crucible wall, the

stainless steel rods were cooled in liquid nitrogen before being loaded into the pre-oxidized Zircaloy crucibles.

Additional experiments were performed to determine the time of dissolution of the ZrO_2 layer while α-Zr(O) was formed. Eleven specimens of Zircaloy were oxidized in steam to produce an oxide layer thickness of 50 μm (using equation 1). Then the specimens were annealed under dynamic vacuum conditions at 1100, 1200, 1250 and 1300°C for different durations at each temperature. The initial and final oxide thicknesses were measured at three locations. The same heatup and cooldown rates were used for dissolution.

The time of ZrO_2 dissolution was compared with the incubation period determined experimentally in the pre-oxidized Zry/ss reaction couples.

3. Results

3.1 Chemical behavior

The Fe-Zr, Ni-Zr, and Cr-Zr phase diagrams indicate that eutectic interactions occur in each system (Figures 4, 5) [8, 9]. The lowest eutectic temperature occurs in the Fe-Zr system at about 930°C on the Zr-rich side. The diffusion of approximately 5 wt. % Fe into Zr results in the formation of a liquid phase even at this low temperature (Fig. 4). The eutectic temperature on the Fe-rich side is about 1337 °C. The Ni-Zr system has four eutectic temperatures which vary between 960 and 1170 °C, while the eutectic temperatures in the binary Cr-Zr system are 1332 and 1592°C.

The cross-sections of metallographically prepared Zry/ss reaction specimens after annealing at 1000, 1100, 1150 and 1200°C for various duration of reaction times are shown in Figure 6. The cross sections of both pre-oxidized Zry/ss reaction specimens (initial ZrO_2 layer thickness: 10 μm) are presented for comparison. In order to recognize better the metallic reaction zone which forms as a result of the chemical interactions, the specimens were etched which produced a dark looking phase (Fig. 6). The eutectic interactions, which occur between 1000°C and higher, result in the formation of liquid reaction products and voids form as some of the molten material relocates.

Although the specimens were annealed in an upright position, the reaction zones of the as-received Zry are not symmetrical around the circumference. Apparently, very small forces are sufficient to induce asymmetric reaction zones in the Zry wall. First interactions have been noticed at 1000°C after annealing times longer than 5 minutes. At 1200°C, the Zry crucible wall of 2.25 mm thickness was already

completly dissolved after 2 minutes. In all cases, the reaction in the Zry was much stronger than in the stainless steel. This may be explained by phase diagram considerations (Figs. 4, 5). Only small amounts ($\geq$ 5 wt. %) of Fe or Ni are necessary to liquefy large quantities of Zr. Also, since the lowest eutectic temperatures in the Fe-Zr, Cr-Zr, and Ni-Zr systems are on the Zr-rich side, Zr can be liquefied at much lower temperatures than Fe, Cr, or Ni. Liquefaction starts as soon as the solid/liquid two phase field has been reached. The cross sections of Zry/ss specimens and typical microstructures produced by the chemical interactions are shown in Figures 7 through 10.

The reaction zones were examined by SEM/EDX. Besides the determination of the element distribution, quantitative measurements were performed. A typical result of a specimen annealed at 1200°C for 2 min is shown in Figure 11. As can be recognized, the molten reaction zone consists mainly of a (Zr-Fe-Ni) alloy with (Zr-Fe-Cr) precipitations. The metallic (Zr-Fe-Ni-Cr) melts decompose into various phases on cooldown. The integral chemical composition of the solidified melt (about 83 wt. % Zr, 12 % Fe, 3 % Ni, 2 % Cr) is very similar to the chemical composition of the eutectic point on the Zr rich side in the Fe-Zr system (Fig. 4).

From the binary (Fe-Zr) and (Ni-Zr) phase diagrams (Fig. 4, 5) and chemical composition of the reaction zone (Figure 11, 12) it is clear that the diffusion of Fe and Ni into Zr causes liquefaction of Zircaloy. Table 1 indicates the chemical composition of the phases in the reaction zone. The chemical analysis indicates that the composition of the different phases is very similar to $ZrFe_2$, Zr_2Fe and β-Zr in the binary Zr-Fe phase diagram (Fig. 4). Apparently, the expected Zr_3Fe does not form, as a result of rapid cooling.

The ternary (Zr-Fe-Ni) and (Zr-Fe-Cr) phase diagrams at 1000°C [10] are shown in Figure 13. The dashed areas indicate the chemical composition of the various phases formed in the reaction zone for specimens tested at different temperatures and times. For comparison, some phases observed in the chemical analysis of samples selected from the TMI-2 reactor core are also included in the (Zr-Fe-Cr) phase diagram [10].

Figure 13 A shows that the integral composition of the reaction zone (dark area) lies in the liquid zone; during cooldown the composition of the two phases, β-Zr and Zr_2 (Fe, Ni) lie on opposite ends of a straight line passing through the original composition point. The point "X" at the end of the connecting tie line indicates the Fe/Ni ratio in the AISI 316 ss.

Figure 13 B shows that the path of composition change of Zr_2 (Fe, Cr) and Zr $(Fe, Cr)_2$ phases deviates from the direct path between Zr/ 76 at. % Fe- 24 at. % Cr,

represented by the tie line as a first approximation of the Zry/AISI 316 ss interaction. This is as a consequence of the large difference in the diffusion velocities of Fe and Cr in Zry which produces a zone enriched in Cr in the ss matrix adjacent to the molten reaction zone. Therefore, the alloy "Y" on the Zr-Cr edge changes its composition and becomes a Cr enriched and Fe depleted zone in the phase diagram. Point "B" shows the point analysis on the ss a few µm away from the ss/liquid interface.

Although the integral analysis of the reaction zone is close to the eutectic composition in the (Zr-Fe) and (Zr-Ni) systems, i. e. 83 wt. % Zr, local compositions deviate from that of the eutectic one. In the case of the Zr $(Fe, Cr)_2$ phase, which forms as a separate primary precipitation at the ss/liquid interface (Cr enriched zone). The volume of this Zr $(Fe, Cr)_2$ phase (with a shape of idiomorphic particles, Figs. 12, 13) changes with the distance from the ss/liquid interface, it has apparently been reduced by the Zr-rich molten alloy. During cooldown, the liquid alloy starts to solidify into the phases Zr_2 (Fe, Cr) and β-Zr; the remnant liquid solidifies as Zr_2 (Fe, Ni) and β-Zr.

3.2 Reaction kinetics

The maximum reaction zone thicknesses in the as-received Zry crucible and ss rod are listed in Tables 2 and 3. The reaction zones in Zry and ss are plotted versus the square root of time in Figures 14 and 15, respectively. The isothermal growth of the reaction zones (dissolution of Zr and ss) obey parabolic rate laws, indicating a diffusion-controlled process. Fe and/or Ni diffuse into Zry and initiate Zry liquefaction as soon as the solid/liquid phase field has been reached. To show the large differences in the amounts of dissolved Zry and ss, the reaction zone thicknesses in Zry and ss are plotted in Figure 16 as a function of the temperature for an annealing time of 5 minutes. Only small amounts of ss are necessary to dissolve large amounts of Zry. Above about 1250 °C complete liquefaction of the specimens occurs.

The growth rates of the reaction zones for the Zry/ss interactions are listed in Table 4 and plotted as a function of the reciprocal temperature in Figure 17. The growth rate equations determined for the temperature range of 1000 to 1200 °C are:

For Zircaloy-4:

$$x^2/t\ (cm^2/s) = 2.78 \times 10^{19} \cdot \exp(-642864/RT) \quad (3)$$

For stainless steel:

$$x^2/t\ (cm^2/s) = 1.08 \times 10^{19} \cdot \exp(-688790/RT) \quad (4)$$

$$R = 8.314\ J/mol \cdot K$$

These equations can be extrapolated to lower temperatures, but not to higher temperatures since fast and complete liquefaction of the materials takes place at about 1250 °C. One can recognize the difference in growth rates of the reaction zones for Zry and ss.

3.3 Influence of oxide layers on the Zry-4/ss interactions

The ZrO_2 layer on the inner Zry crucible wall delays and reduces the chemical interactions between Zry and ss, but cannot prevent them. Stainless steel does not interact with stoichiometric ZrO_2, but the oxide layer will be dissolved by the Zry during a time-dependent incubation period, t_0. The cross sections of Zry/ss reaction specimens annealed at 1000, 1100, 1150 and 1200°C for various reaction times are shown in Fig. 6. The cross sections of both as-received and pre-oxidized specimens (initial ZrO_2 layer thickness 10 µm) are presented for comparison.

The experimental studies with preoxidized Zry specimens (10, 20 and 50 µm thick ZrO_2 layers) have shown that the liquefaction of the specimens is shifted to higher temperatures. The chemical reaction rate was slower when compared with those of the specimens tested in the as-received condition. In the experiments with the thicker oxide layer, 50 µm ZrO_2, the interaction process can be described in three stages with different reaction rates; the difference was more evident at the lower temperatures due to the slower reaction rate. The first stage, in which the chemical interaction between Zry/ss does not occur, extends till the disappearance of the oxide layer; this stage is called incubation period.

The second stage, in which the eutectic Zr-Fe interaction begins, extends from the end of the incubation period till the moment at which the eutectic liquid reaches

the α-Zr(O)/ β-Zry interface. The reaction rate in this stage is relatively low. The eutectic interaction develops mainly along the grain boundaries.

The third stage begins when the liquid phase comes into contact with the Zircaloy β phase which has a low oxygen content. In this stage, the reaction rate increases and the liquid phase moves forward as a continuous front, as in the as-received condition. The reaction rate in this last stage is higher than in the second, but is lower compared with the reaction rate of the experiments performed with Zircaloy in the as - received condition. The difference could be attributed to the smaller number of Fe atoms available to produce the eutectic reaction with Zr, due to the "filter" effect caused by the α-Zr(O) phase.

These three stages developing in the interaction process can be clearly seen in Figures 18, 19, 20 and 21. The photos show the reaction zone of specimens annealed at 1100°C with an initial oxide layer of 50 μm. According to Figure 18 there is no interaction after 4 hours due to the remaining, but reduced oxide layer. Figures 19 and 20 show the reaction after an annealing time of 10 hours. The oxygen supplied by the ZrO_2 layer diffused into the Zircaloy, stabilizing the α-Zr(O) phase at high temperatures. In this zone the eutectic reaction due to the Zr - Fe interaction develops and moves forward mainly through the grain boundaries, reaching a zone in the vicinity of the α-Zr(O) / β-Zry interface where small regions start to melt. Such small regions, liquid at temperature, form as a result of the lower oxygen content in the α-Zr(O) phase. Figure 20 also shows a mapping of Fe in the eutectic region; Fe was selected because it is the main component of steel which forms a eutectic alloy with Zr at low temperatures. With longer annealing times, the local molten regions become larger and finally approach the β-Zr phase, as can be seen in Figure 21. The α-Zr(O) grains are surrounded and partially dissolved by the liquid of eutectic composition whose front advances as a continuous interface into β - Zry.

The three stages of material-interaction behaviour on the reaction rate could have developed in the whole range of temperatures and oxide layer thicknesses, but it was more clearly seen at the lower temperatures and thicker oxide layers. Due to the low reaction rate in the second stage, the annealing time could be selected in a wide range in order to observe the reaction layer morphology in the narrow α-Zr(O) phase.

The reaction zone thicknesses in Zry and ss measured for the preoxidized Zry/ss reaction specimens are listed in Tables 6 and 7 and plotted versus the square root of time in Figures 22 through 27. The figures show the strong impact of the oxide layers on the chemical interactions between Zry and ss. The reaction zone growth

rates are listed in Tables 8, 9 and 10 and plotted as a function of the reciprocal temperature in Figure 28. The growth rate equation and "t_0" values were determined from x^2 versus t correlations of the experimental data. The values of the reaction zone growth rate of Zry shown in Figure 28 apply to the third stage of reaction kinetics. The difference is only noticeable in the experiments performed at 1100°C with an initial oxide layer of 50 µm, see Figure 26.

3.4 Influence of oxygen dissolved in Zry on the Zry-4/ss interaction

The chemical interaction between α-Zr(O) and stainless steel shows that the reaction rate and morphology of the reaction zone are different from those in the experiments carried out in the as-received condition with an initial oxide layer at the Zry/ss interface. The differences are a consequence of the high oxygen content of Zry of around 3.5 wt. %. Figures 29 and 30 show the reaction zone generated by the chemical interactions of specimens annealed at 1200 and 1300°C for 10 min. The liquid phase (which forms as a result of eutectic interactions between Zr and Fe and/or Ni) does not advance as a continuous interface, but develops along the grain boundaries. Metallic Fe and/or Ni penetrate and/or diffuse into the α-Zry(O), primarily along grain boundaries, to interact chemically with oxygen - poor Zr. The reaction zone also shows many small previously molten regions within the grains with some Fe dissolved in the α-Zry (O) matrix. These regions, liquid at the annealing temperature, are larger and connected to each other in the vicinity of the interface, the number of these liquid regions decreases with the distance from the interface.

The measurement of the lengths of the liquid phase regions, which develop along the grain boundaries, is difficult. The Zry crucibles are very brittle due to the high oxygen content; they show cracks and voids produced mainly by the different thermal expansions between the steel rod and the Zry crucible. These defects act as a liquid short-circuit. Therefore, it was necessary to differentiate between these zones and the liquid regions which formed exclusively along the grain boundaries by a diffusion process. The diffusion rate and morphology of the reaction zone in Zry indicate that Fe diffuses slowly in α-Zry (O); the diffusion rate depends on the oxygen content. The lower the oxygen content in Zry, the faster is the diffusion process.

The reaction morphology on stainless steel was different depending on whether the experiments were carried out at 1300°C and above or at lower temperatures. At 1300°C, the reaction zone shows two different layers, Figure 31; the first nearer to the Zry/ss interface is liquid due to the diffusion of Zr into the ss, the

second consists of stringers, which develop in the radial direction. In the experiments performed at 1350 and 1400°C, the steel rods have liquefied (with the exception of the experiment performed at 1350°C/10 min). The diffusion of Zr into stainless steel attained the eutectic composition between Fe and Zr, which forms at 1337°C with a Zr content of 15 wt. %; Figure 4.

Due to the growth of the liquid phase in Zry, which is mainly intergranular and not a continuous interface, the growth of the reaction zone was calculated from the measurements of the maximum length of the liquid branch at four positions along the circumference, starting from a random point of the specimen. The values are given in Table 11 and plotted vs. the square root of time in Figure 32. Table 11 also shows the reaction thicknesses measured in stainless steel for the two reaction layers. In Figure 33 the values are plotted of the homogeneous liquid zone in ss vs. the square root of time. The reaction zone growth versus the reciprocal temperature plotted in Figure 34 is a comparison with the results in the as-received condition and with an initial oxide layer of ZrO_2 of 10 µm. The growth rate equations determined for the temperature range of 1100 to 1400°C are:

For Zircaloy-4:

$$x^2/t\ (cm^2/s) = 5.04 \times 10^4 \cdot \exp(-281100/RT) \qquad (5)$$

For stainless steel:

$$x^2/t\ (cm^2/s) = 5.98 \times 10^{30} \cdot \exp(-1098800/RT) \qquad (6)$$

$$R = 8.314\ J/mol \cdot K$$

Figure 34 indicates a very strong reduction in the reaction rate compared with the previous experiments; for example, in the as-received condition, a Zry tube of 0.7 mm wall thickness at 1200°C would melt in less than 15 seconds, in the case of specimens with 3.5 weight percent of oxygen, the results indicate that the wall thickness would be crossed by a liquid branch after about 13 minutes. The same occurs with the steel rod, i.e. in the as-received condition, the same wall thickness at 1200°C would melt in 23 minutes, but in contact with α-Zry (O) at 1200°C, the wall would be molten after about 210 hours.

Although liquid phase formation on the Zircaloy does not affect the whole material (but develops mainly along grain boundaries), the reaction rate was calculated considering the maximum length of the intergranular liquid branch.

Figures 35 and 36 show the reaction depth and the reaction zone growth rate as a function of temperature for all experimental conditions.

3.5 Dissolution of the ZrO_2 layer; Experimental determination

Additional experiments were performed to determine the time until disappearance of the ZrO_2 layer on the Zry surface and to correlate this time with the delay in the beginning of Zry/ss interactions; this time is called the incubation time. The measured oxide layer thicknesses remaining after annealing at different temperatures for various times are listed in Table 13 and plotted versus the square root of time in Figure 37. The initial oxide layer thickness was 50 μm. The time for the disappearance of the ZrO_2 layer and the incubation time for the Zr/ss interactions are plotted in Figure 38 versus the reciprocal temperature. The time until disappearance of the ZrO_2 layer calculated with the DISOL code [7] (which describes the dissolution of the oxide layer when the oxygen supply is interrupted) is also included; the agreement in the activation energy between the experimental and calculated results is reasonably good; small differences in the dissolution time can be attributed to experimental procedures. Some differences can be recognized when the experimentally determined dissolution time for the ZrO_2 layer and the incubation time in the Zry/ss interactions are inter-compared. At higher temperatures the incubation time is shorter than the time necessary to dissolve the ZrO_2 layer; this means that the liquid phase due to Zry/ss interactions begins before the oxide layer has completely disappeared. This was proved by metallographic examinations; remnants of oxide layers still exist in the liquid reaction zone, Figure 39.

The chemical behavior can be explained on the basis of the (Zr, Fe, O) ternary phase diagram, Figure 40 [10]. Fe does not interact with ZrO_2, but different phases can form with a sub-stoichiometric ZrO_2 (ZrO_{2-x} can form due to oxygen diffusion into Zry to form oxygen stabilized α-Zr(O)). In this way, Zr from the oxide layer can interact with Fe, producing a liquid phase which penetrates into the cracks of the brittle and porous oxide layer reaching the narrow α-Zry(O) phase. Figure 39 shows the chemical interactions and the liquid phase in the stainless steel when in contact with a Zry specimen with an initial oxide layer thickness of 50 μm annealed at 1300 °C for 10 min.

At lower temperatures ($T < 1150°C$), the incubation time in the Zry/ss interactions seems to be slightly longer than the ZrO_2 dissolution time (Fig. 38), the reason is the effect of the α-Zry(O) layer described as a second stage in Chapter 3.3. This α-Zry(O) phase produce a certain delay in the formation of a

liquid phase in the β-Zry phase, which is more pronounced at lower temperatures and greater initial oxide layer thicknesses.

4. Discussion

In the Zry/ss system, a considerable amount of a Zr-rich liquid phase is formed around 1000°C, and the amount of liquefied material increases with increasing temperature and time.

These results are in agreement with results of integral tests (CORA experiments) in which fuel rod bundles containing absorber rods were heated to temperatures of about 2000°C [2, 11, 12]. The onset of liquid-phase formation and the complete liquefaction of the absorber rod components at temperatures above 1200°C were detected by video systems. The low-temperature failure of the absorber rods initiated core melt progression. The resulting melt attacked the fuel rods chemically dissolving the Zry cladding and some of the UO_2 fuel. By this process, "molten" fuel relocation and early fission product release can take place even well below the melting point of the Zry cladding ($\approx$ 1760°C). The melts relocate towards cooler regions of the core where they may produce coolant channel blockages on solidification.

The main purpose of this work has been to determine the kinetics of reactions between Zry and stainless steel absorber rod components. Although some interaction experiments have been described in the literature, no Arrhenius equation had previously been developed from the data. In all cases, the maximum reaction zone thickness was used in the evaluation of the kinetics data to obtain conservative results.

Thin oxide layers on the Zry surface can delay the chemical interactions with the ss, but cannot prevent them. ZrO_2 interacts with metallic Zr while forming oxygen-stabilized α-Zr(O) and sub-stoichiometric ZrO_{2-x} which is then able to interact with the ss components.

The reaction zone growth rates of pre-oxidized Zry are slower than those of as-received Zry (Fig. 36). The oxygen dissolved in the Zr lattice exerts an influence on the diffusion and/or dissolution processes; the reaction rates are slower. The delay in the interaction of Zry with ss, called the incubation time, t_0, increases with increasing ZrO_2 thickness, and complete meltdown of the components is shifted to higher temperatures. The ZrO_2 layers on metallic Zry disappear only if no further oxygen is available in the environment or has no access to Zry to continue the oxidation. In all other cases, the reaction of Zry with oxygen or

steam is more favorable thermodynamically than the reactions with stainless steel. But, as the integral LWR bundle meltdown experiments [2, 12, 13] show, a steam environment cannot prevent the chemical interactions between Zry and ss since steam starvation conditions may exist locally. In these experiments, the bundle components were used in the as-received condition. The chemical/physical behavior of heavily preoxidized bundle components has produced similar results [4].

During a severe reactor accident not only Zry but also ss will be oxidized by steam at comparable rates [13]. If the resulting oxide layers are in solid contact with each other, eutectic interactions will take place with liquid phase formation between 1200 and 1400 °C [14]. Therefore, the oxide layers offer only limited protection from the chemical interactions. In all cases, liquefaction of the non-oxidized and oxidized components will occur below their melting points.

The metallographic and chemical/analytical examinations of the specimens revealed a large number of various phases at room temperature. Since only a limited number of mainly binary phase diagrams are available, the observed phases cannot all be described by phase diagram considerations. In addition, some of the phases will not be in equilibrium since cooldown of the specimens occurred rather fast. The integral chemical compositions of the solidified melts indicate for the Zry/ss system that only small amounts of ss are needed to dissolve large quantities of Zry (Fig. 4, 5). The integral compositions are nearly identical for all interaction temperatures examined.

The kinetic evaluation of these interaction experiments is problematic since a liquid phase forms as a reaction product. The liquid causes relative movements between the Zry crucible and the ss rod during annealing of the diffusion couple. Depending on the annealing conditions of the specimens (upright, horizontal), the ss rod can penetrate into the Zry crucible wall by liquefying it at different velocities. As a result, the interaction zones in the Zry crucible or the amount of Zry dissolved are not uniform along their axes and circumference. This can be clearly recognized in Figure 41. It shows specimens which were annealed at 1100 °C for 15 minutes in upright and horizontal positions. In a few cases the inserted ss rod turned even by about 90° at higher temperatures (Figure 42). The penetration of the ss rod into Zry is deepest at locations where the liquid film is thinnest. Thus, for the kinetic evaluation of the Zry/ss reaction experiments the maximum attack of Zry was considered. The different extents of Zry liquefaction by ss are shown in Figure 43 as a function of the annealing conditions. The ss rod behaves the same as Zry, but, at lower temperatures the differences with respect

to the reaction zone growth rates between the two annealing conditions examined become larger.

5. Summary and Conclusions

- Failure of the stainless steel cladding of the absorber rod takes place as a result of either internal pressurization (high Cd vapor pressure) or chemical interactions with the Zircaloy guide tube (bowing of the rods at high temperatures).
- As soon as solid state contact is established between stainless steel and Zircaloy, eutectic interactions take place which can be described by parabolic rate laws. Liquid phases form at around 1000°C, and a fast and complete liquefaction of both components takes place above 1250°C.
- Only small amounts of stainless steel are necessary to dissolve great amounts of Zircaloy, and it takes only a little more than 2 minutes to destroy the 2.25 mm thick Zircaloy crucible wall at 1200°C.
- Thin ZrO_2 layers on the Zircaloy surface delay the eutectic interactions of Zircaloy with stainess steel, but cannot prevent them; the interaction processes can be described in three different stages with different reaction rates. The incubation period depends on the initial ZrO_2 thickness and temperature.
- Oxygen dissolved in the Zircaloy, forming oxygen-stabilized α-Zr(O), reduces the reaction rates and shifts the liquefaction temperature to slightly higher levels.
- The liquid phase could have a substantial influence on further damage progression of the fuel bundle components; the liquefaction of components provides a mechanism for low-temperature material relocation and blockage formation.

6. Acknowledgement

The authors wish to thank Dr. T. Haste (AEA Technology, Winfrith) for his thorough and critical review of this paper.

This work was partially funded by the Commission of the European Communities under the Reinforced Concerted Action Project "Core Degradation", Contract Number FI3S-CT-0001.

7. References

[1] P. Hofmann, M. Markiewicz; Chemical behavior of (Ag, In, Cd) absorber rods in severe LWR accidents, KfK 4670 (1990).

[2] S. Hagen, P. Hofmann; Physical and chemical behavior of LWR fuel element up to very high temperatures, KfK 4104 (1987).

[3] P. Hofmann, M. Markiewicz, J. Spino; Reaction behavior of B_4C absorber material with stainless steel and Zircaloy in severe LWR accidents, Nuclear Technology 90 (1990) 226 - 244.

[4] P. Hofmann, S. Hagen, G. Schanz, L. Sepold; Chemical-physical behavior of LWR core components at high temperatures, IAEA Meeting on "Behavior of Core Materials and Fission Product Release in Accident Conditions in LWRs", Aix-en-Provence, France, March 16 - 20, 1992.

[5] R. Pawel, J. Cathcart; The kinetics of oxidation of Zircaloy-4 in steam at high temperatures, J. Elect. Soc. Vol 126, (1979) 7.

[6] R. Ballinger, W. Dobson, R. Biederman, Oxidation reaction kinetics of Zry-4 in an unlimited steam environment, Journal of Nuclear Materials 62 (1976) 213 - 220.

[7] E. Garcia, P. Hofmann, A. Denis; Analysis and Modelling of the Chemical Interactions between Inconel Grid Spacers and Zircaloy Cladding of LWR Fuel Rods; Formation of Liquid Phases due to Chemical Interactions, KfK 4921, CNEA NT-1/91, July 1992.

[8] T.B. Massalski; Binary alloy phase diagrams, Vol. 1,2, American Society for Metals, Ohio (1986).

[9] D. Arias, J.P. Abriata; The Fe-Zr system, Bulletin of Alloy Phase Diagrams, Vol. 9 No. 5 (1988) 597-604.

[10] H. Kleykamp, R. Pejsa; Chemical and X-Ray Diffraction Analysis on Selected Samples form the TMI-2 Reactor Core. KfK 4872; May 1991.

[11] S. Hagen, P. Hofmann, G. Schanz, L. Sepold; CORA Experiments on the behavior of LWR fuel rod bundles under SFD conditions, Kerntechnik 53, No. 1 (1988) 15.

[12] S. Hagen, P. Hofmann, G. Schanz, L. Sepold; Out-of-pile-experiments on LWR severe fuel damage behavior (Tests CORA-5 and CORA-12), KfK 4419 (1990).

[13] P. Hofmann, S. Hagen, G. Schanz, A. Skokan; Reactor core materials interactions at very high temperatures, Nuclear Technology 87 (1989) 147-182.

[14] M.E. Reser (Editor), Phase Diagrams for Ceramists, The American Ceramic Society (1975).

List of Tables

List of Figures

Fig. 19: Chemical interaction between Zry-4 and ss 1.4919 (AISI 316); 1100°C/600 min.

Fig. 20: Chemical interaction between Zry-4 and ss 1.4919 (AISI 316); 1100°C/600 min. Fe distribution within the previously liquid reaction products.

Fig. 21: Chemical interaction between Zry-4 and ss 1.4919 (AISI 316); 1100°C/900 min.

Fig. 22: Maximum reaction zone thicknesses in Zircaloy for the pre-oxidized Zircaloy-4/stainless steel 1.4919 (AISI 316) system versus the square root of time; initial ZrO_2 layer thickness: 10 µm. The interactions start after the incubation time t_0 has passed (Table 5).

Fig. 23: Maximum reaction zone thicknesses in stainless steel for the pre-oxidized Zircaloy-4/stainless steel 1.4919 (AISI 316) system versus the square root of time; initial ZrO_2 layer thickness: 10 µm. The interactions start after the incubation time t_0 has passed (Table 5).

Fig. 24: Maximum reaction zone thicknesses in Zircaloy for the pre-oxidized Zircaloy-4/stainless steel 1.4919 (AISI 316) system versus the square root on time; initial ZrO_2 layer thickness: 20 µm. The interactions start after the incubation time t_0 has passed (Table 6).

Fig. 25: Maximum reaction zone thicknesses in Zircaloy for the pre-oxidized Zircaloy-4/stainless steel 1.4919 (AISI 316) system versus the square root of time; initial ZrO_2 layer thickness: 20 µm. The interactions start after the incubation time t_0 has passed (Table 6).

Fig. 26: Maximum reaction zone thicknesses in Zircaloy for the pre-oxidized Zircaloy-4/stainless steel 1.4919 (AISI 316) system versus the square root of time; initial ZrO_2 layer thickness: 50 µm. The interactions start after the incubation time t_0 has passed (table 7).

Fig. 27: Maximum reaction zone thicknesses in Zircaloy for the pre-oxidized Zircaloy-4/stainless steel 1.4919 (AISI 316) system versus the square root of time; initial ZrO_2 layer thickness: 50 µm. The interactions start after the incubation time t_0 has passed (Table 7).

Fig. 28: Reaction zone growth rates for the pre-oxidized Zry-4/ss 1.4919(AISI 316) system; initial ZrO_2 layer thicknesses: 10, 20 and 50 µm.

Fig. 29: Chemical interaction between oxygen-stabilized α-Zry (O) and ss 1.4919 (AISI 316); 1200°C/10 min.

Fig. 30: Chemical interaction between oxygen-stabilized α-Zry (O) and ss 1.4919 (AISI 316); 1300°C/10 min.

Fig. 31: Chemical interaction between oxygen-stabilized α-Zry (O) and ss 1.4919 (AISI 316); 1350°C/10 min.

Fig. 32: Maximum reaction zone thicknesses in Zry for the oxygen-stabilized α-Zry (O) / ss 1.4919 (AISI 316) system versus the square root of time between 1100 und 1400°C.

Fig. 33: Maximum reaction zone thicknesses in stainless steel for the oxygen-stabilized α-Zry (O)/ss 1,4919 (AISI 316) system versus the square root of time for 1200 and 1300°C.

Fig. 34: Reaction zone growth rates for the oxygen-stabilized α-Zry(O)/ss 1.4919 (AISI 316) reaction system. Comparison with as-received and pre-oxidized Zry (ZrO_2 layer 10 μm).

Fig. 35: Comparison of the reaction zone thicknesses in Zry versus annealing temperature for all conditions tested.

Fig. 36: Reaction zone growth rates for the Zry-4/ss 1.4919 (AISI 316) system for all conditions tested.

Fig. 37: Dissolution of the oxide layer with the formation of α-Zry(O); initial ZrO_2 layer thickness: 50 μm.

Fig. 38: Time of dissolution of the ZrO_2 layer versus reciprocal temperature. Comparison with the incubation time and calculation by the DISOL code [7].

Fig. 39: Chemical interaction between Zry-4 and ss 1.4919 (AISI 316); 1300°C/10 min; initial ZrO_2 layer thickness: 50 μm.

Fig. 40: Ternary phase diagram of the Fe-Zr-O system [10].

Fig. 41: Extent of chemical interactions between Zircaloy and stainless steel as a function of annealing conditions (upright or horizontal arrangement of the specimens).

Fig. 42: Turning of the stainless steel rod within the Zircaloy crucible as a result of liquid phase formation. The relocated melt forms a large void.

Fig. 43: Reaction zone growth rates for the Zircaloy/stainless steel 1.4919 (AISI 316) reaction system for two modes of annealing conditions (upright or horizontal arrangement of the specimens).

Table 1: Quantitative analysis of phases in the Zircaloy-4/stainless steel 1.4919 (AISI 316) reaction zone.

Position (see Fig. 11, 12)	Element	Conc. in at. %	Phase
1	Zr Fe Cr	36 34 30	$Zr(Cr, Fe)_2$
2	Zr Fe Cr	67 20 13	Zr_2 (Fe, Cr)
3	Zr Fe Ni Cr, Sn Mn	68 23 7 2	Zr_2 (Fe, Ni)
4	Zr Fe Sn, Cr, Ni	94 4 2	α-Zr

Table 2: Measured maximum reaction zone thickness in Zircaloy for the diffusion couple Zircaloy-4/stainless steel 1.4919 (AISI 316) as a function of temperature and time (Fig. 14).

Specimen	Temperature °C	Time min	Reaction zone thickness µm
177	1000	5	0
178	"	15	80
179	"	15	80
198	"	30	150
197	"	30	120
192	1100	2	370
189	"	5	670
196	"	10	840
180	"	15	1200
182	"	30	1610
193	1150	1	550
184	"	2	960
183	"	5	1530
194	1200	1	1390
187	"	1	1150
188	"	2	1740
185	"	3	2250

Table 3: Measured maximum reaction zone thickness in stainless steel for the diffusion couple Zircaloy-4/stainless steel 1.4919 (AISI 316) as a function of temperature and time (Fig. 15).

Specimen	Temperature °C	Time min	Reaction zone thickness µm
177	1000	5	0
178	"	15	0
179	"	15	0
198	"	30	15
197	"	30	6
192	1100	2	35
181	"	5	15
189	"	5	65
196	"	10	105
180	"	15	65
193	1150	1	30
184	"	2	60
183	"	5	110
194	1200	1	145
188	"	2	190
199	"	4.5	375

Table 4: Reaction zone growth rates in Zircaloy and stainless steel for the diffusion couple Zircaloy-4/stainless steel 1.4919 (AISI 316) (Fig. 17).

Temperature		Reaction zone growth rate, x^2/t cm^2/s	
°C	1/K	Zircaloy-4	stainless steel
1000	$7.855 \cdot 10^{-4}$	$9.48 \cdot 10^{-8}$	$5.74 \cdot 10^{-10}$
1100	$7.283 \cdot 10^{-4}$	$1.44 \cdot 10^{-5}$	$8.72 \cdot 10^{-8}$
1150	$7.027 \cdot 10^{-4}$	$7.69 \cdot 10^{-5}$	$3.81 \cdot 10^{-7}$
1200	$6.789 \cdot 10^{-4}$	$3.33 \cdot 10^{-4}$	$4.79 \cdot 10^{-6}$

Growth rate equation:

For Zircaloy-4:

$$x^2/t\ (cm^2/s) = 2.78 \cdot 10^{19} \cdot \exp(-642864/RT)$$

For stainless steel:

$$x^2/t\ (cm^2/s) = 1.08 \cdot 10^{19} \cdot \exp(-688790/RT)$$

$$R = 8.314\ J/mol \cdot K$$

Table 5: Measured maximum reaction zone thickness in Zircaloy and stainless steel for the diffusion couple pre-oxidized Zircaloy-4/stainless steel 1.4919 (AISI 316); initial ZrO_2 oxide layer thickness: 10 µm (Figs. 22 and 23).

Specimen	Temperature °C	Time min	Reaction zone thickness µm	
			Zircaloy-4	1.4919 ss
29	1000	15	0	0
22	"	30	0	0
37	"	30	0	0
38	"	60	0	0
25	1100	3	0	0
33	"	10	198	54
21	"	15	287	66
27	"	30	513	119
34	1150	2	0	0
26	"	5	263	57
30	"	5	192	45
35	"	10	440	95
23	"	15	683	124
36	1200	1	0	0
32	"	2	160	40
31	"	3	393	73
24	"	5	490	112
28	"	10	793	151

Table 6: Measured maximum reaction zone thickness in Zircaloy and stainless steel for the diffusion couple pre-oxidized Zircaloy-4/stainless steel 1.4919 (AISI 316); initial ZrO_2 oxide layer thickness: 20 µm (Figs. 24 and 25).

Specimen	Temperature °C	Time min.	Reaction zone thickness µm	
			Zircaloy-4	1.4919 ss
201 B	1050	90	0	0
202 B	"	120	0	0
212	"	180	463	100
212 B	"	240	872	175
213	"	300	1195	255
205	1100	30	0	0
204	"	45	123	24
204 B	"	60	425	115
206	"	90	755	170
210	"	120	1207	275
203	1200	10	127	38
201	"	20	827	158
202	"	30	1240	290
208	"	30	1115	258
214	"	45	1630	385
218	1250	5	155	197
216	"	10	977	395
215	"	15	1473	635
217	"	20	1890	837
209	1300	3	430	160
220	"	5	850	407
207	"	7	1930	627

Table 7: Measured maximum reaction zone thickness in Zircaloy and stainless steel for the diffusion couple pre-oxidized Zircaloy-4/stainless steel 1.4919 (AISI 316); initial ZrO_2 oxide layer thickness: 50 µm (Figs. 26 and 27)

Specimen	Temperature °C	Time min.	Reaction zone thickness µm	
			Zircaloy-4	1.4919 ss
233	1100	180	0	0
234	"	240	0	0
235	"	300	37	0
239	"	420	175	0
236	"	600	340	20
237	"	900	1493	381
222	1200	60	0	0
221	"	90	687	38
240	"	90	810	120
223	"	120	1237	202
224	"	180	2500	485
241	" "	180	melted	-
231	1250	30	190	313
232	"	30	305	-
230	"	40	802	-
229	"	60	1787	1175
243	"	60	1815	850
228	1300	5	0	0
227	"	10	0	253
246	"	10	195	315
225	"	15	836	670
226	"	20	1180	1477
245	"	20	1185	-
244	"	25	2190	-

Table 8: Reaction zone growth rates in Zircaloy and stainless steel for the diffusion couple pre-oxidized Zircaloy-4/stainless steel 1.4919 (AISI 316); initial ZrO_2 oxide layer thickness: 10 µm (Fig. 34).

Temperature		Reaction zone growth rate, x^2/t cm^2/s	
°C	1/K	Zircaloy-4	stainless steel
1000	$7.855 \cdot 10^{-4}$	–	–
1100	$7.283 \cdot 10^{-4}$	$1.9 \cdot 10^{-6}$	$9.7 \cdot 10^{-8}$
1150	$7.027 \cdot 10^{-4}$	$6.7 \cdot 10^{-6}$	$2.1 \cdot 10^{-7}$
1200	$6.789 \cdot 10^{-4}$	$1.2 \cdot 10^{-5}$	$4.3 \cdot 10^{-7}$

Growth rate equation:

For Zircaloy-4:

$$x^2/(t - t_0)\ (cm^2/s) = 1.43 \cdot 10^6 \cdot \exp(-311100/RT)$$

For stainless steel:

$$x^2/(t - t_0)\ (cm^2/s) = 3.4 \cdot 10^2 \cdot \exp(-250817/RT)$$

$$R = 8.314\ J/mol \cdot K$$

t_0 values (10 µm ZrO_2 layer), s

Temperature	Zry	ss
1000 °C	–	–
1100 °C	426	371
1150 °C	239	176
1200 °C	83	56

Table 9: Reaction zone growth rates in Zircaloy and stainless steel for the diffusion couple pre-oxidized Zircaloy-4/stainless steel 1.4919 (AISI 316); initial ZrO_2 layer thickness: 20 µm (Fig. 36).

Temperature		Reaction zone growth rate, x^2/t cm^2/s	
°C	1/K	Zircaloy-4	stainless steel
1050	$7.558 \cdot 10^{-4}$	$1.666 \cdot 10^{-6}$	$7.639 \cdot 10^{-8}$
1100	$7.283 \cdot 10^{-4}$	$2.502 \cdot 10^{-6}$	$1.662 \cdot 10^{-7}$
1200	$6.789 \cdot 10^{-4}$	$1.249 \cdot 10^{-5}$	$7.158 \cdot 10^{-7}$
1250	$6.566 \cdot 10^{-4}$	$3.95 \cdot 10^{-5}$	$7.428 \cdot 10^{-6}$
1300	$6.357 \cdot 10^{-4}$	$1.54 \cdot 10^{-4}$	$1.531 \cdot 10^{-5}$

Growth rate equation:

For Zircaloy-4:

1050 °C ≤ T ≤ 1200° C

$$x^2 / (t-t_0)\ (cm^2/s) = 1030 \cdot \exp(-224062 / RT)$$

1200 °C ≤ T ≤ 1300° C

$$x^2 / (t-t_0)\ (cm^2/s) = 1.582 \cdot 10^{12} \cdot \exp.(-482794 / RT)$$

For stainless steel:

1050 °C ≤ T ≤ 1200° C

$$x^2 / (t-t_0)\ (cm^2/s) = 282 \cdot \exp(-242428 / RT)$$

1200 °C ≤ T ≤ 1300° C

$$x^2 / (t-t_0)\ (cm^2/s) = 9.36 \cdot 10^{14} \cdot \exp(-592439 / RT)$$

$R = 8.314\ J/mol \cdot K$

t_0 values (20 µm ZrO_2 layer), s

Temperature	Zry	ss
1050	7450	9770
1100	3170	2870
1200	800	710
1250	250	310
1300	205	170

Table 10: Reaction zone growth rates in Zircaloy and stainless steel for the diffusion couple pre-oxidized Zircaloy-4/stainless steel 1.4919 (AISI 316); initial ZrO_2 layer thickness: 50 µm (Fig. 36).

Temperature		Reaction zone growth rate, x^2/t cm^2	
°C	1/K	Zircaloy-4	stainless steel
1100	$7.855 \cdot 10^{-4}$	$1.174 \cdot 10^{-6}$	$8.033 \cdot 10^{-8}$
1200	$6.789 \cdot 10^{-4}$	$9.473 \cdot 10^{-6}$	$4.482 \cdot 10^{-7}$
1250	$6.566 \cdot 10^{-4}$	$1.78 \cdot 10^{-5}$	$5.294 \cdot 10^{-6}$
1300	$6.357 \cdot 10^{-4}$	$4.67 \cdot 10^{-5}$	$3.29 \cdot 10^{-5}$

Growth rate equation:

For Zircaloy-4:

$$x^2 / (t-t_0)\ (cm^2/s) = 8.925 \cdot 10^7 \cdot \exp(-368975 / RT)$$

For stainless steel:

1100 °C ≤ T ≤ 1200° C

$$x^2 / (t-t_0)\ (cm^2/s) = 8152 \cdot \exp(-289244 / RT)$$

1200 °C ≤ T ≤ 1300° C

$$x^2 / (t-t_0)\ (cm^2/s) = 1.107 \cdot 10^{23} \cdot \exp(-827825 / RT)$$

R: 8.314 J/mol·K

t_0 values (50 µm ZrO_2 layer), s

Temperature	Zry	ss
1100	34060	35950
1200	4750	5470
1250	1660	1890
1300	640	610

Table 11: Measured reaction zone thickness in the oxygen stabilized α-Zry(O)/ stainless steel 1.4919 (AISI 316) system (Figs. 32 and 33). Initial oxygen content about 3.5 wt. %.

			Reaction zone thickness, µm		
Specimen	Temperature °C	Time min	Zircaloy-4	1.4919 ss	
				Zone 1 [A]	Zone 2 [B]
42	1100	60	650	-	-
58	"	90	740	-	-
43	"	120	804	-	-
52	"	120	866	-	-
53	1200	10	475	18	-
41	"	15	675	25	-
45	"	25	960	28	-
44	"	40	1270	42	-
48	"	60	1510	48	-
54	1300	5	525	182	420
47	"	10	995	155	-
55	"	15	1150	467	935
46	"	25	1637	868	1378
49	"	40	1730	-	470
57	1350	40	2330	457	1210
50	"	5	1348	molten	-
51	"	10	1625	978	1267
56	"	15	1910	molten	-
59	1400	5	1743	molten	-
60	"	15	3000	molten	-

[A]: Length of the eutectic liquid zone, Figure 31
[B]: Length of the total reaction zone (eutectic plus radial stringers), Figure 31

Table 12: Reaction zone growth rates in Zircaloy and stainless steel for the diffusion couple α-Zry(O)/stainless steel 1.4919 (AISI 316), (Fig. 34).

Temperature		Reaction zone growth rate, x^2/t cm^2/s	
°C	1/K	Zircaloy-4	stainless steel
1100	$7.283 \cdot 10^{-4}$	$9.97 \cdot 10^{-7}$	-
1200	$6.789 \cdot 10^{-4}$	$6.31 \cdot 10^{-6}$	$6.51 \cdot 10^{-9}$
1300	$6.357 \cdot 10^{-4}$	$1.73 \cdot 10^{-5}$	$1.99 \cdot 10^{-6}$
1350	$6.161 \cdot 10^{-4}$	$4.29 \cdot 10^{-5}$	-
1400	$5.977 \cdot 10^{-4}$	$1.00 \cdot 10^{-4}$	-

Growth rate equation:

For Zircaloy-4:

$$x^2/(t - t_0)\ (cm^2/s) = 54078 \cdot \exp(-282106/RT)$$

For stainless steel:

$$x^2/(t - t_0)\ (cm^2/s) = 7.588 \cdot 10^{30} \cdot \exp(-1101622/RT)$$

$$R = 8.314\ J/mol \cdot K$$

Table 13: Dissolution of the oxide layer; initial oxide layer thickness: 50 µm (Fig. 37).

Specimen	Temperature °C	Time min	Oxide thickness µm
11	1100	60	25
12	"	90	20
13	1200	10	34
15	"	20	28
14	"	30	21
16	1250	5	35
18	"	10	29
17	"	15	23
19	1300	3	36
21	"	7	27
20	"	10	20

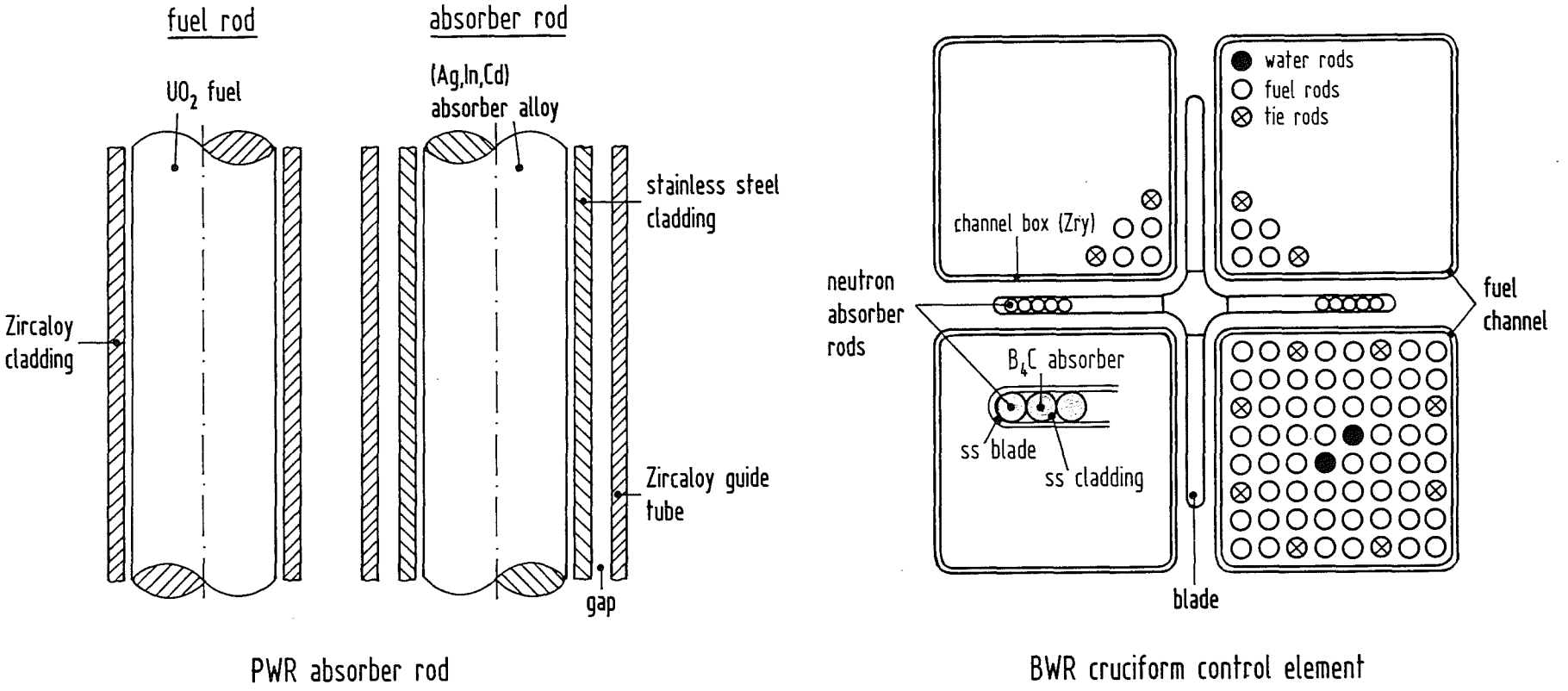

Fig. 1: Schematic of PWR and BWR absorber assembly arrangements.

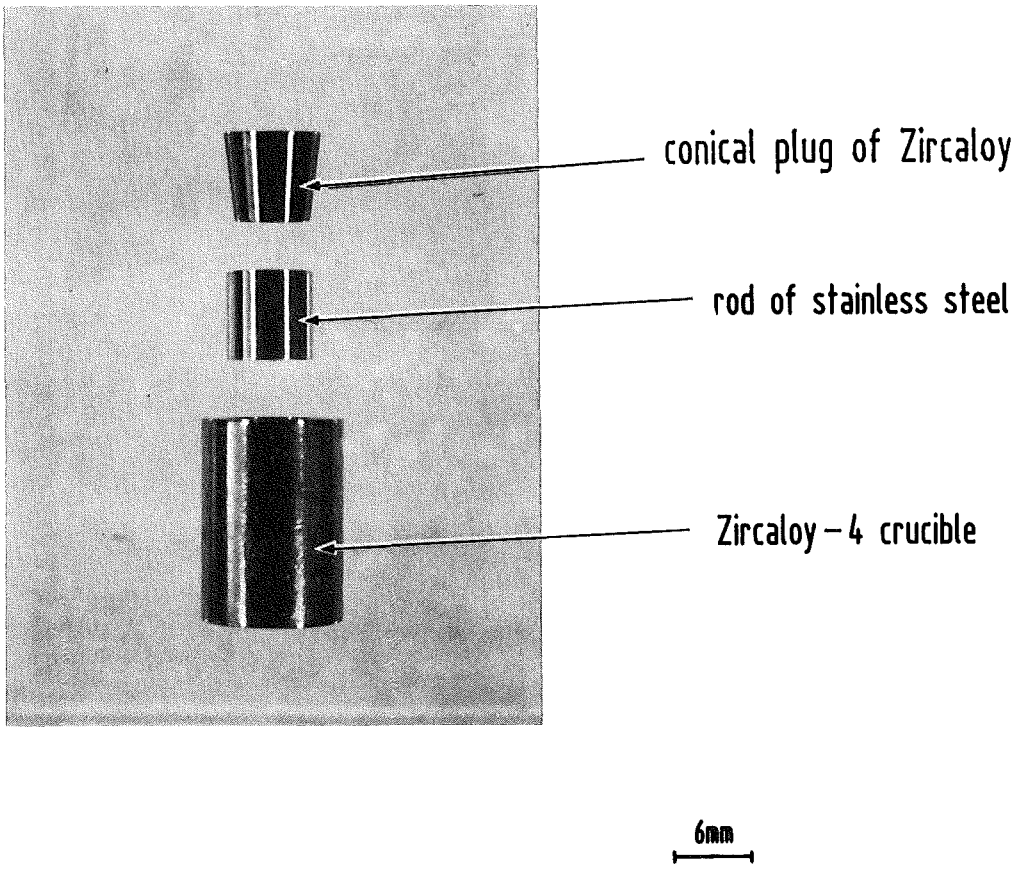

Fig. 2: Setup of the reaction couples.

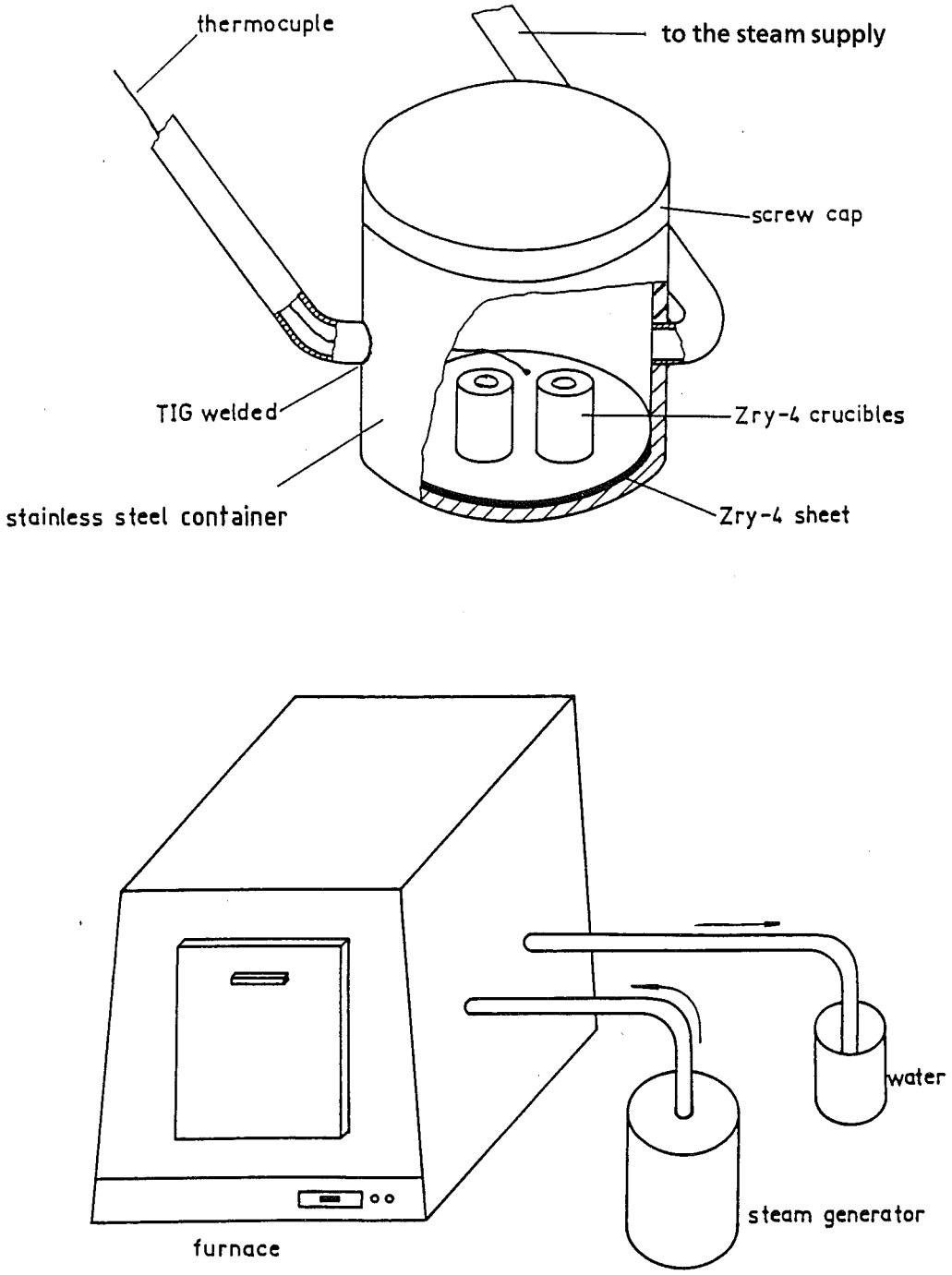

Fig. 3: Schematic of the apparatus used for the oxidation of the Zry-4 capsules.

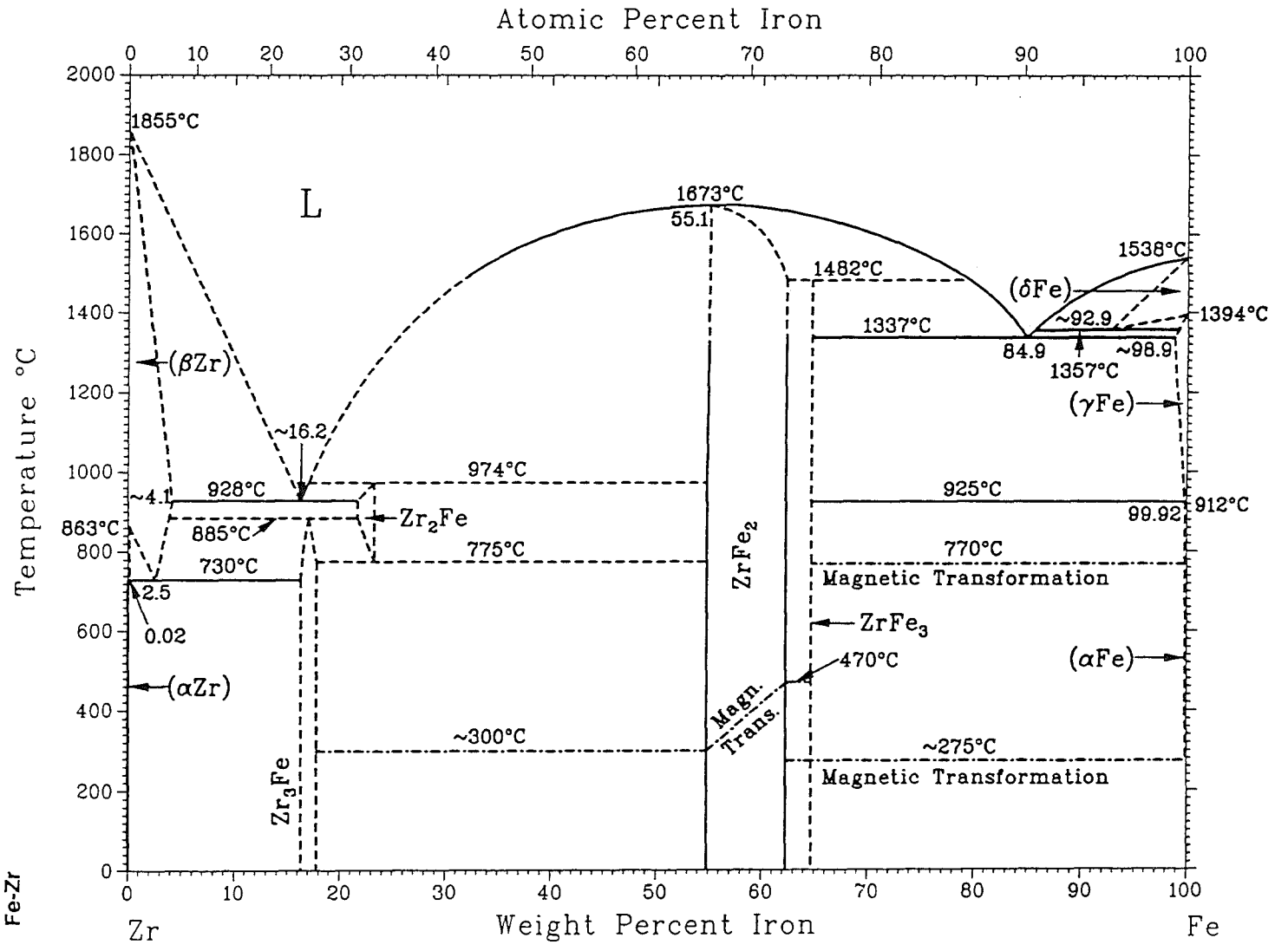

Fig. 4: Binary alloy phase diagrams of the Fe-Zr system [8, 9].

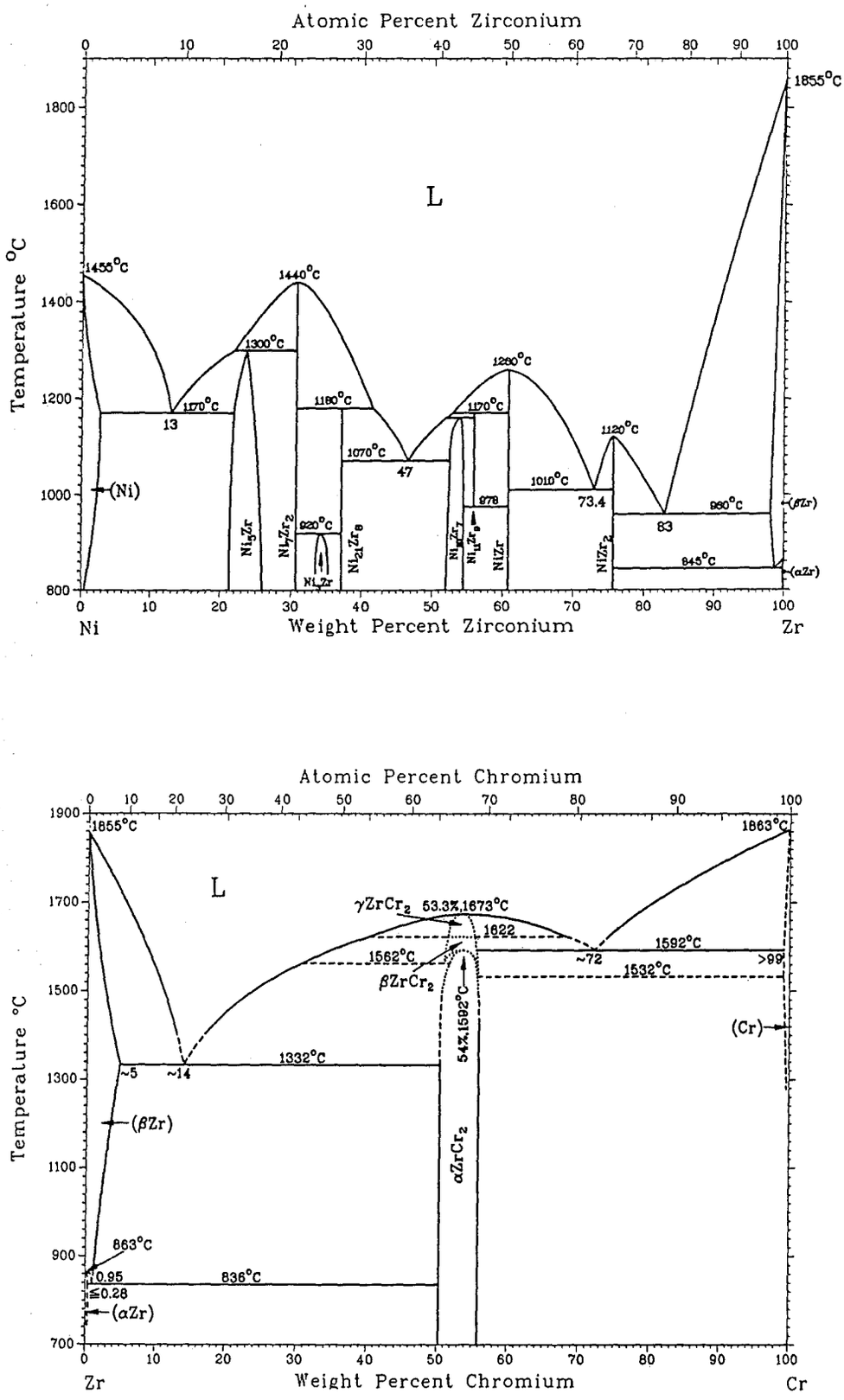

Fig. 5: Binary alloy phase diagrams of the Ni-Zr and Cr-Zr systems [8].

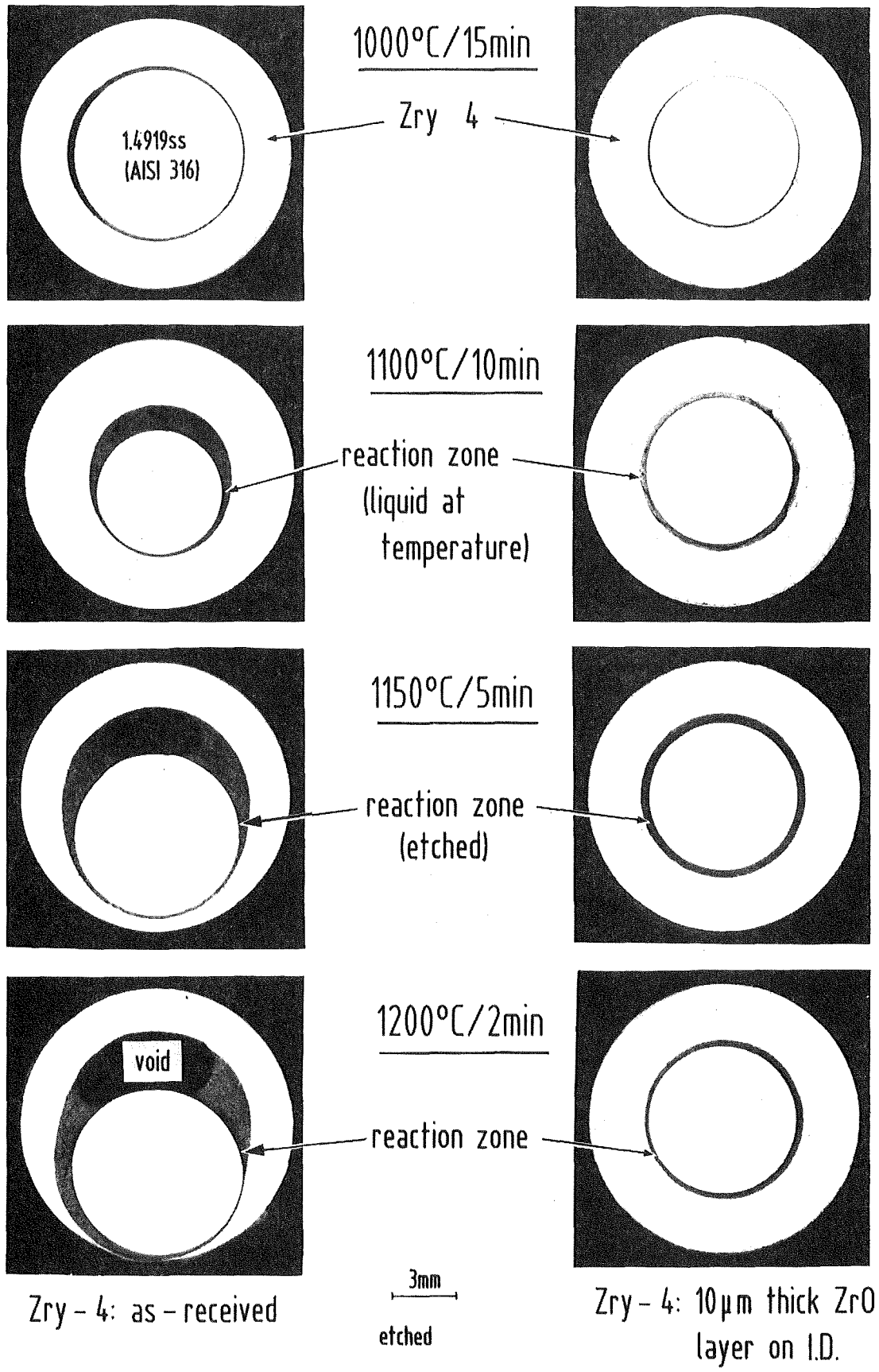

Fig. 6: Chemical interactions between Zircaloy-4 and stainless steel 1.4919 (AISI 316) at different temperatures; influence of a thin ZrO_2 layer on the reaction behavior (right row of pictures).

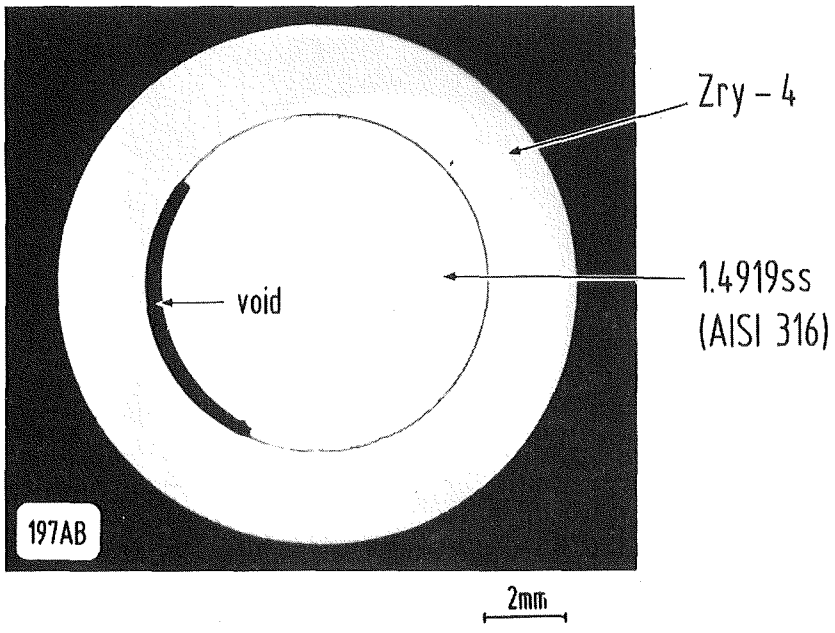

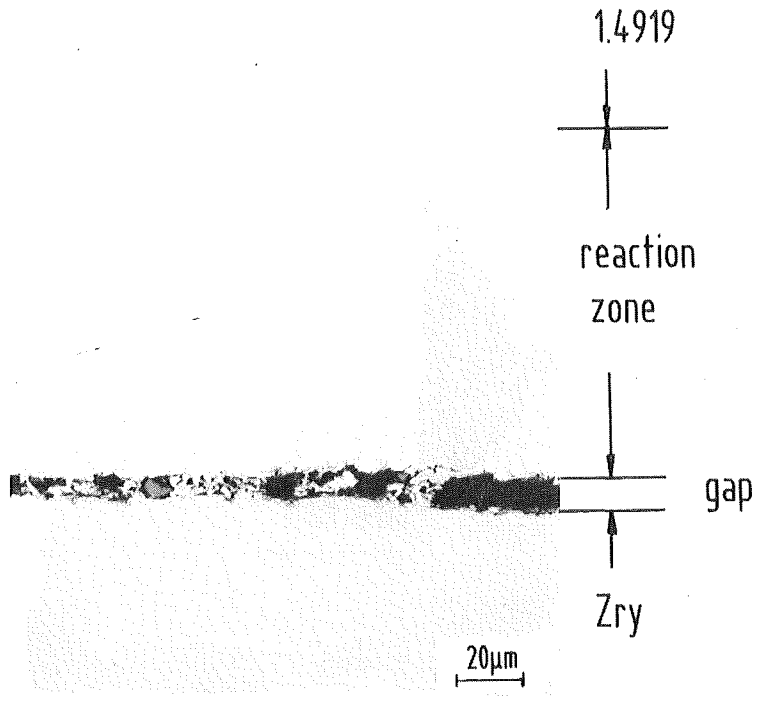

Fig. 7: Chemical interactions between Zircaloy-4 and stainless steel 1.4919 (AISI 316); 1000°C/15 min.

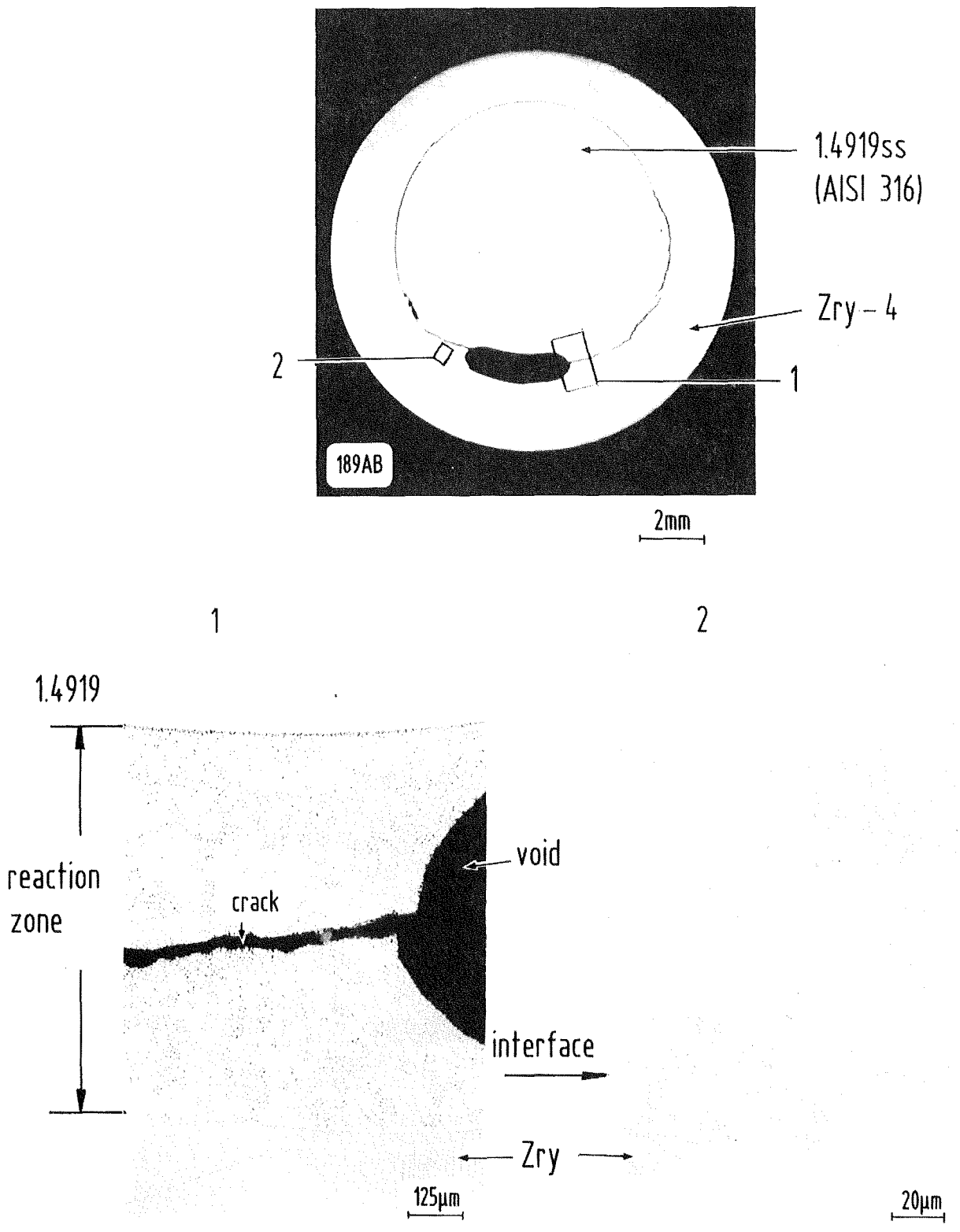

Fig. 8: Chemical interactions between Zircaloy-4 and stainless steel 1.4919 (AISI 316); 1100°C/5 min.

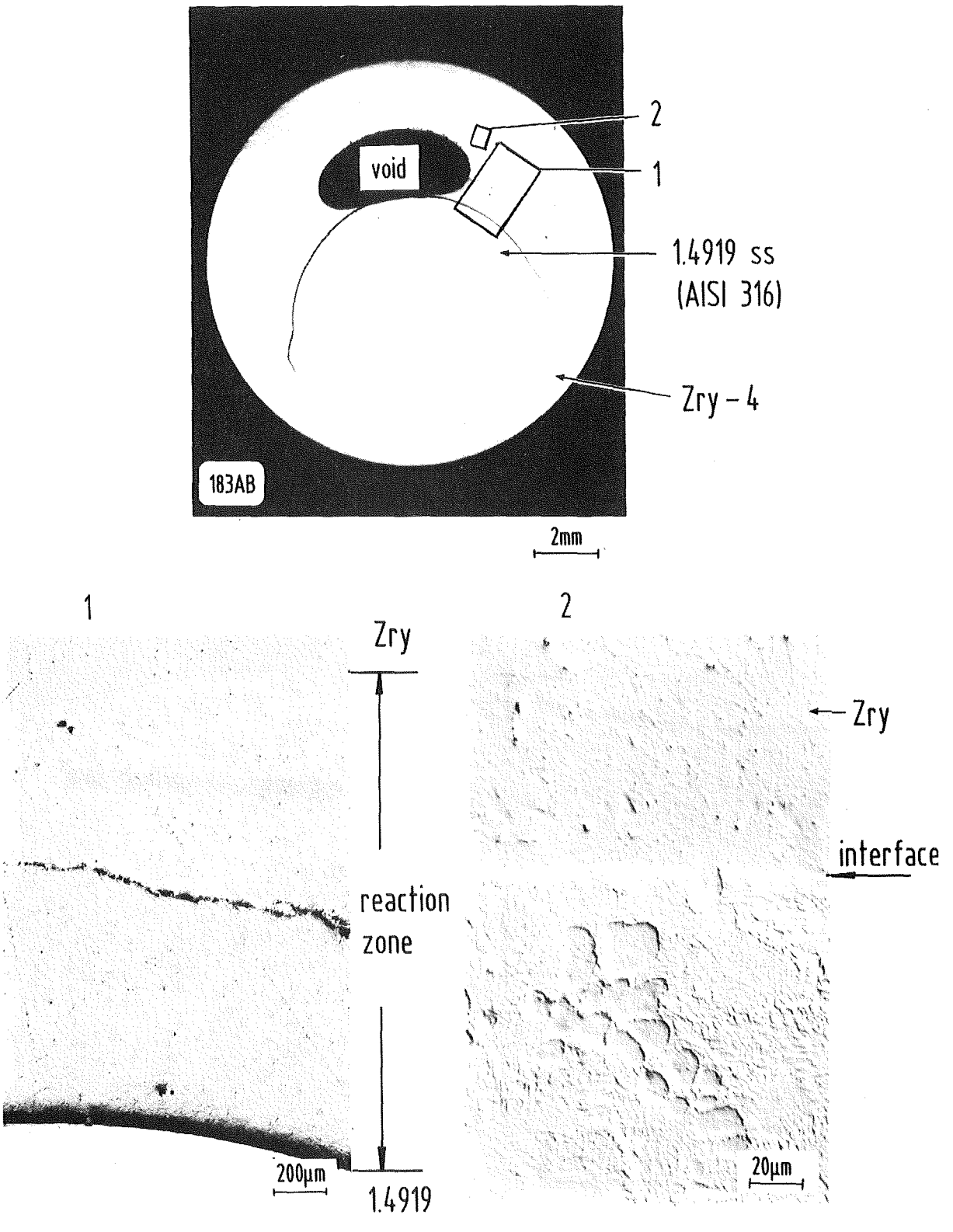

Fig. 9: Chemical interactions between Zircaloy-4 and stainless steel 1.4919 (AISI 316); 1150°C/5min.

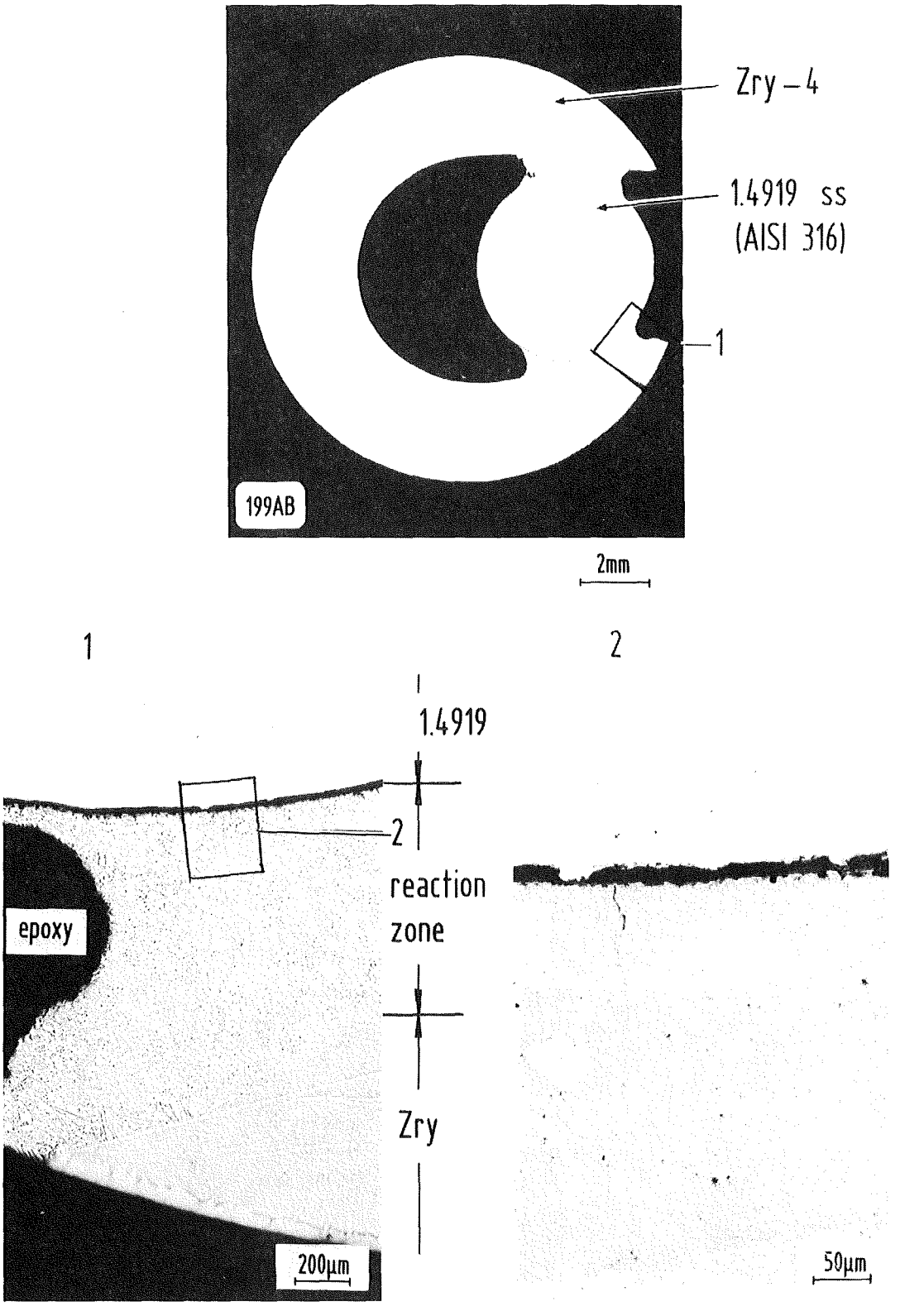

Fig. 10: Chemical interactions between Zircaloy-4 and stainless steel 1.4919 (AISI 316); 1200°C/4.5 min.

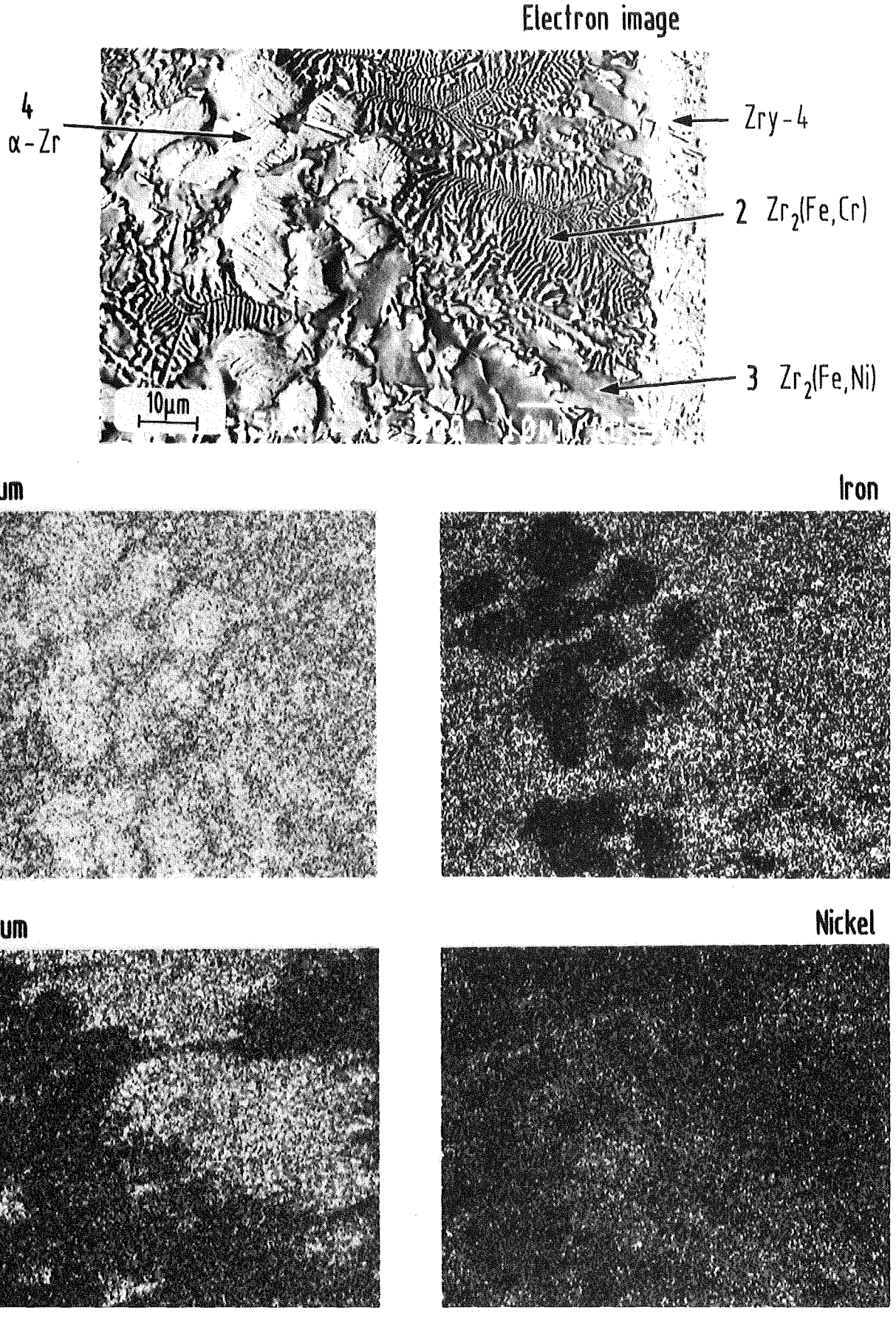

Fig. 11: Chemical composition of the Zry-4/ss 1.4919 (AISI 316) reaction zone after 2 min at 1200°C.

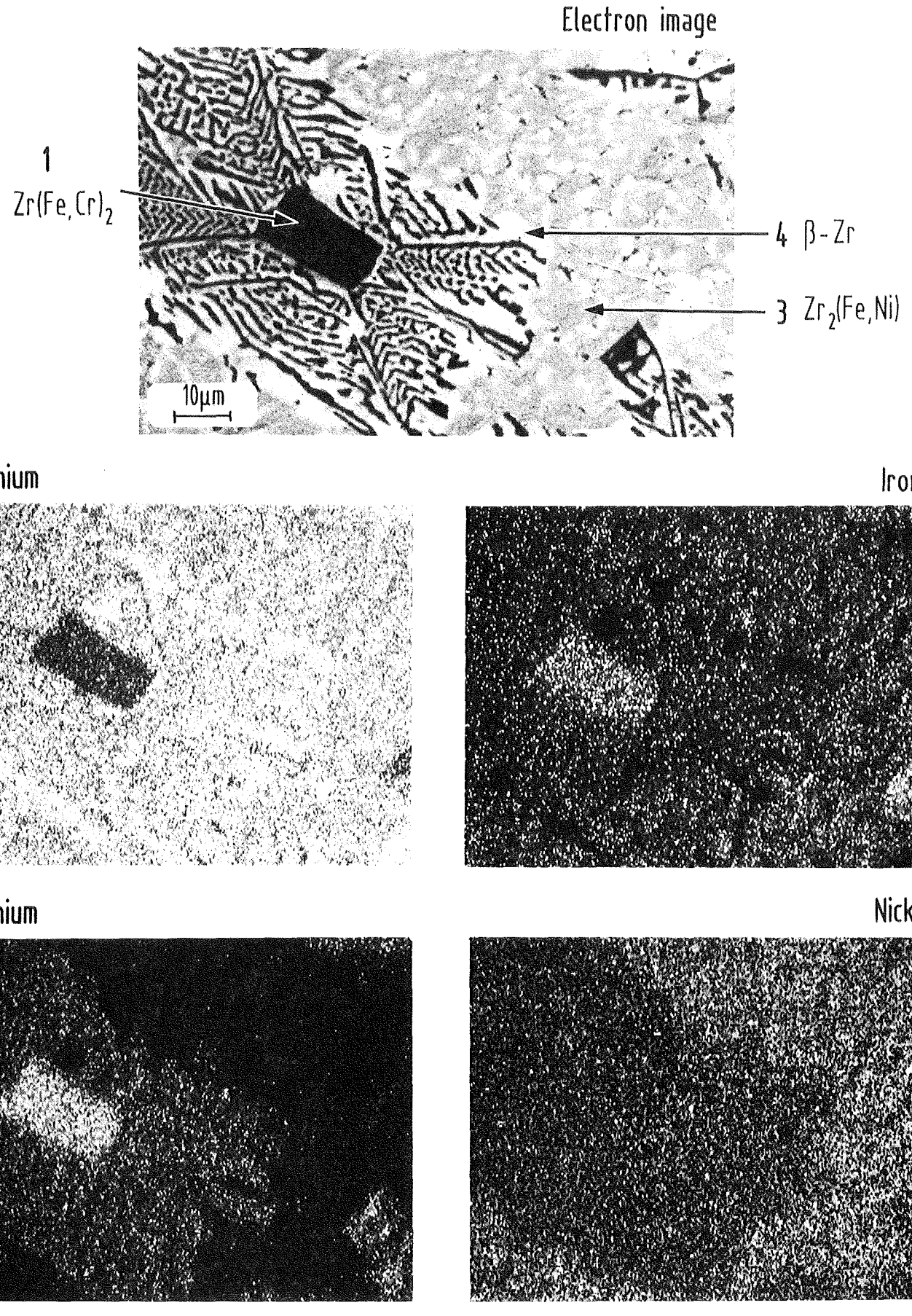

Fig. 12: Chemical composition of the Zry-4/ss 1.4919 (AISI 316) reaction zone after 5 min at 1150°C.

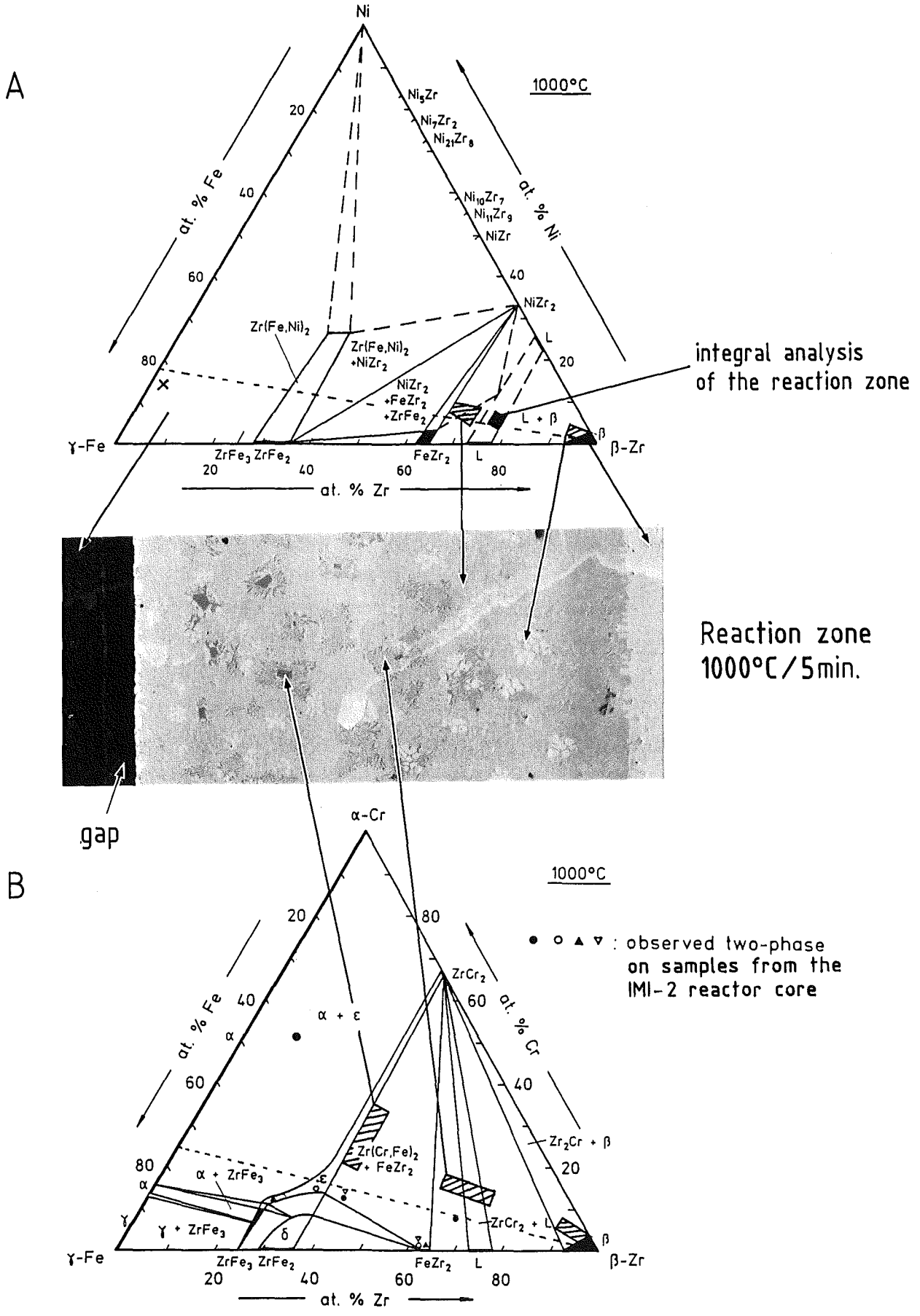

Fig. 13: Isothermal sections of the Fe-Zr-Ni and Fe-Zr-Cr systems at 1000°C [10]. Relation between the observed microstructure and phase diagrams.

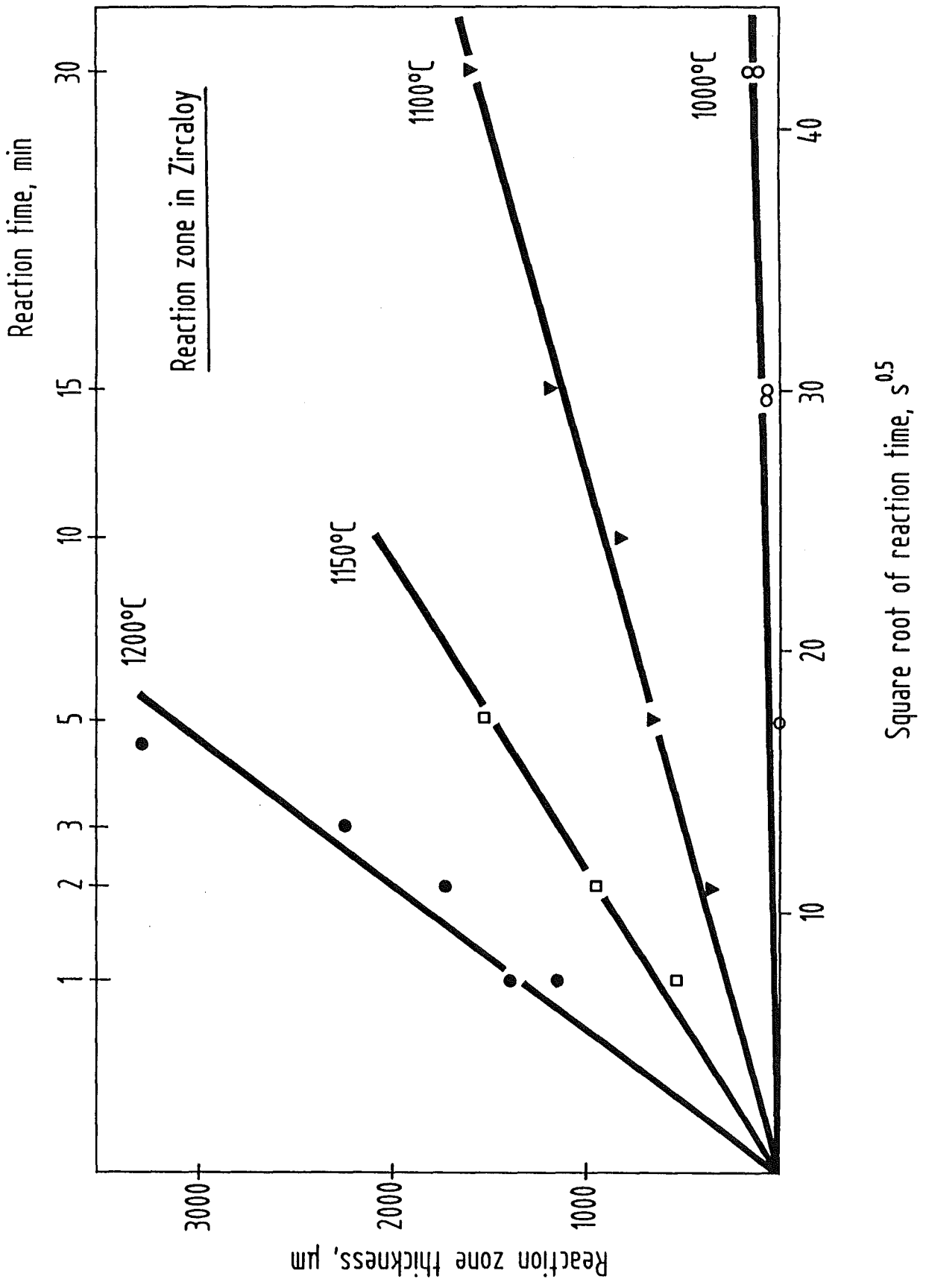

Fig. 14: Maximum reaction zone thicknesses in Zircaloy for the Zircaloy-4 stainless steel 1.4919 (AISI 316) system versus the square root of time between 1000 and 1200°C (Table 2).

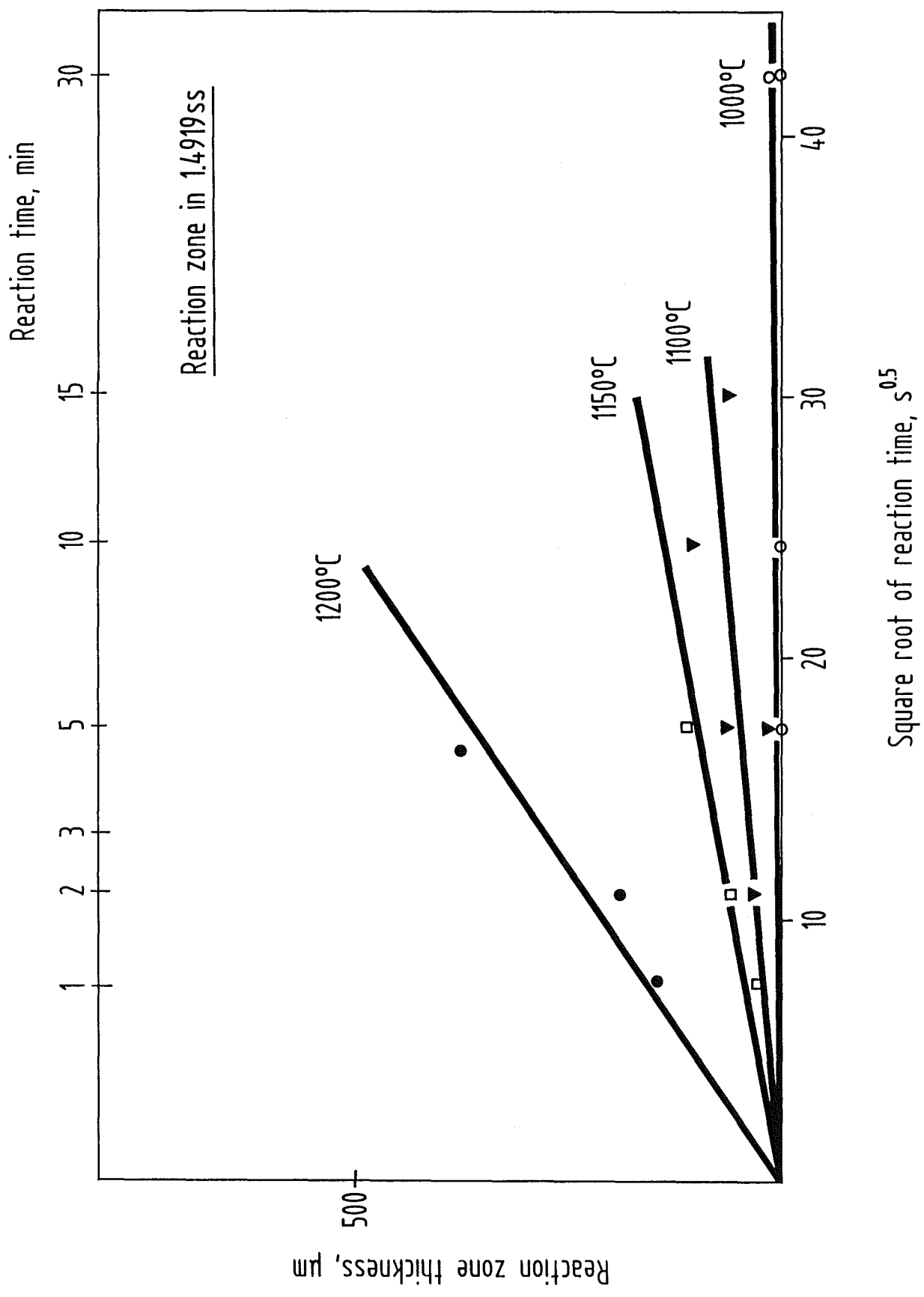

Fig. 15: Maximum reaction zone thicknesses in stainless steel for the Zircaloy-4/stainless steel 1.4919 (AISI 316) system versus the square root of time between 1000 and 1200°C (Table 3).

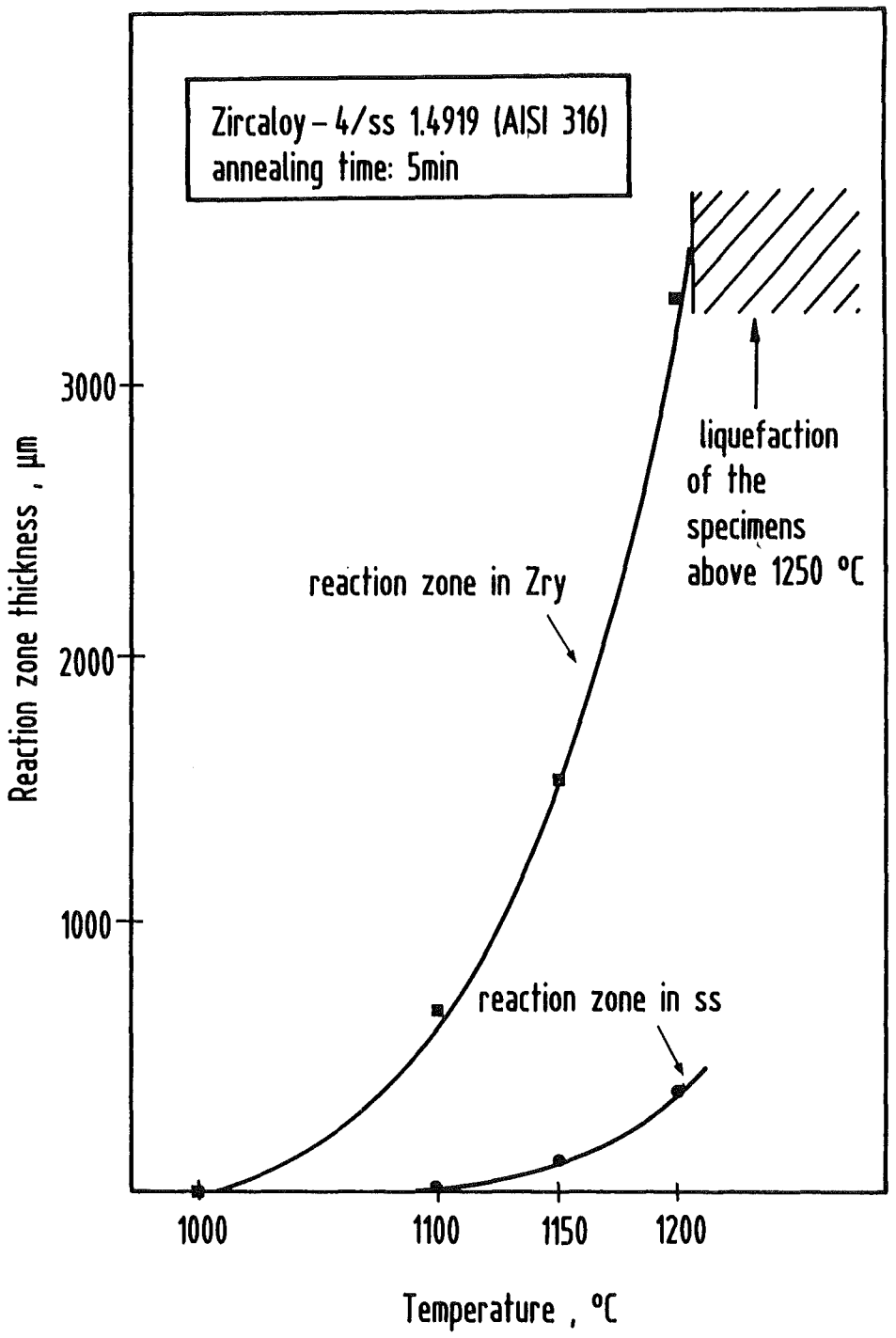

Fig. 16: Comparison of the reaction zone thicknesses in Zircaloy and stainless steel for the Zircaloy-4 / stainless steel 1.4919 (AISI 316) system versus temperature; annealing time: 5 min.

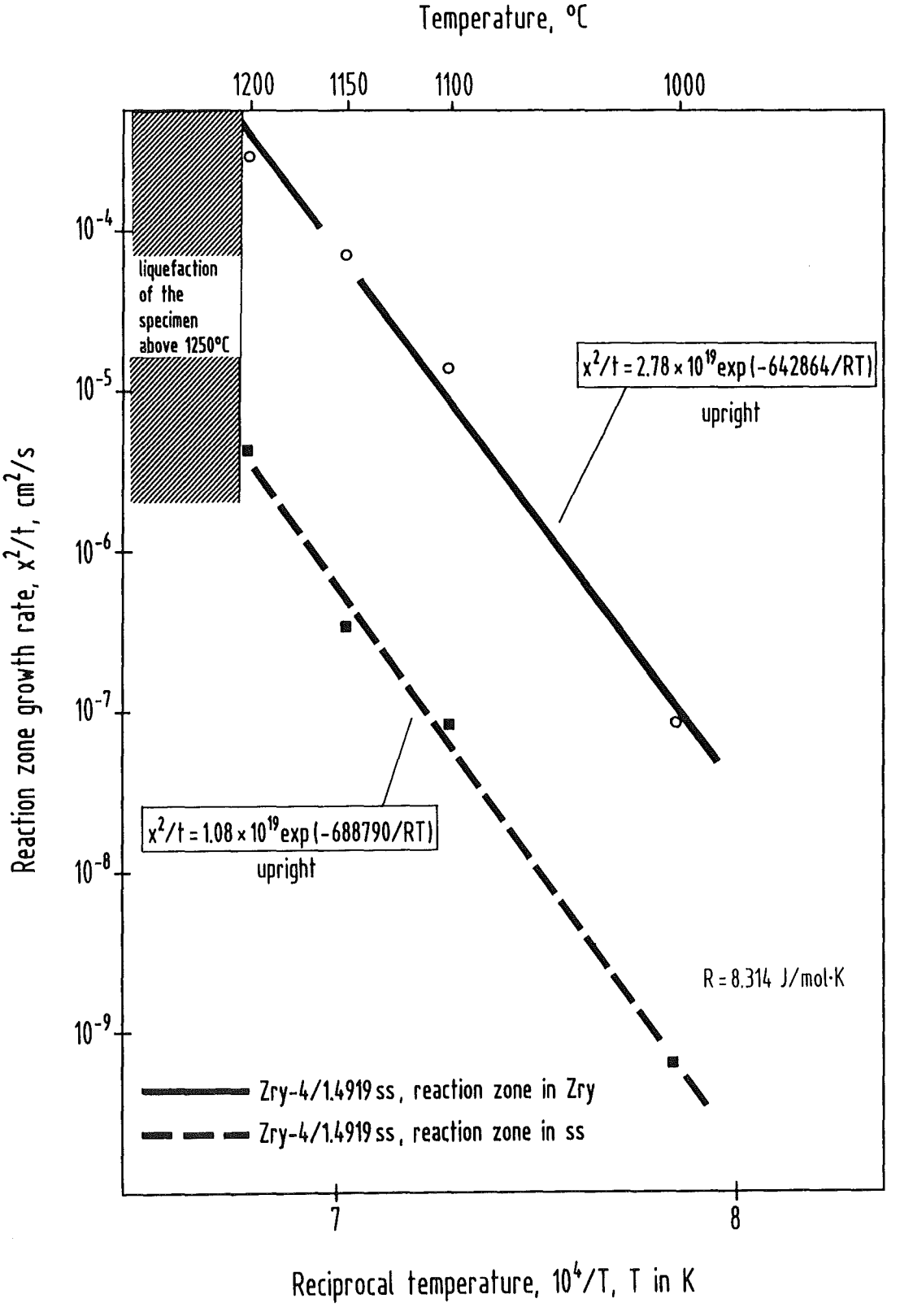

Fig. 17: Reaction zone growth rates for the Zircaloy-4/stainless steel 1.4919 (AISI 316) reaction system (Table 4).

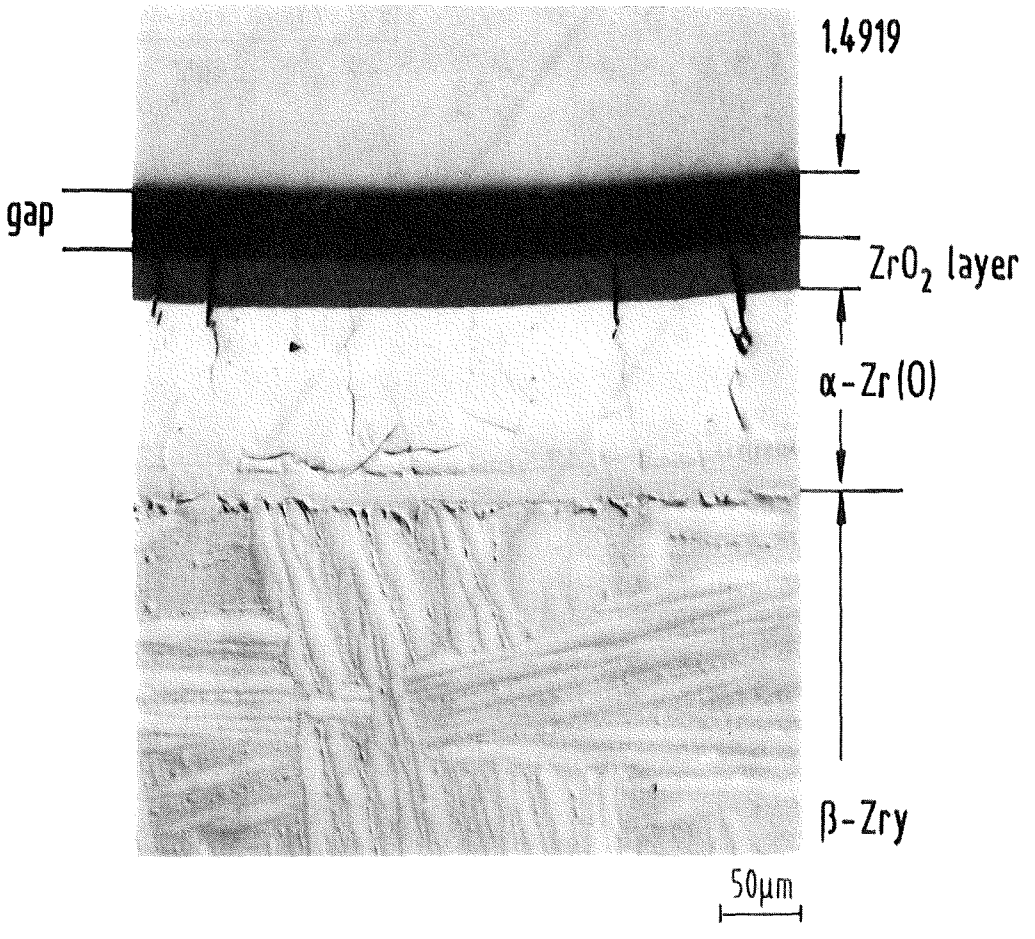

Fig. 18: Chemical interaction between Zry-4 and ss 1.4919 (AISI 316); 1100°C/240 min. Initial ZrO_2 layer thickness: 50 µm.

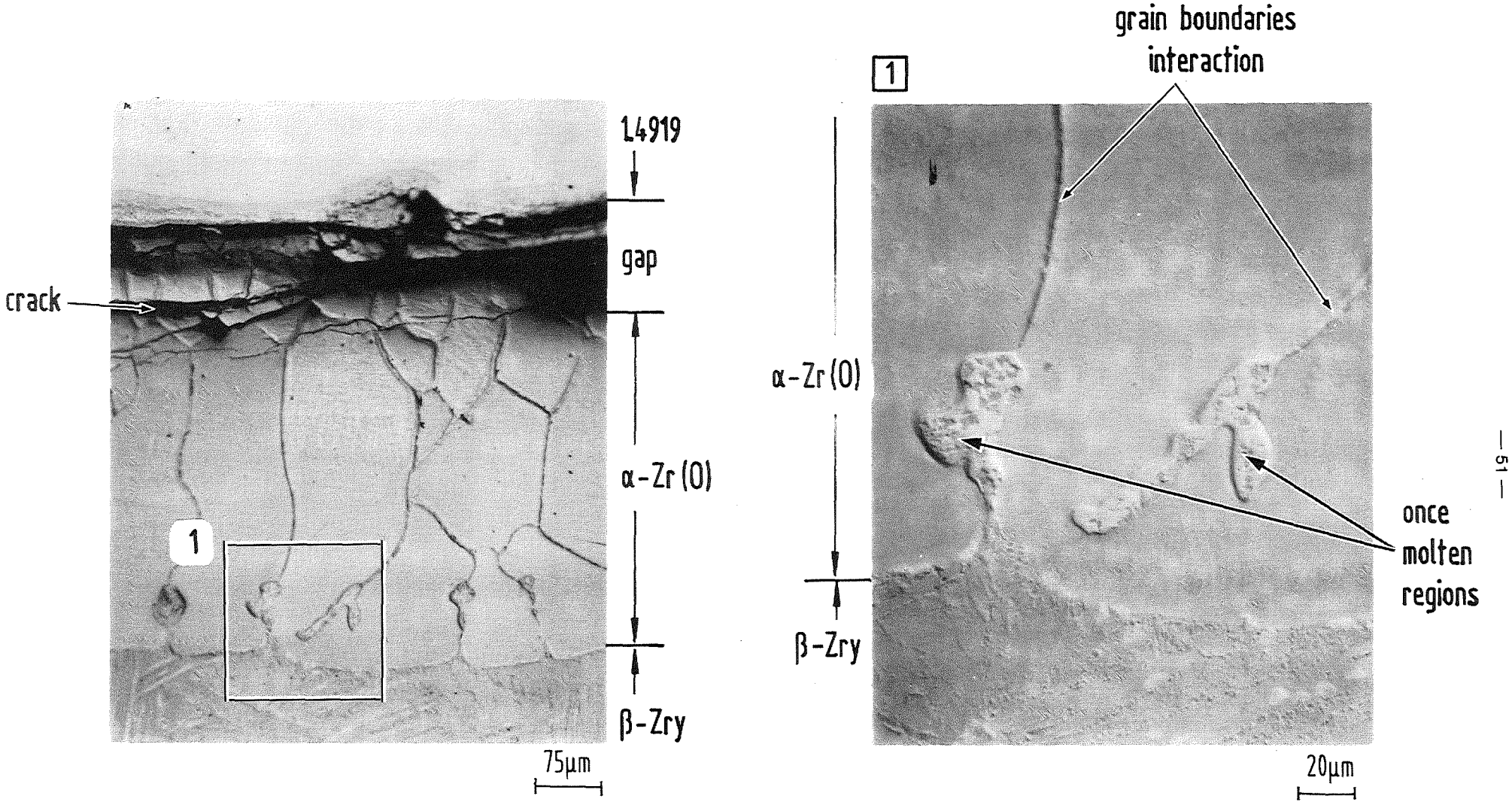

Fig. 19: Chemical interaction between Zry-4 and ss 1.4919 (AISI 316); 1100°C/600 min.

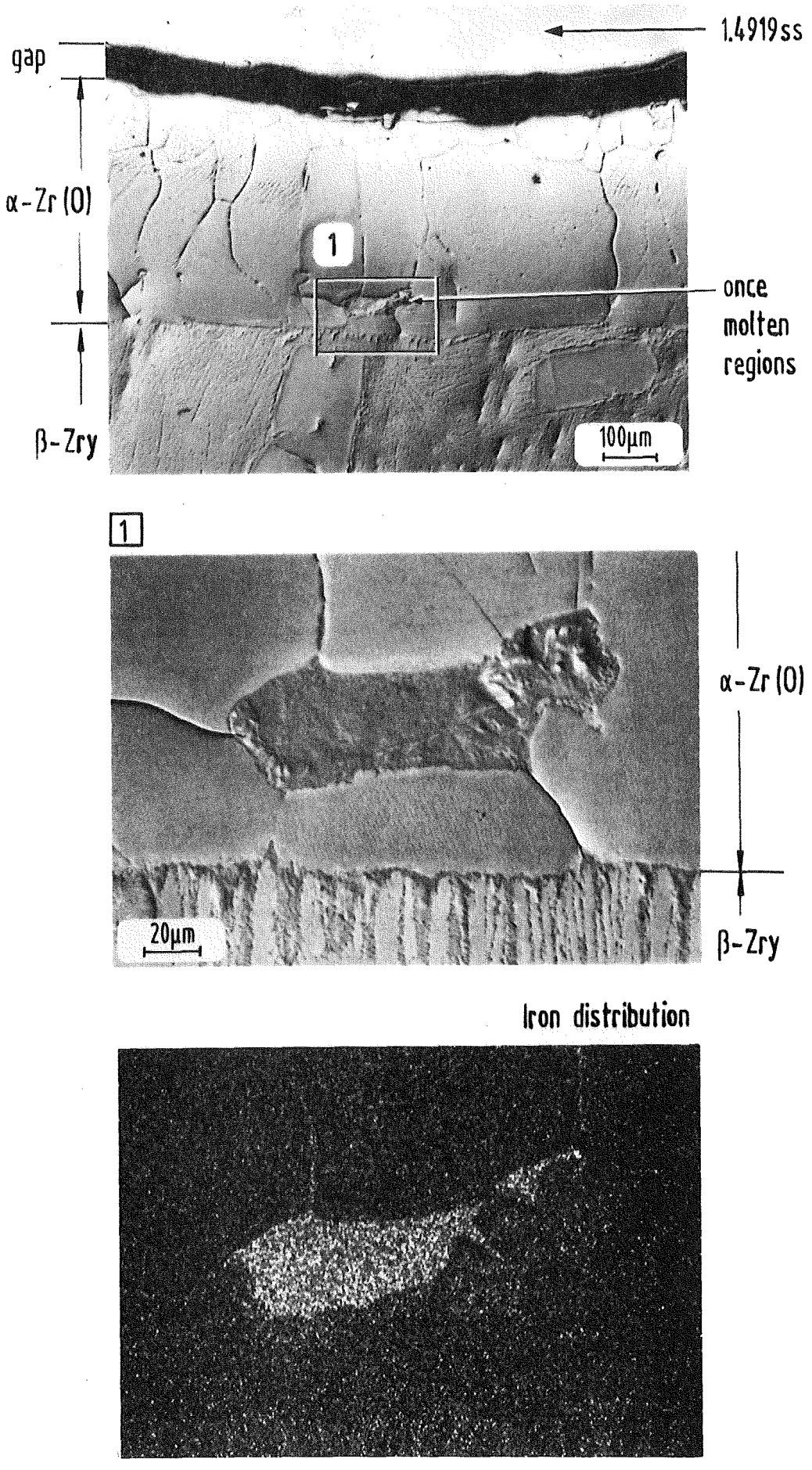

Fig. 20: Chemical interaction between Zry-4 and ss 1.4919 (AISI 316); 1100°C/600 min. Fe distribution within the previously liquid reaction products.

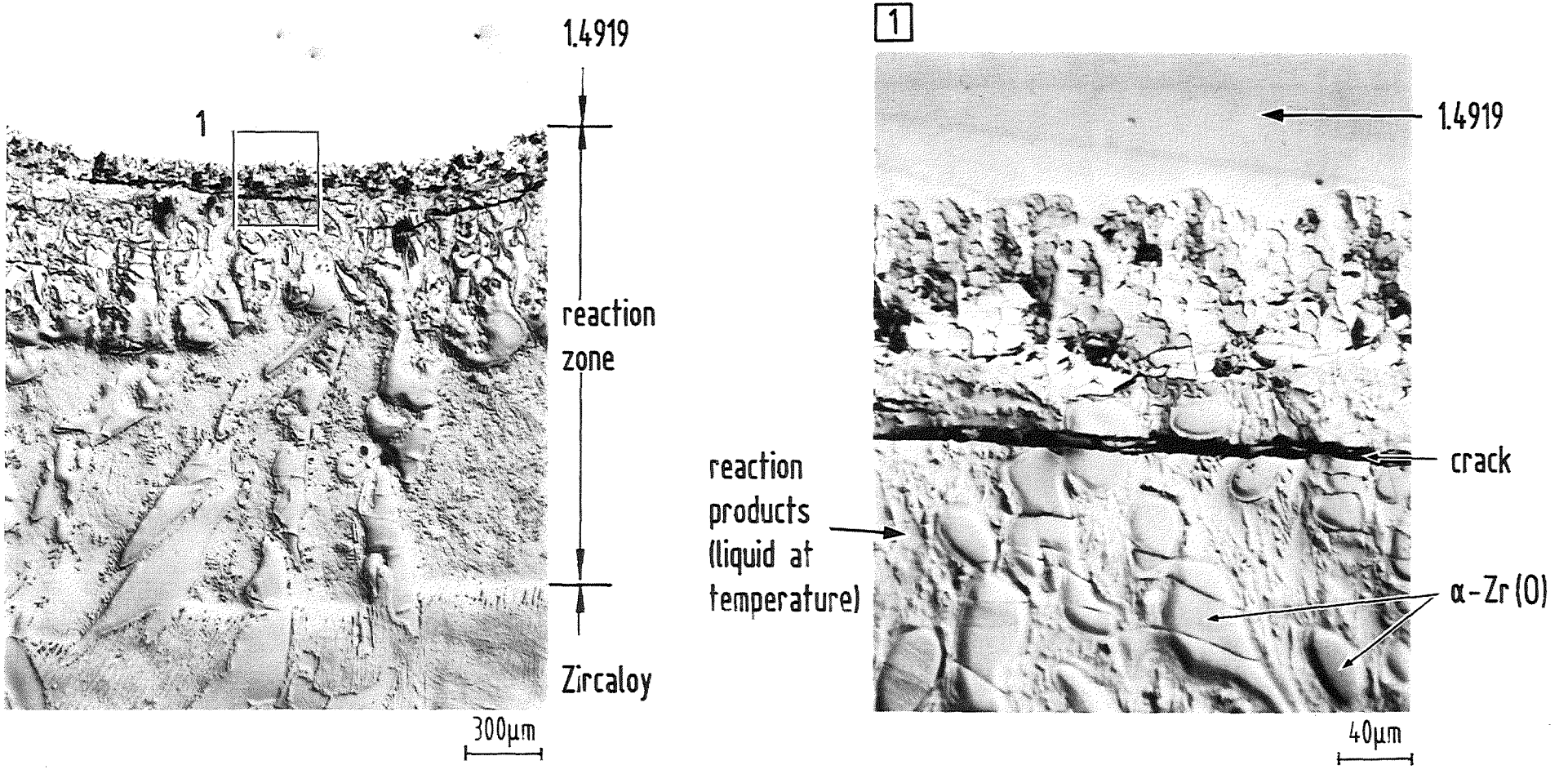

Fig. 21: Chemical interaction between Zry-4 and ss 1.4919 (AISI 316); 1100°C/900 min.

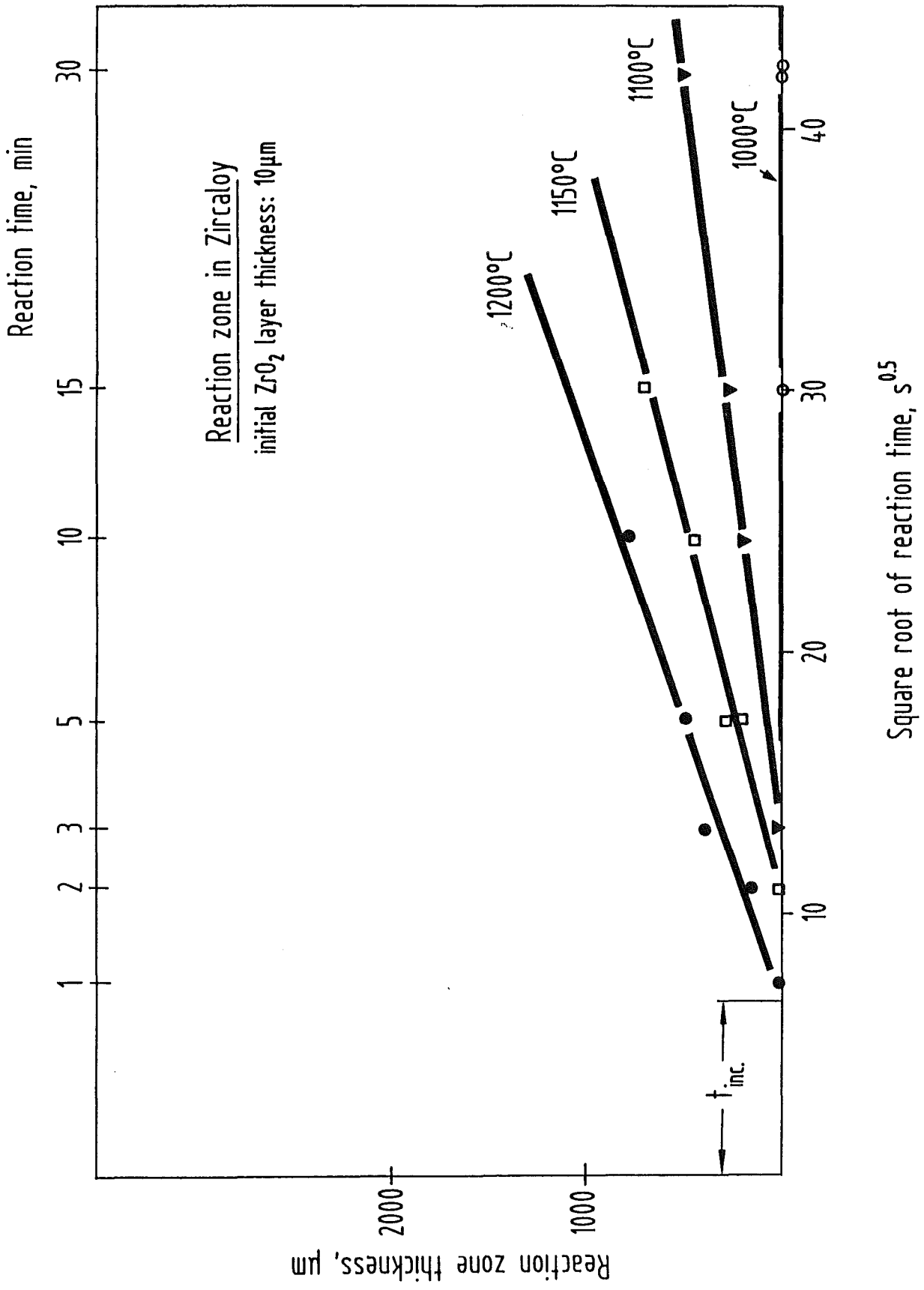

Fig. 22: Maximum reaction zone thicknesses in Zircaloy for the pre-oxidized Zircaloy-4/stainless steel 1.4919 (AISI 316) system versus the square root of time; initial ZrO_2 layer thickness: 10 µm. The interactions start after the incubation time t_0 has passed (Table 5).

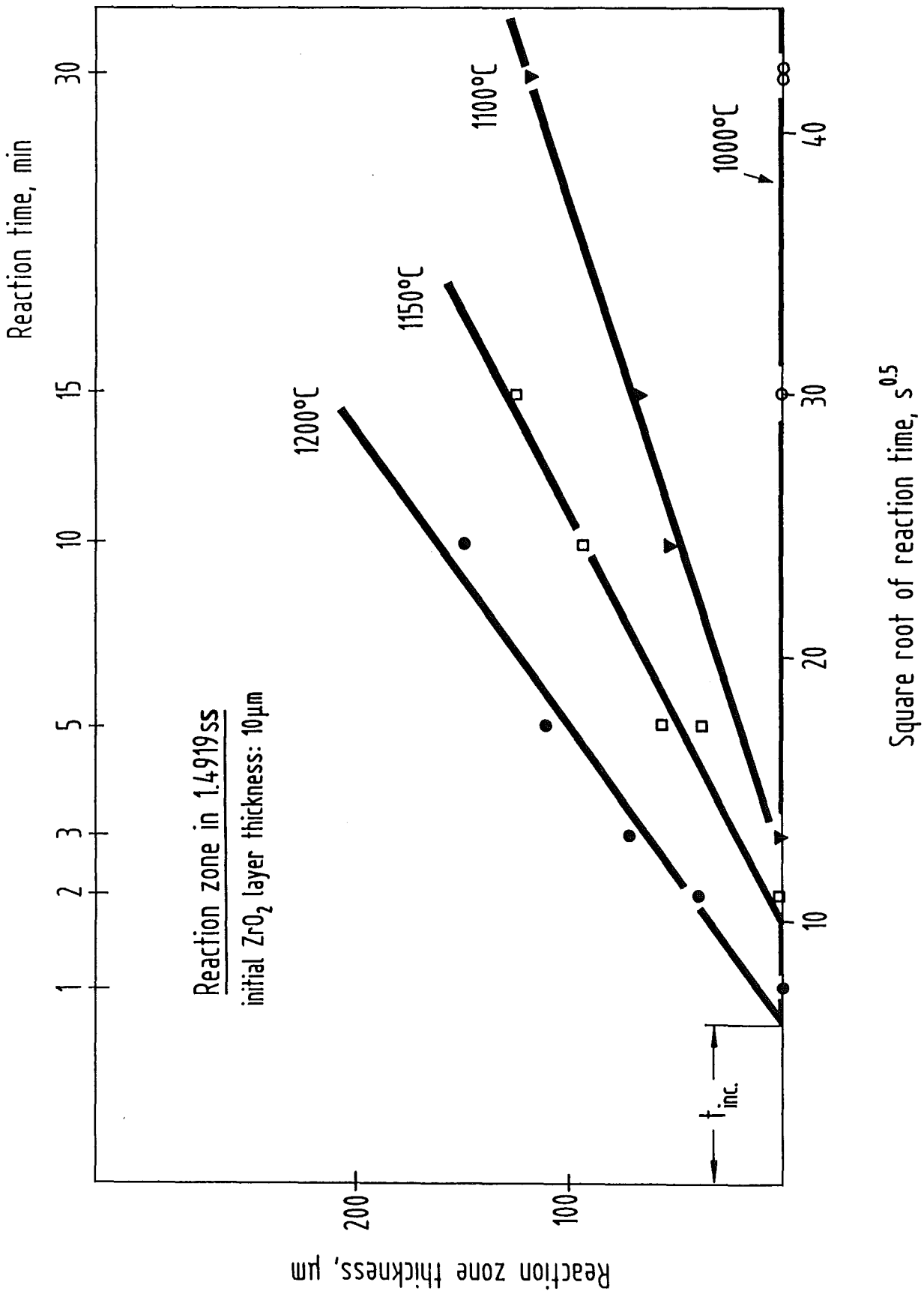

Fig. 23: Maximum reaction zone thicknesses in stainless steel for the pre-oxidized Zircaloy-4/stainless steel 1.4919 (AISI 316) system versus the square root of time; initial ZrO_2 layer thickness: 10 µm. The interactions start after the incubation time t_0 has passed (Table 5).

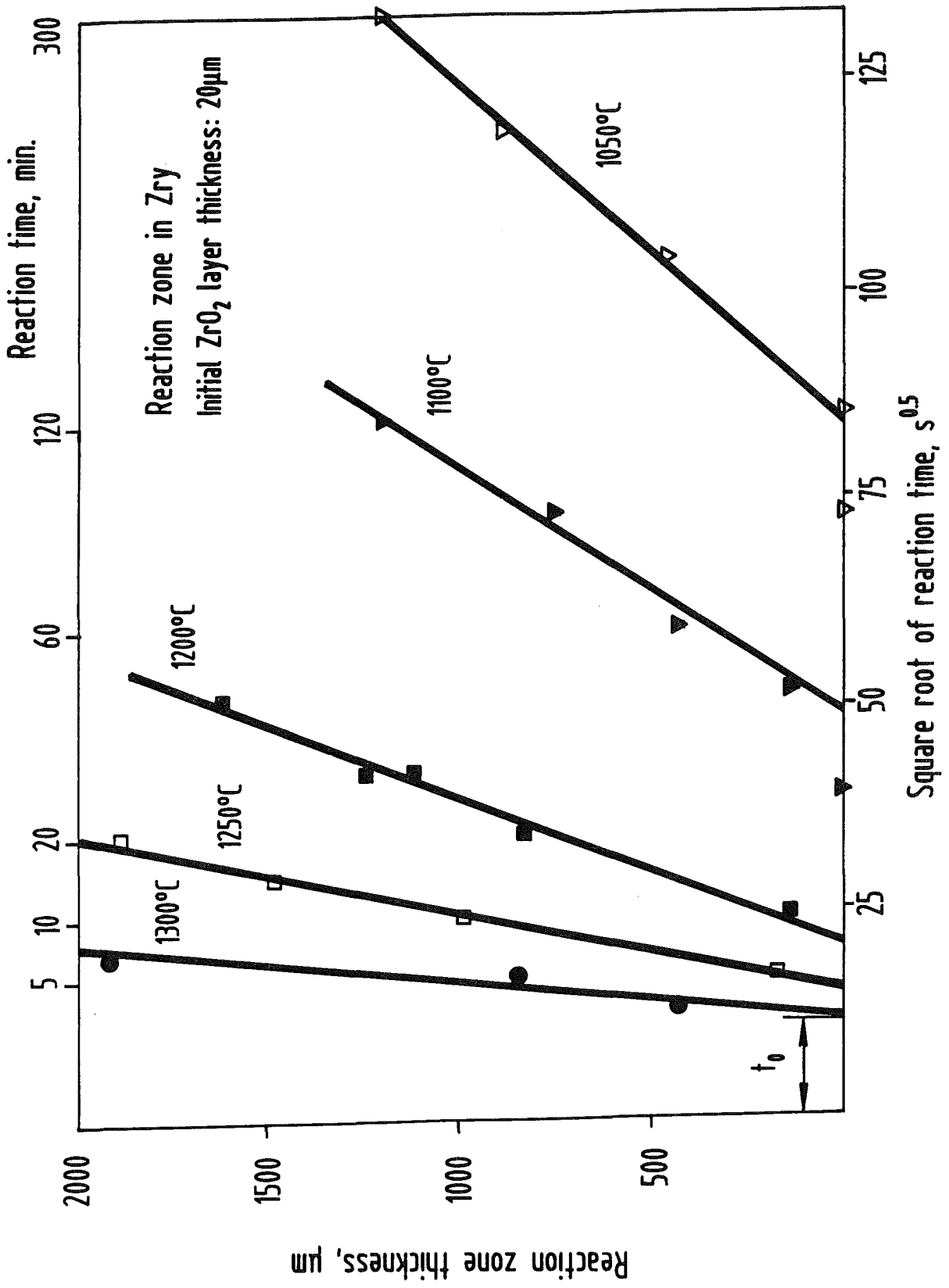

Fig. 24: Maximum reaction zone thicknesses in Zircaloy for the pre-oxidized Zircaloy-4/stainless steel 1.4919 (AISI 316) system versus the square root on time; initial ZrO_2 layer thickness: 20 µm. The interactions start after the incubation time t_0 has passed (Table 6).

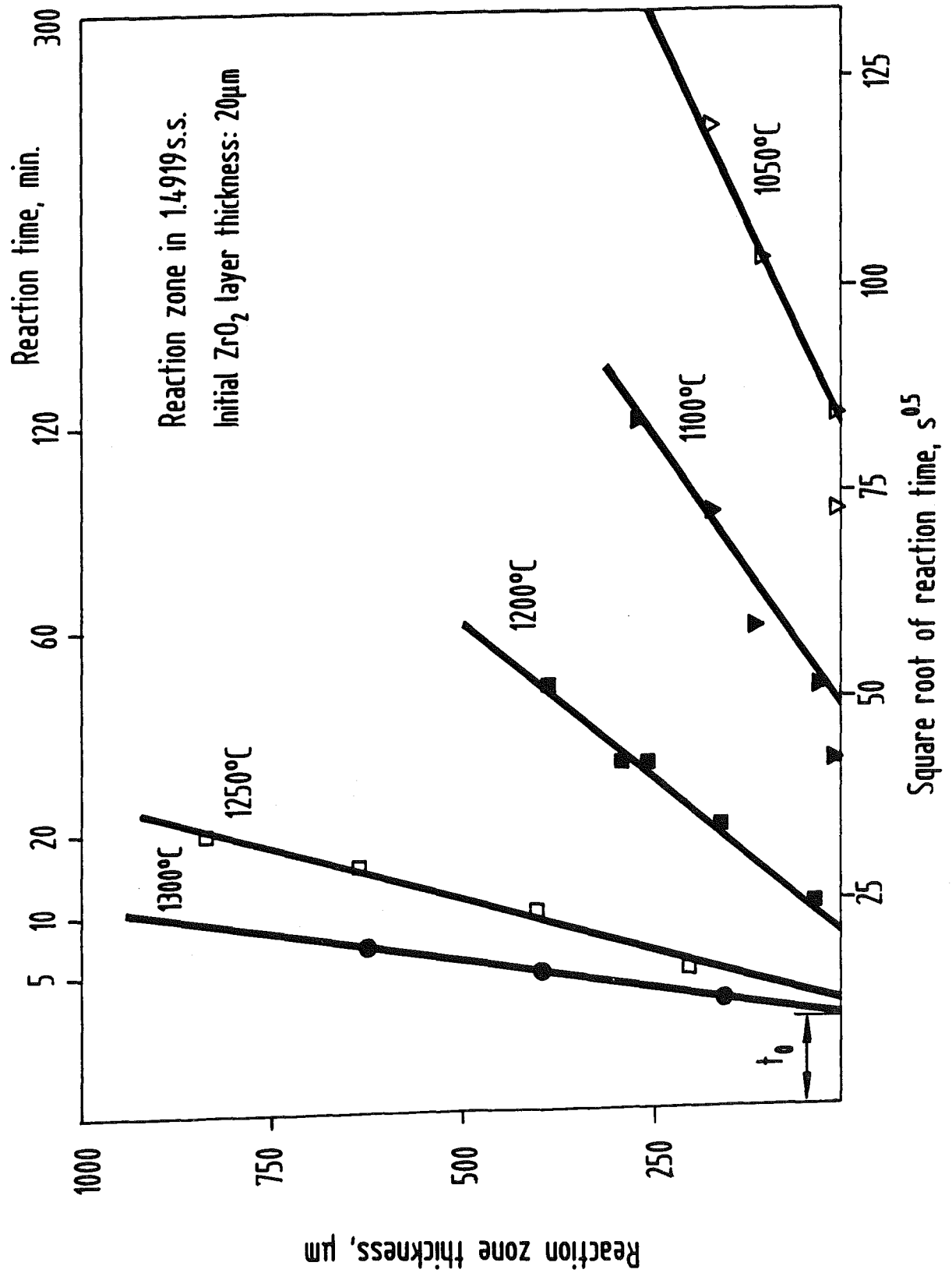

Fig. 25: Maximum reaction zone thicknesses in Zircaloy for the pre-oxidized Zircaloy-4/stainless steel 1.4919 (AISI 316) system versus the square root of time; initial ZrO_2 layer thickness: 20 µm. The interactions start after the incubation time t_0 has passed (Table 6).

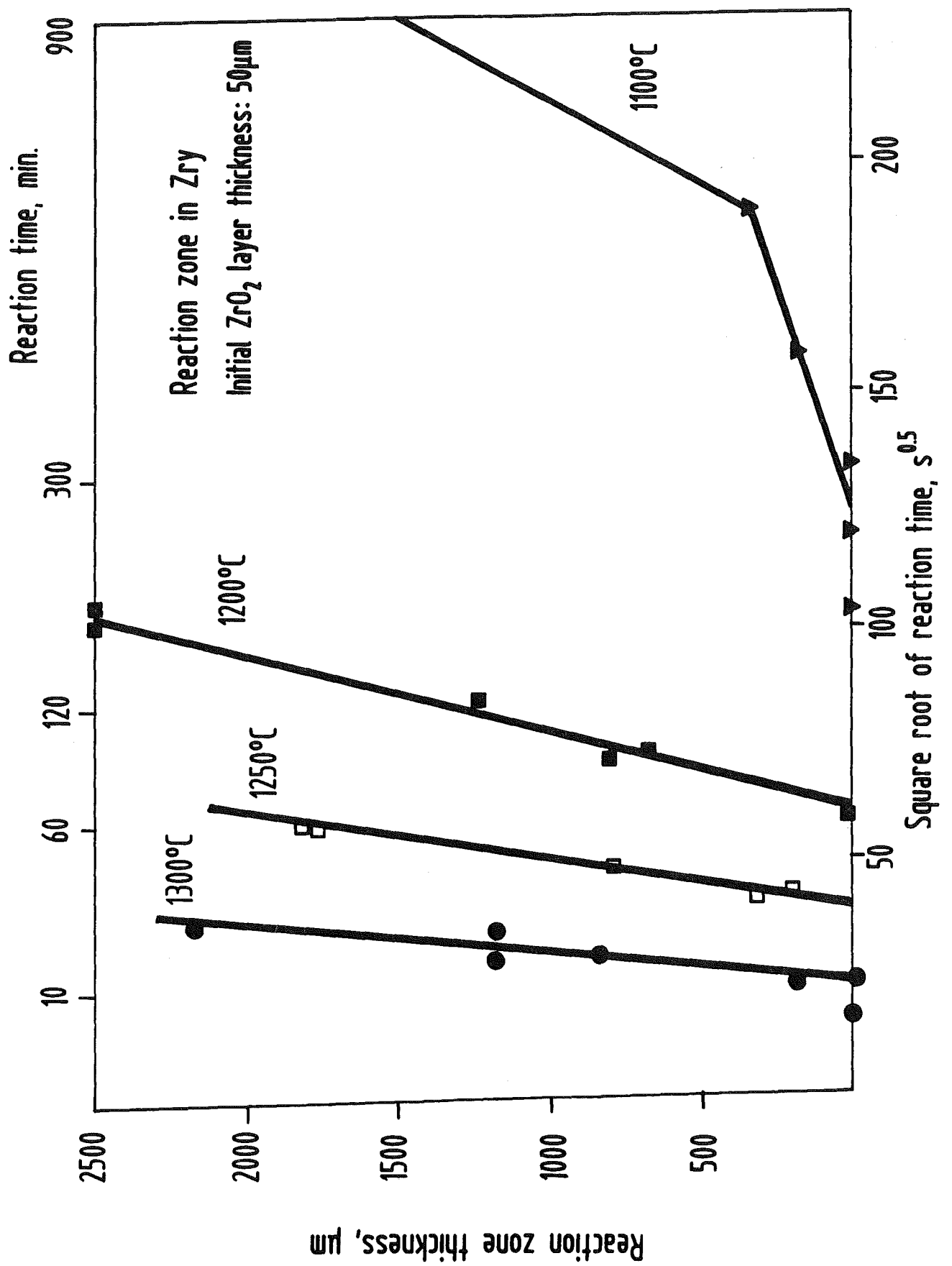

Fig. 26: Maximum reaction zone thicknesses in Zircaloy for the pre-oxidized Zircaloy-4/stainless steel 1.4919 (AISI 316) system versus the square root of time; initial ZrO_2 layer thickness: 50 µm. The interactions start after the incubation time t_0 has passed (table 7).

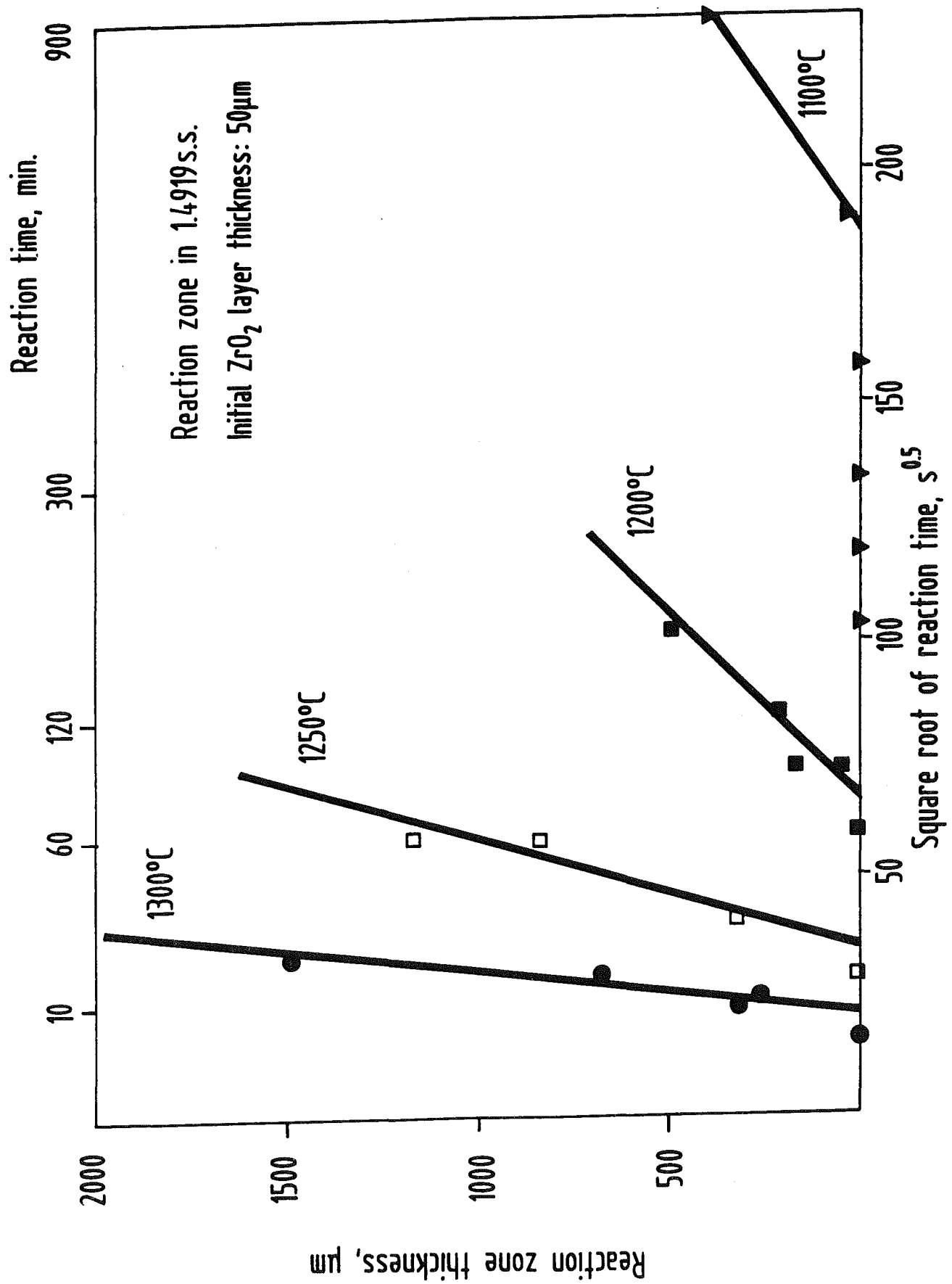

Fig. 27: Maximum reaction zone thicknesses in Zircaloy for the pre-oxidized Zircaloy-4/stainless steel 1.4919 (AISI 316) system versus the square root of time; initial ZrO_2 layer thickness: 50 µm. The interactions start after the incubation time t_0 has passed (Table 7).

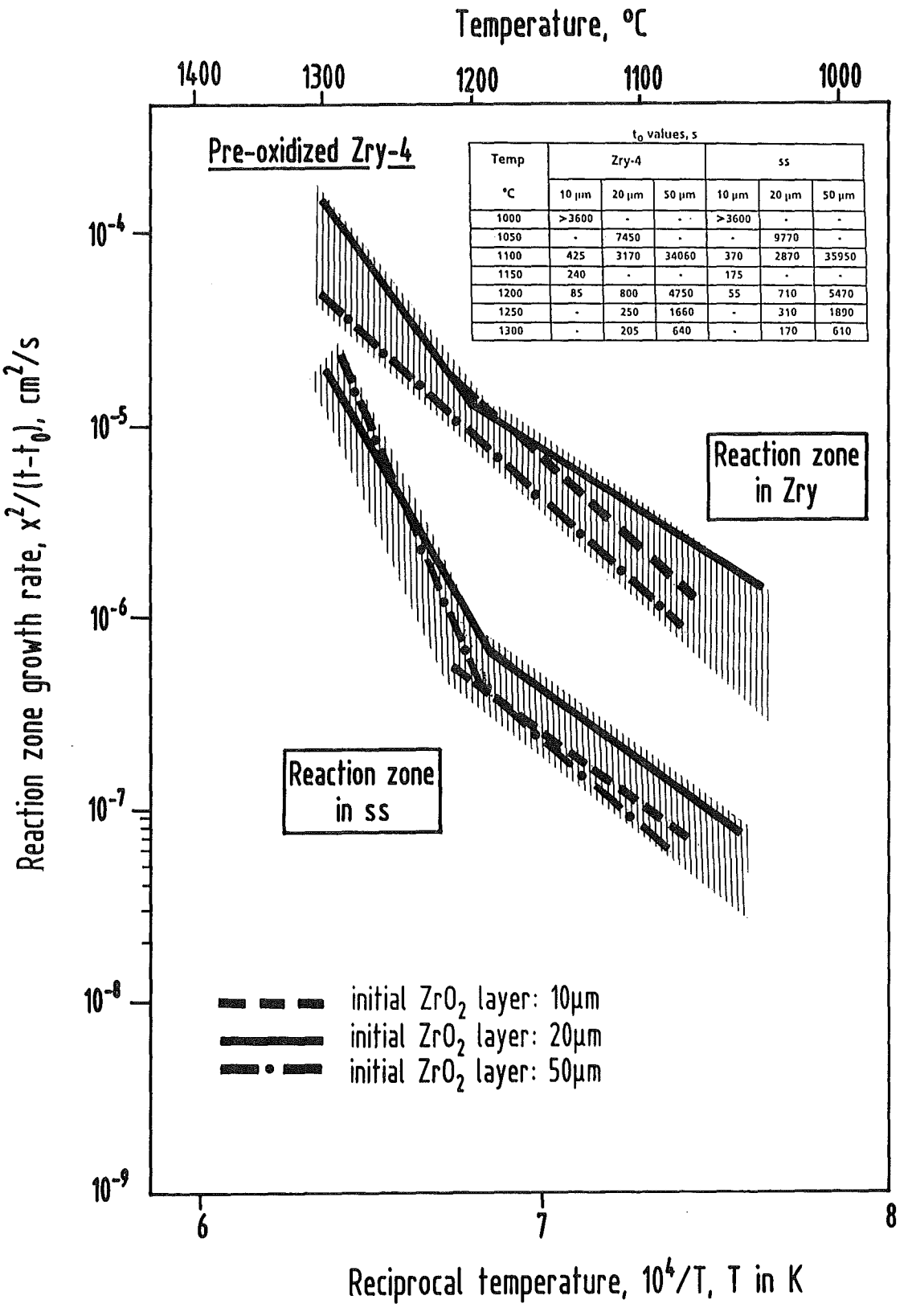

Fig. 28: Reaction zone growth rates for the pre-oxidized Zry-4/ss 1.4919(AISI 316) system; initial ZrO_2 layer thicknesses: 10, 20 and 50 µm.

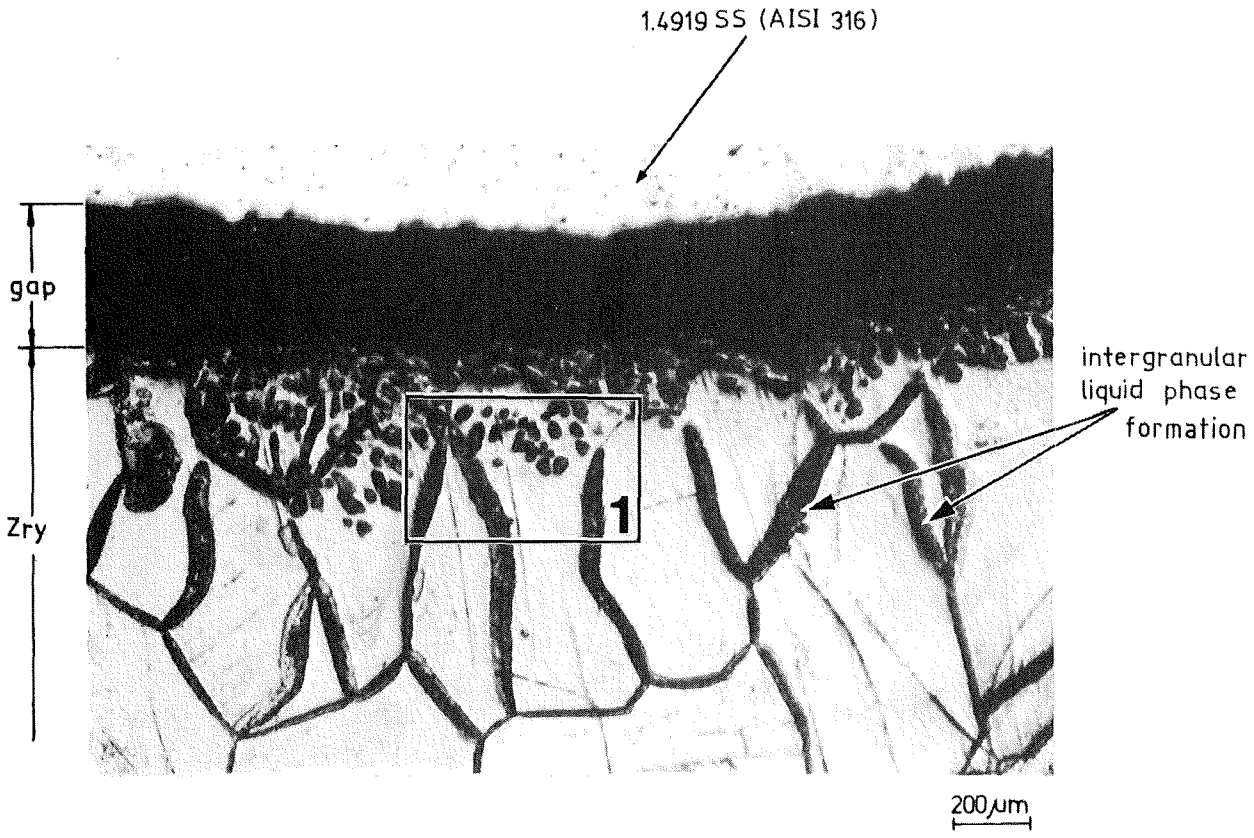

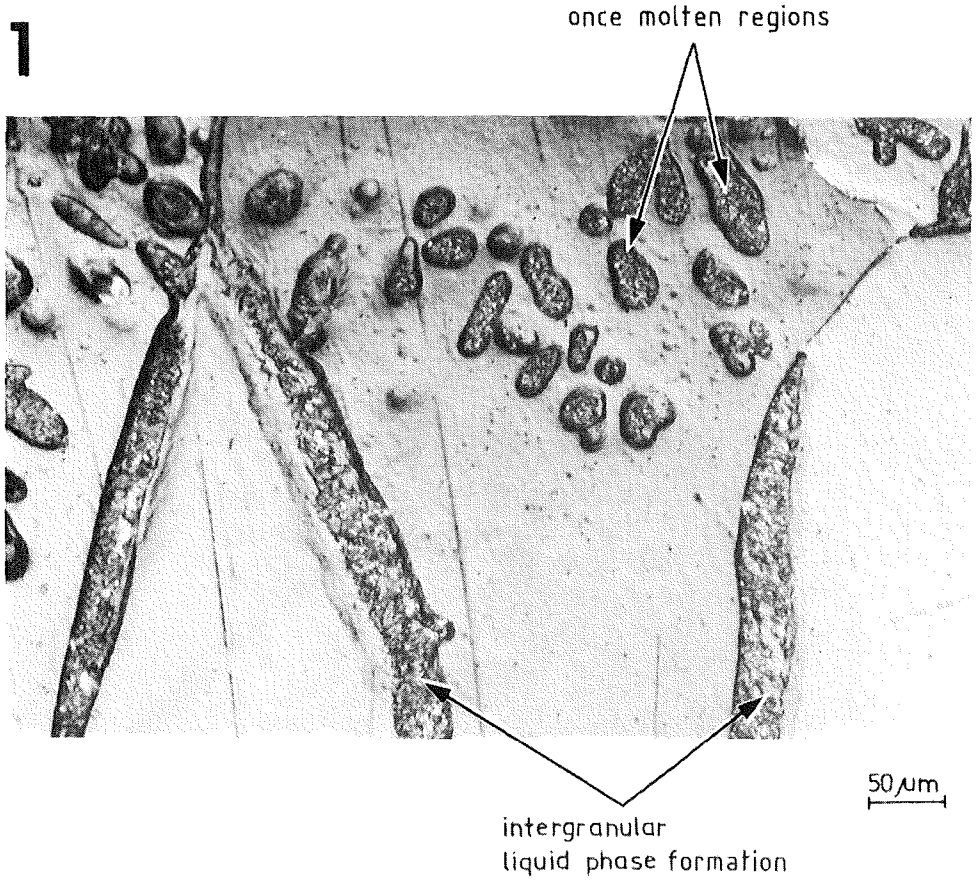

Fig. 29: Chemical interaction between oxygen-stabilized α-Zry (O) and ss 1.4919 (AISI 316); 1200°C/10 min.

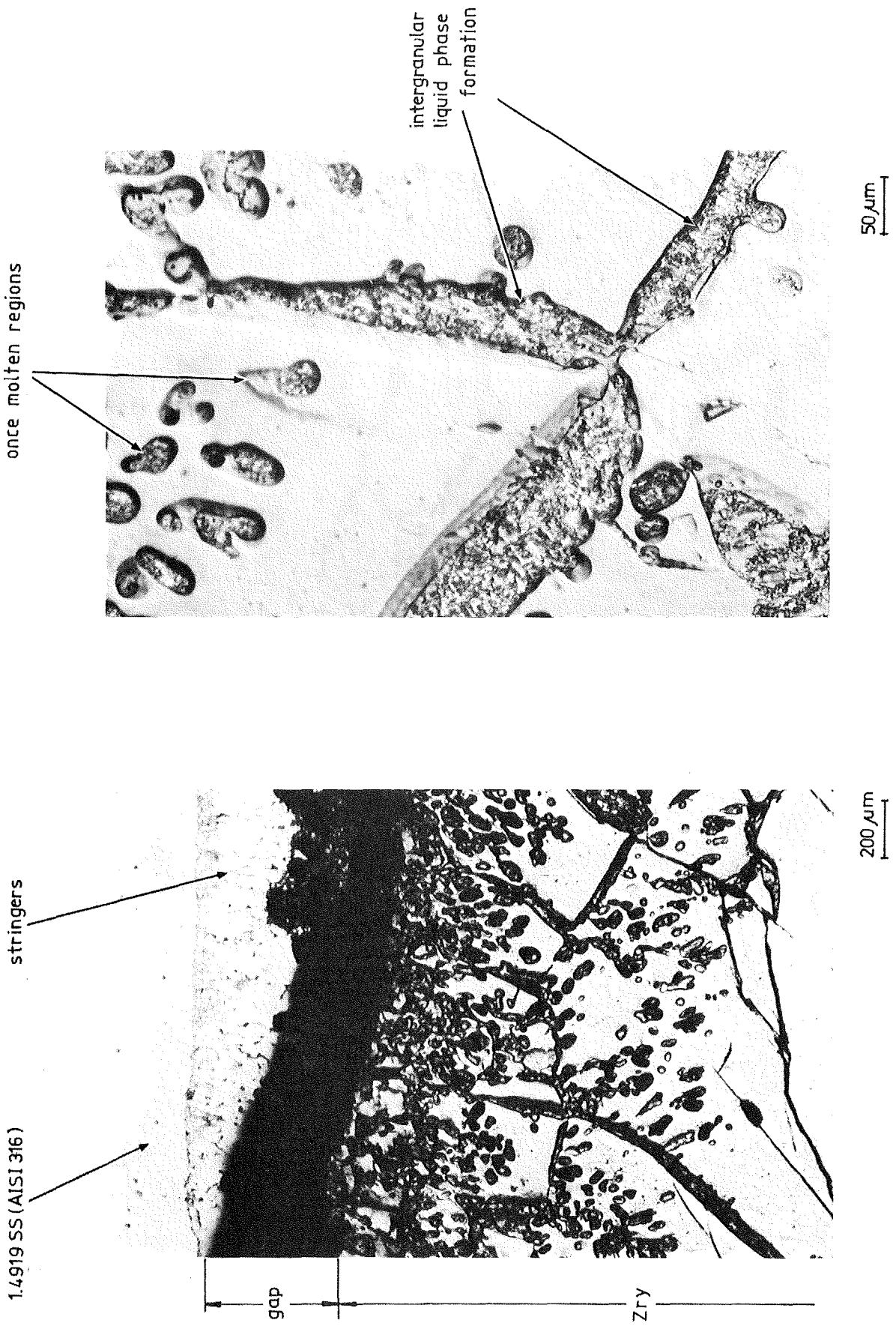

Fig. 30: Chemical interaction between oxygen-stabilized α-Zry (O) and ss 1.4919 (AISI 316); 1300°C/10 min.

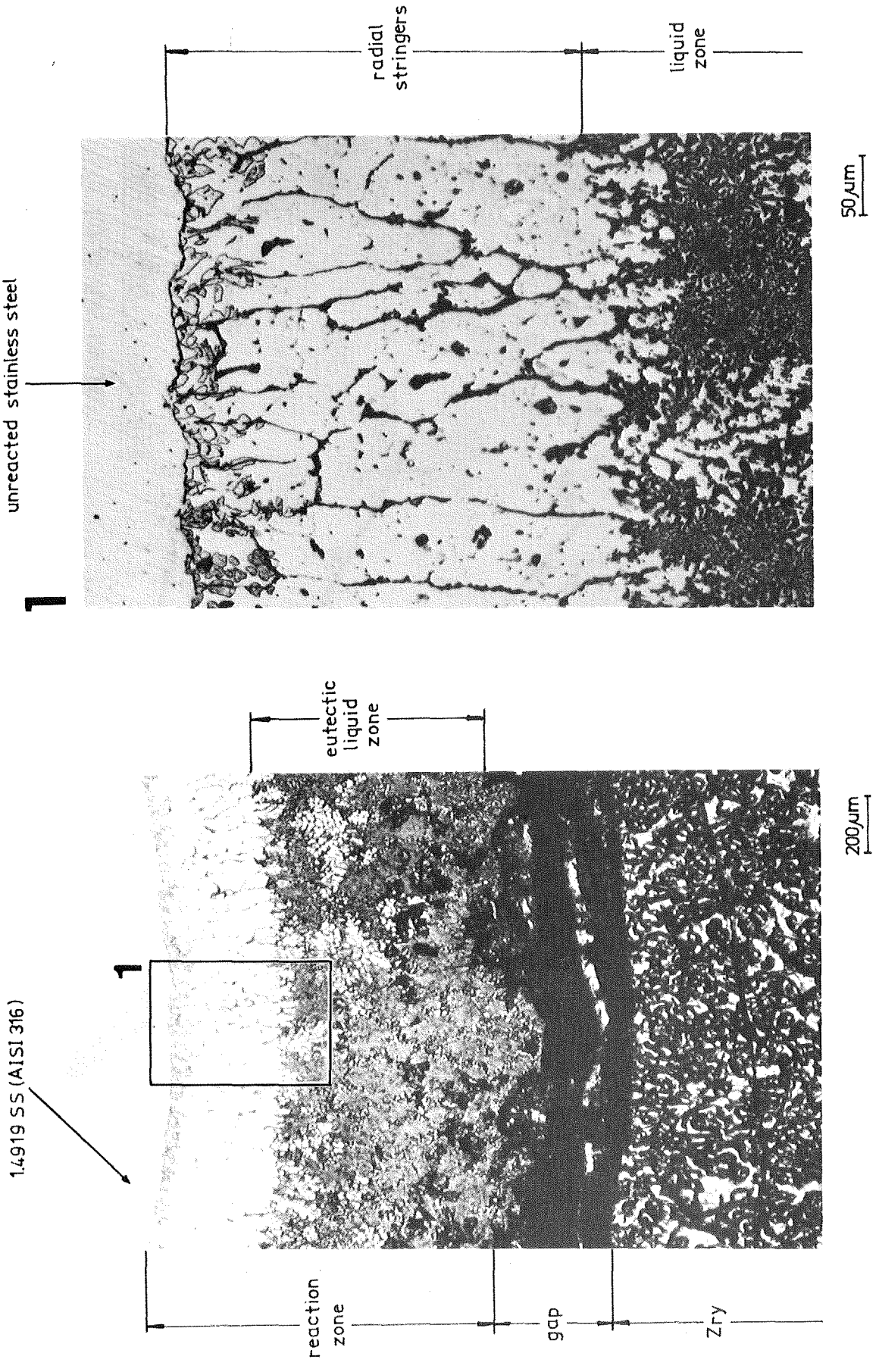

Fig. 31: Chemical interaction between oxygen-stabilized α-Zry (O) and ss 1.4919 (AISI 316); 1350°C/10 min.

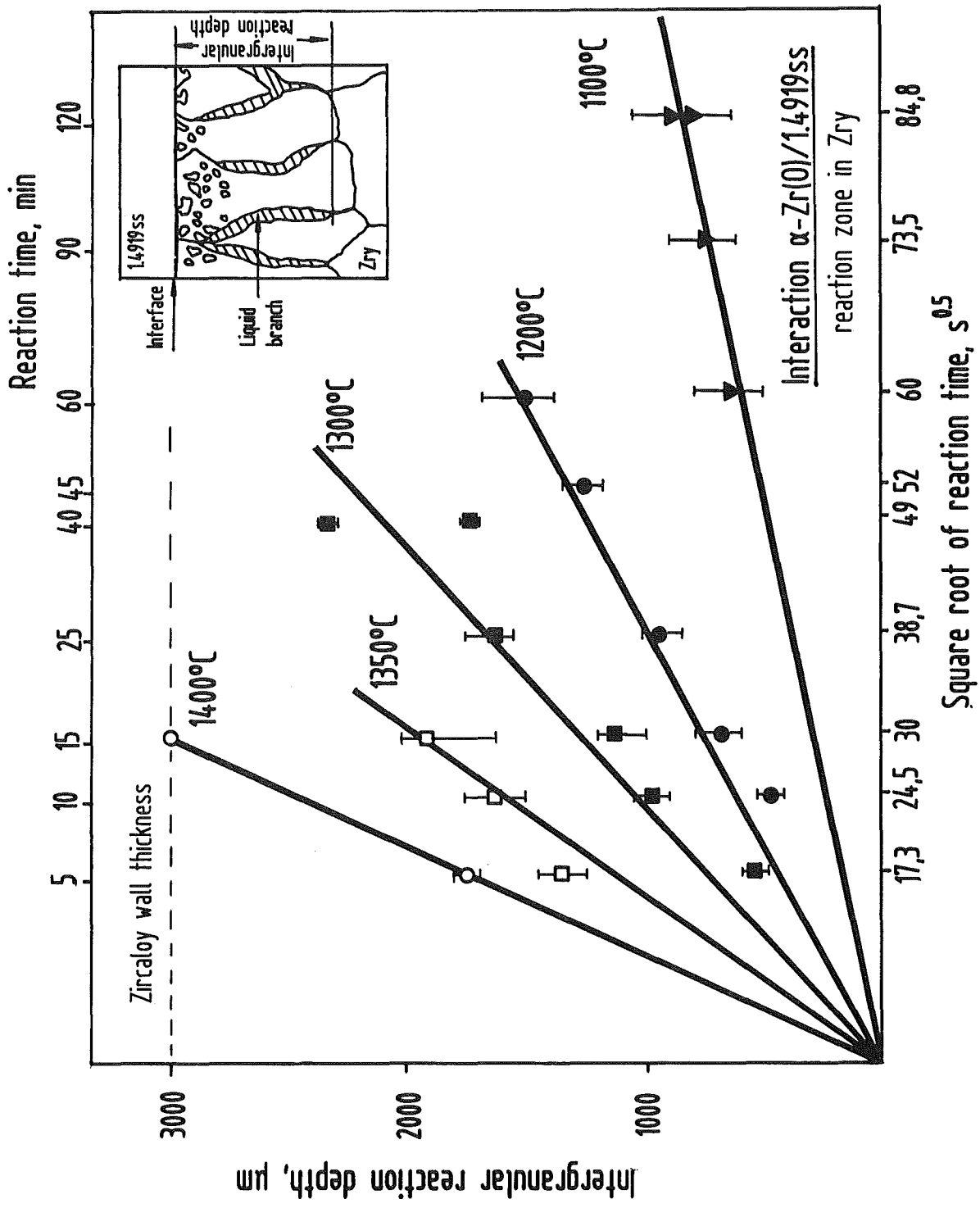

Fig. 32: Maximum reaction zone thicknesses in Zry for the oxygen-stabilized α-Zry (O) / ss 1.4919 (AISI 316) system versus the square root of time between 1100 und 1400°C.

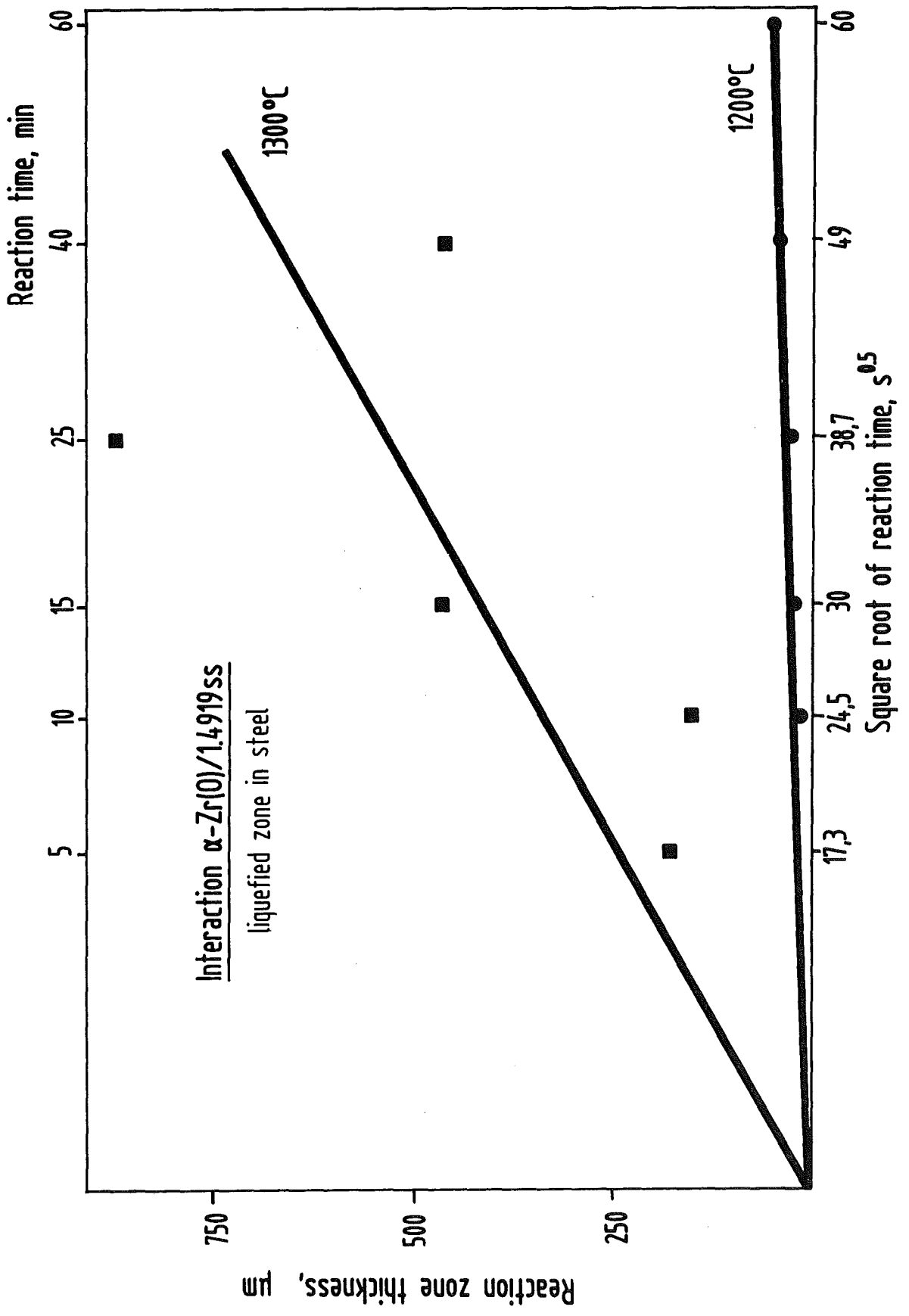

Fig. 33: Maximum reaction zone thicknesses in stainless steel for the oxygen-stabilized α-Zry (O)/ss 1,4919 (AISI 316) system versus the square root of time for 1200 and 1300°C.

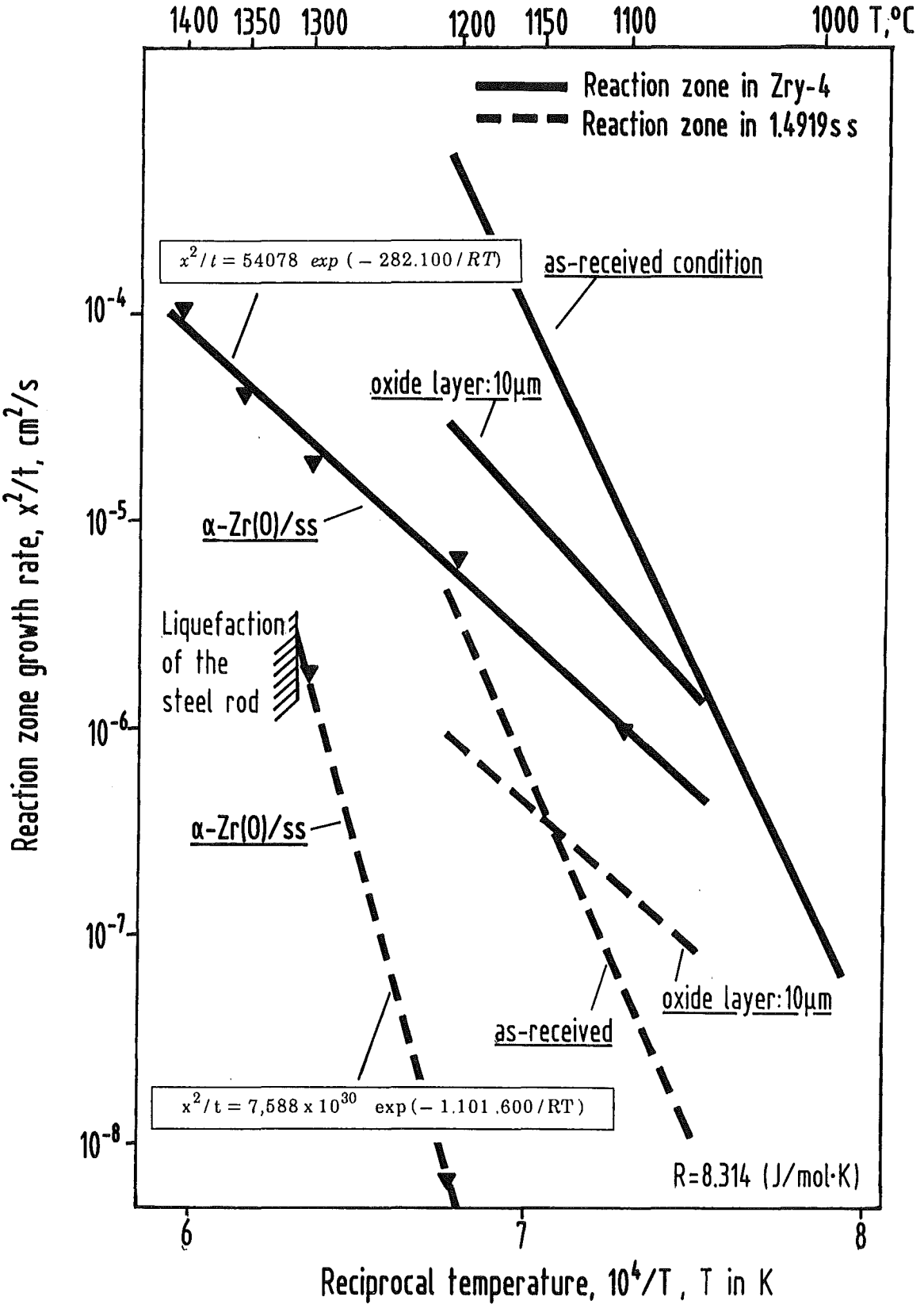

Fig. 34: Reaction zone growth rates for the oxygen-stabilized α-Zry(O)/ss 1.4919 (AISI 316) reaction system. Comparison with as-received and pre-oxidized Zry (ZrO_2 layer 10 µm).

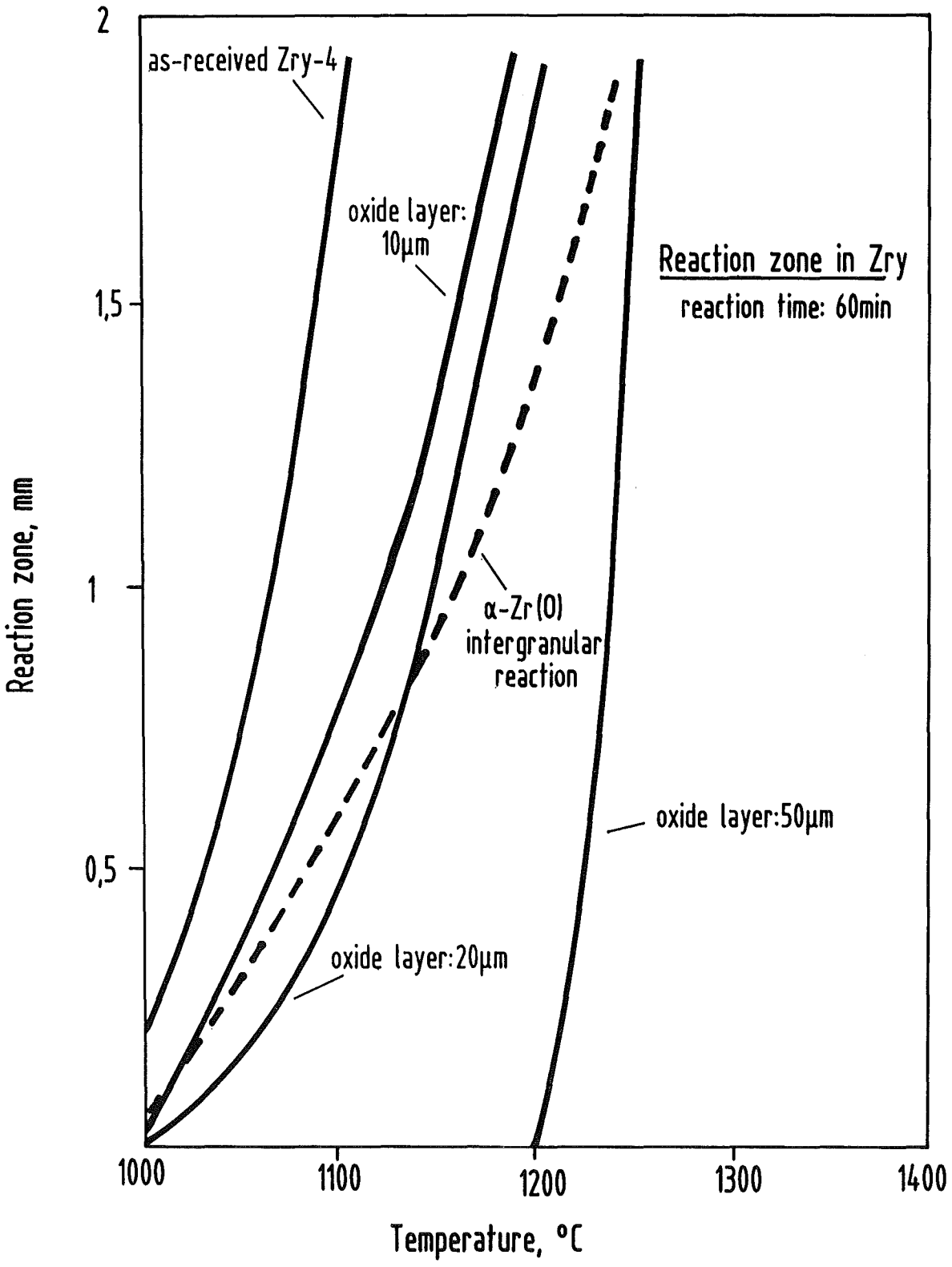

Fig. 35: Comparison of the reaction zone thicknesses in Zry versus annealing temperature for all conditions tested.

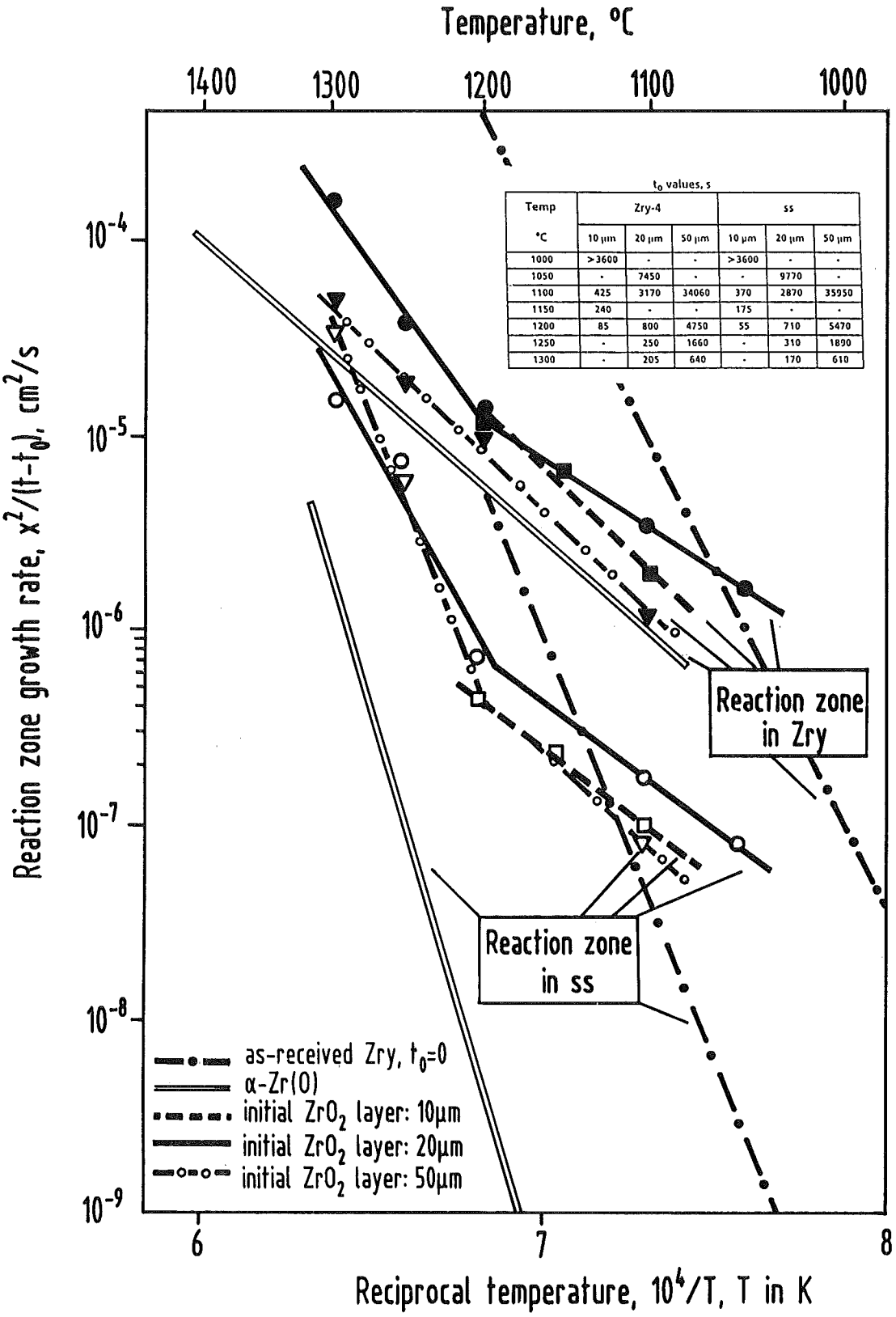

Fig. 36: Reaction zone growth rates for the Zry-4/ss 1.4919 (AISI 316) system for all conditions tested.

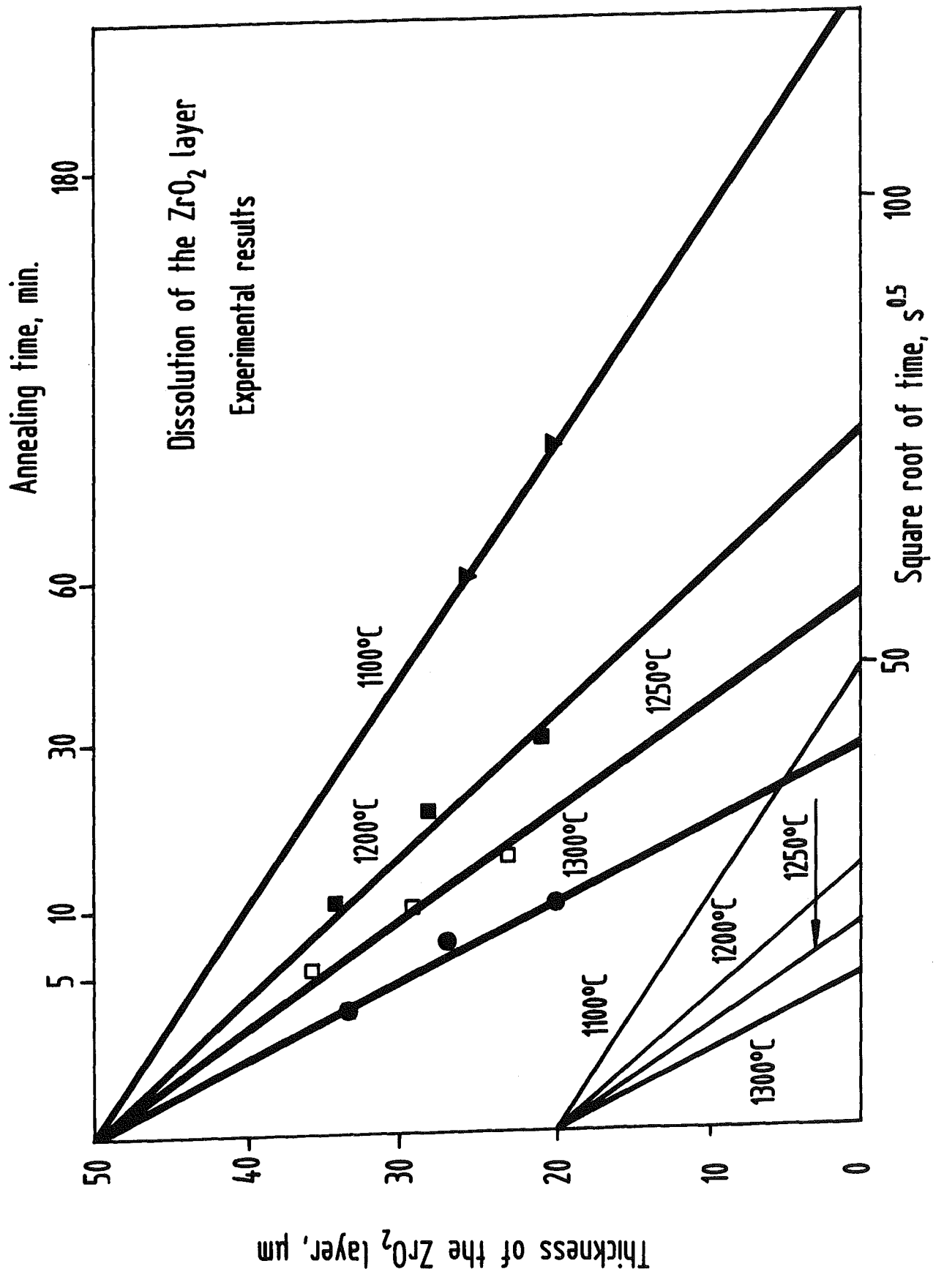

Fig. 37: Dissolution of the oxide layer with the formation of α-Zry(O); initial ZrO_2 layer thickness: 50 μm.

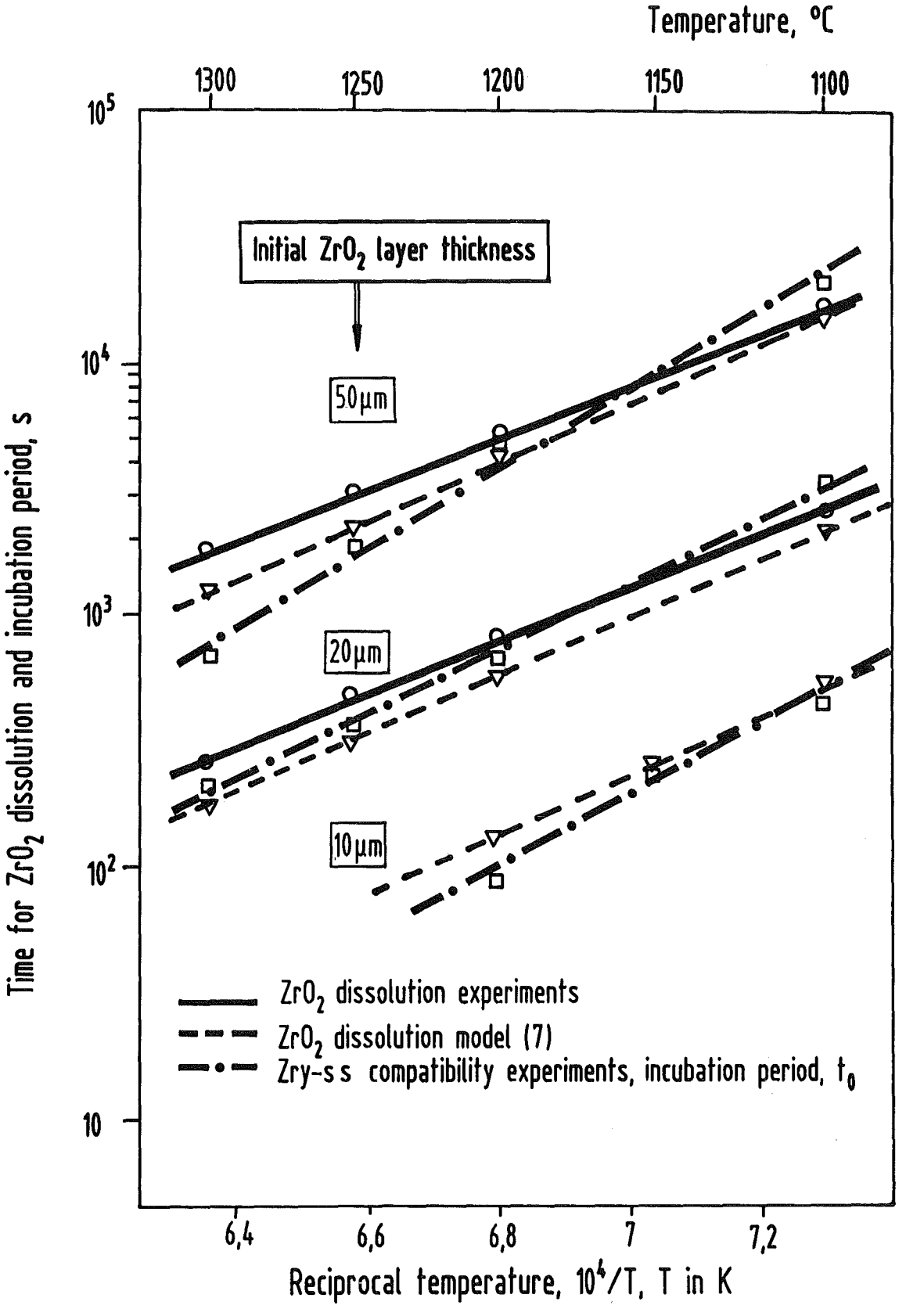

Fig. 38: Time of dissolution of the ZrO_2 layer versus reciprocal temperature. Comparison with the incubation time and calculation by the DISOL code [7].

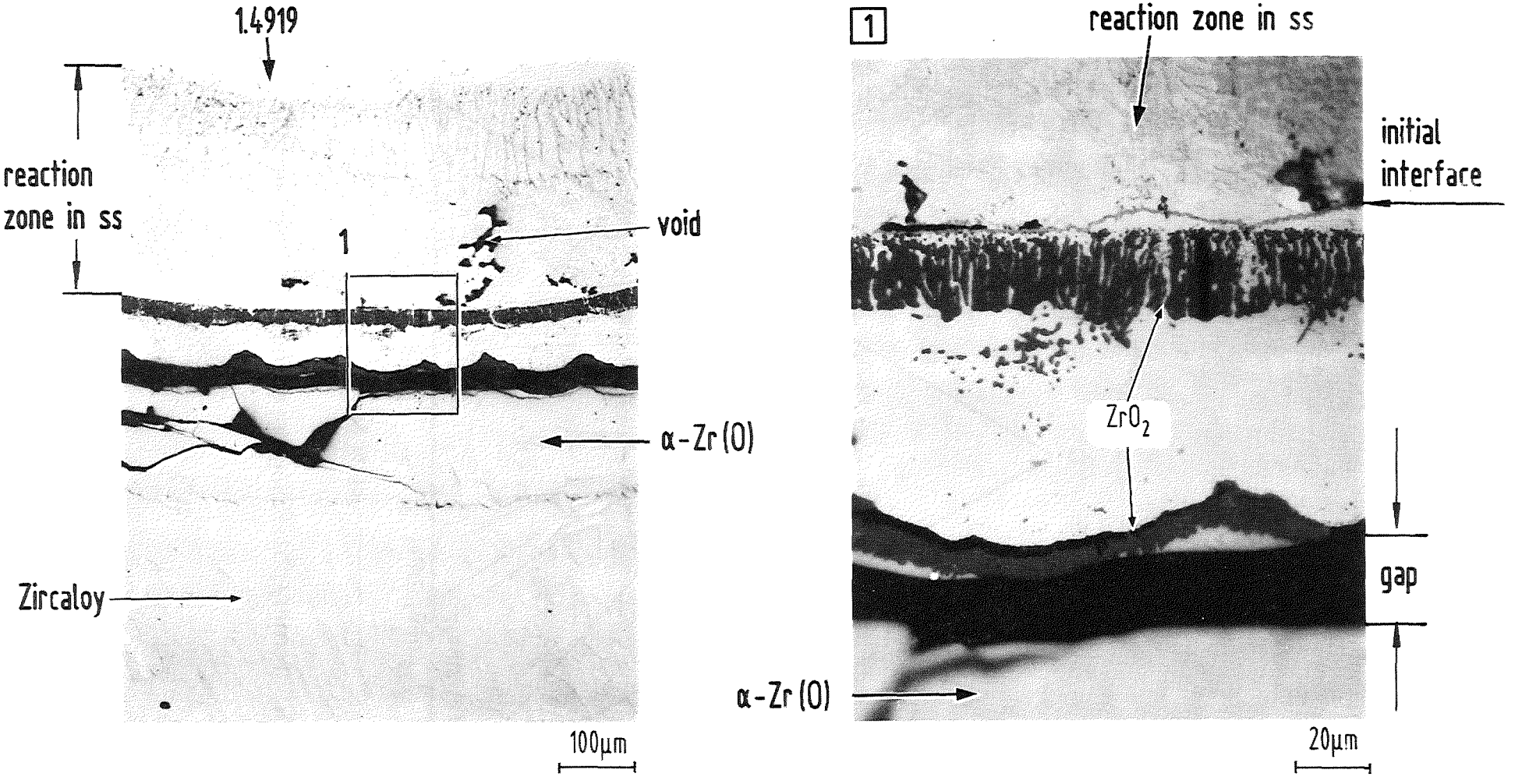

Fig. 39: Chemical interaction between Zry-4 and ss 1.4919 (AISI 316); 1300°C/10 min; initial ZrO_2 layer thickness: 50 µm.

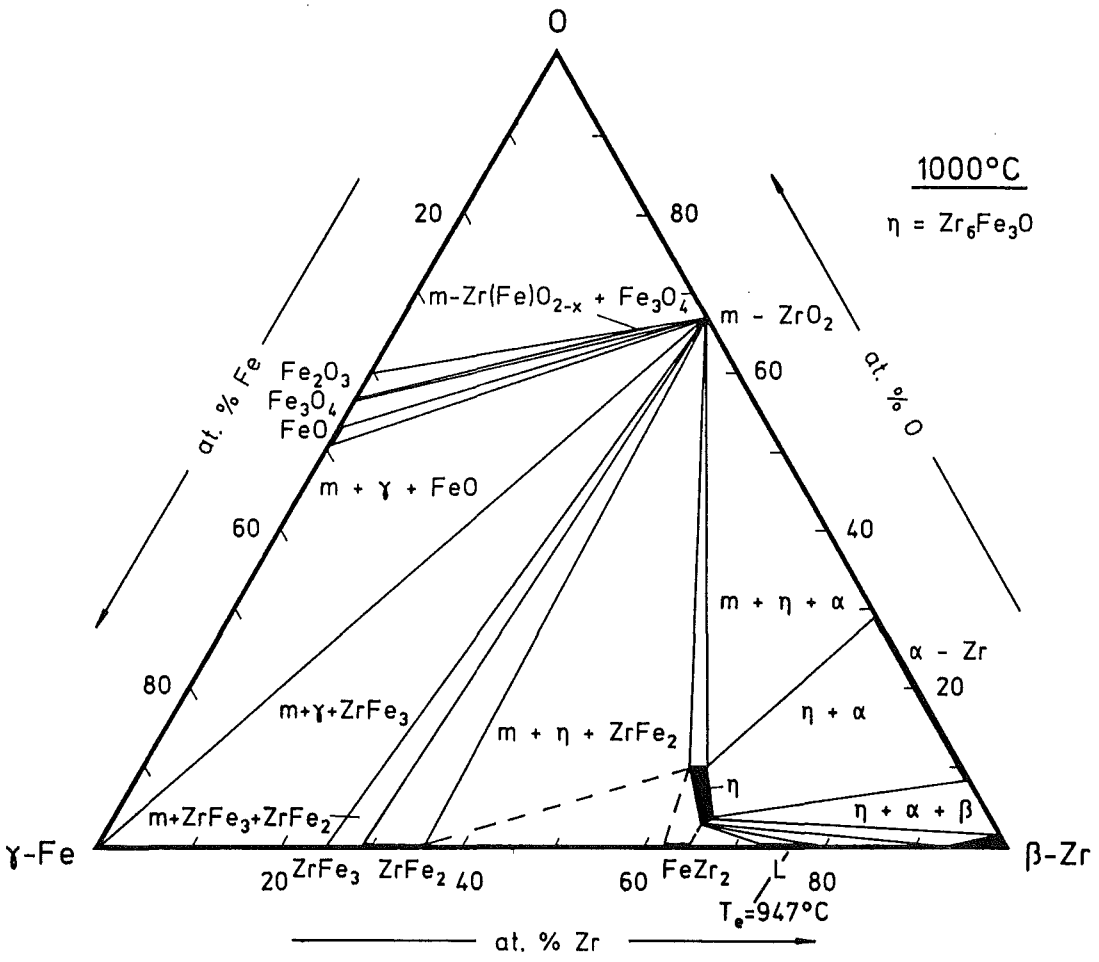

Fig. 40: Ternary phase diagram of the Fe-Zr-O system [10].

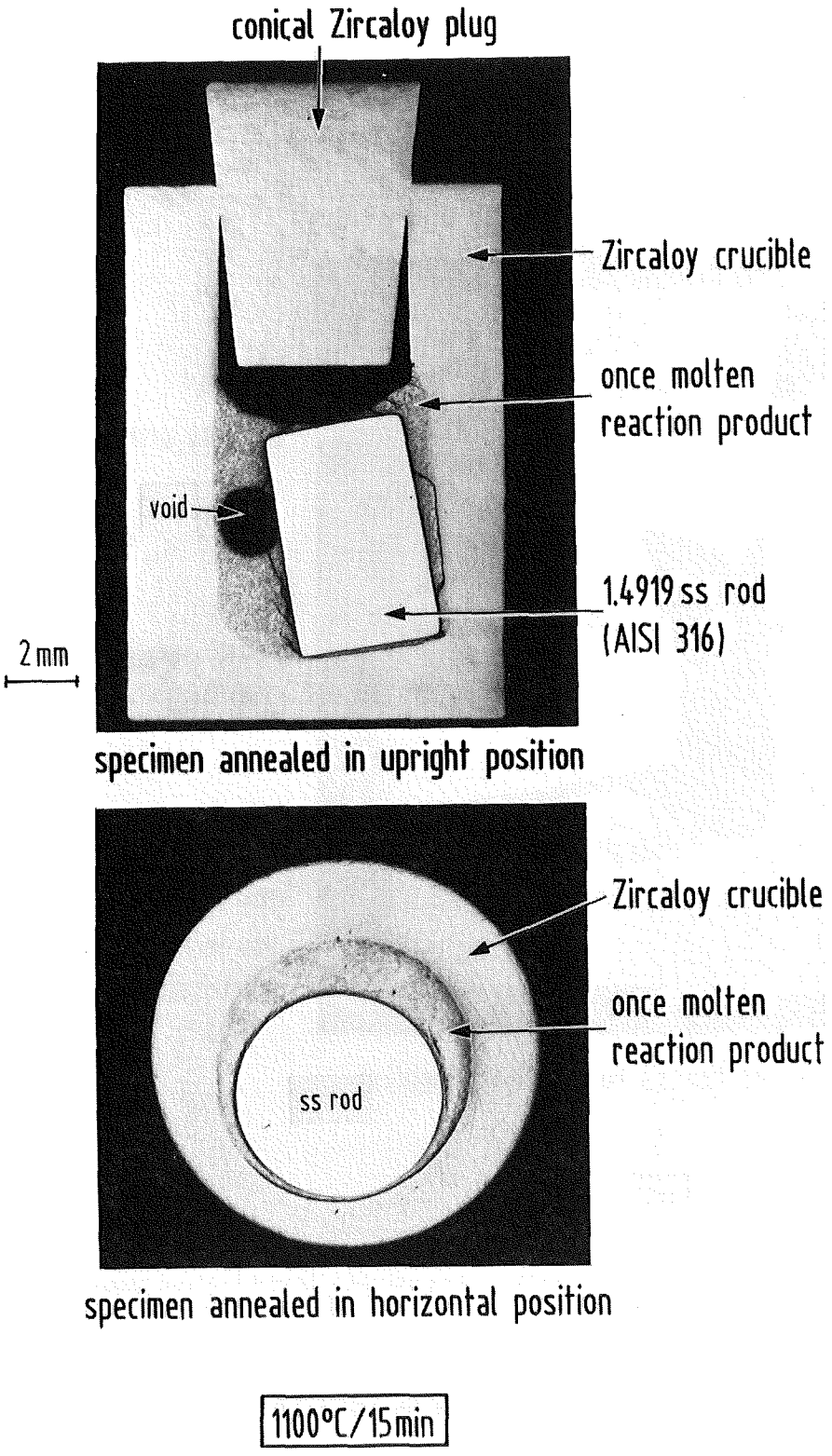

Fig. 41: Extent of chemical interactions between Zircaloy and stainless steel as a function of annealing conditions (upright or horizontal arrangement of the specimens).

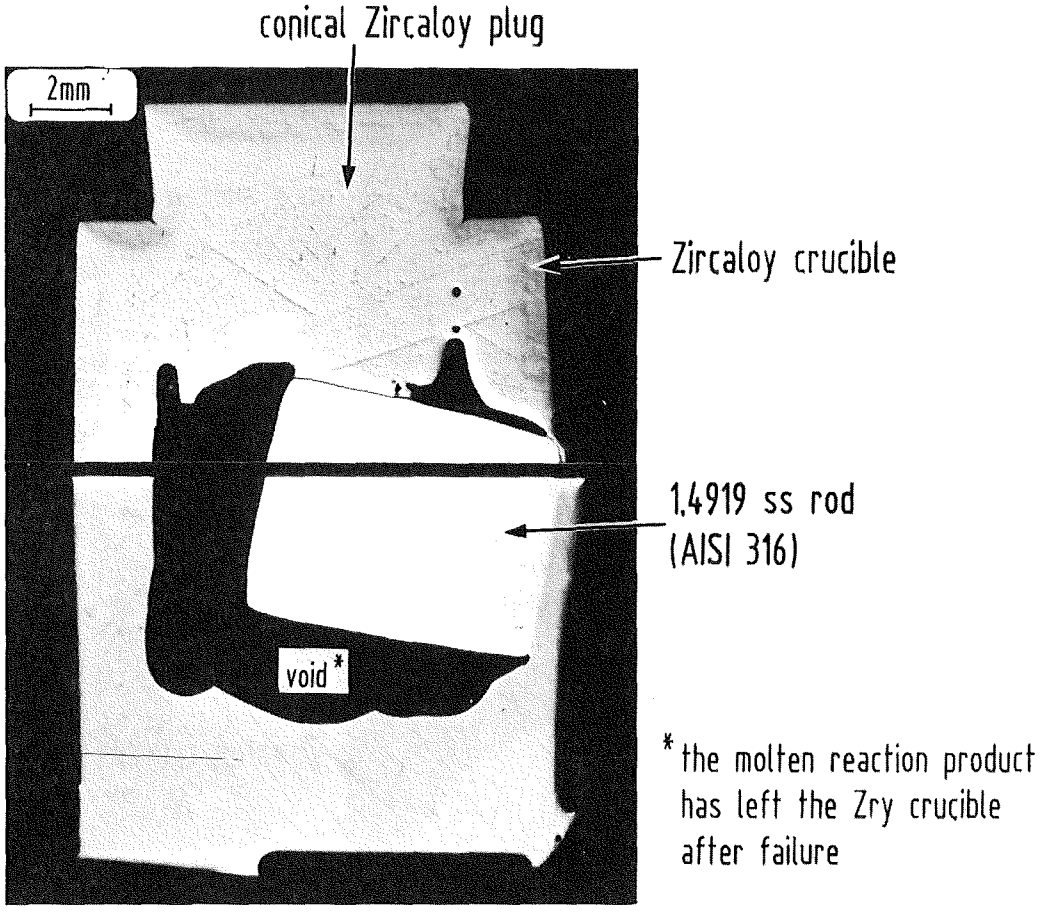

Fig. 42: Turning of the stainless steel rod within the Zircaloy crucible as a result of liquid phase formation. The relocated melt forms a large void.

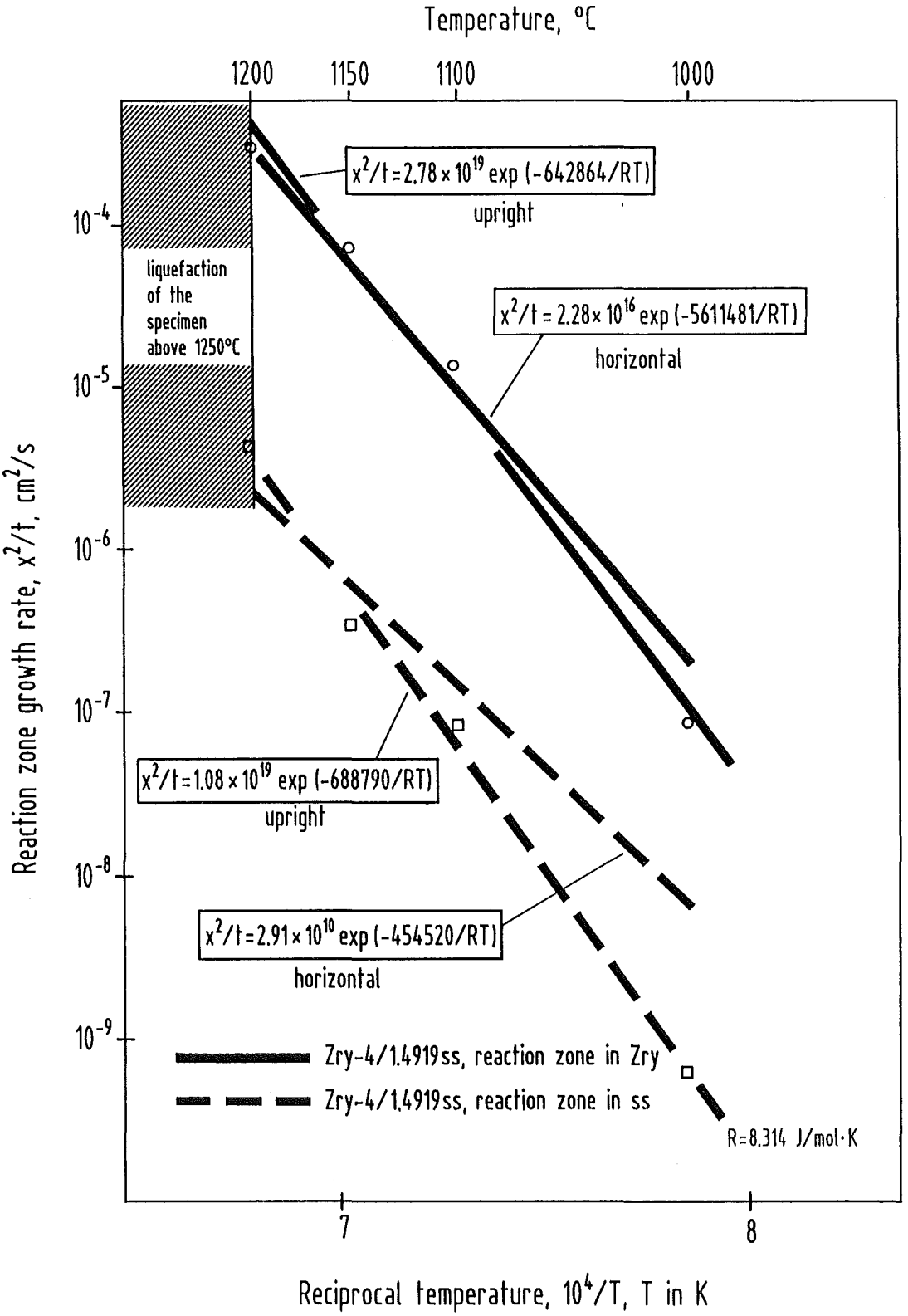

Fig. 43: Reaction zone growth rates for the Zircaloy/stainless steel 1.4919 (AISI 316) reaction system for two modes of annealing conditions (upright or horizontal arrangement of the specimens).